THESE

Présentée à

L'Université des Sciences et Technologies de Lille

Pour obtenir le titre de

DOCTEUR EN CHIMIE

Spécialité : Sciences de la Matière, du Rayonnement et de l'Environnement

Par

Ajay GHALWADKAR

Etude de catalyseurs d'ammoxydation du glycérol en acrylonitrile

Soutenance le 22 octobre 2014 devant la commission d'examen :

Rapporteurs :

Prof. Fabrizio Cavani, Université de Bologne (Italie)

Prof. Pedro Jesus Maireles Torres, Université de Malaga (Espagne)

Examinateurs :

Prof. Philippe Gaucher, Ecole Centrale de Paris

Dr. Axel Löfberg, Chargé de recherche CNRS

Dr. Bruno Vuillemin, Senior Manager TOTAL

M. Gérard Hecquet, Consultant

Directeur :

Prof. Franck Dumeignil, Université de Lille 1

Co-directeur :

Prof. Sébastien Paul, Ecole Centrale de Lille

Acknowledgement

Firstly, I would like to express the deepest appreciation to my supervisor Prof. Franck Dumeignil and co-supervisor Prof. Sébastien Paul for their emphatic guidance and support in steering my dissertation towards completion. I am deeply affected by their scientific method and attitude.

I also would like to thank Dr. Benjamin Katryniok for the help, valuable discussions, ideas and advices during my research work. Thanks to your guidance, I was able to stay focused, structured and motivated. I also would like to thank Prof. Nouria Fatah for her guidance.

I owe my gratitude towards *Unité de Catalyse et Chimie du Solide* (UCCS, UMR 8181) of *Université des Sciences Technologies de Lille* (USTL) and *Ecole centrale de Lille* (ECLille) for providing scientific environment and experimental platform. It is impossible to complete the work without help of all the team. Special thanks to all the technicians for their consistent help, especially Mr. Johann Jezequel and Mr. Gérard Cambien.

I am grateful to the TOTAL Pvt. Ltd for the financial support during my stay in France, as well as Dr. Bruno Vuillemin and Mr. Gérard Hecquet for their kind attention.

I am also thankful to Prof. Fabrizio Cavani and Prof. Pedro Jesus Maireles Torres for accepting the role of Referees for my thesis as well as Prof. Philippe Gaucher and Dr. Axel Lofberg for examining the thesis.

I should not forget to thank all of my colleagues and friends of ECLille Dr.Cyrille Guillon, Dr.Jorge Beiramar, Dr.Fangli Jing, Dr.Svetlana Heyte, Thomas Bonnette, Samadhan Lomate, David Melendez, Mengnan Lu for their helping hands and making my stay in France more memorable.

Finally, I express my special thanks to my parents, my sister and my wife for their love, enduring support and encouragement throughout my studies.

Index

Index

Abstract

The aim of this work is to study the conversion of glycerol to acrylonitrile through the indirect route *via* acrolein as an intermediate. In the indirect route, glycerol is first dehydrated to acrolein over an acidic catalyst and then the as-formed acrolein is ammoxidized to acrylonitrile over a multicomponent catalyst in the presence of oxygen and ammonia. The glycerol dehydration to acrolein process is widely studied and lot of research efforts have been devoted to the development of catalysts and process technologies. For the moment, the major problem remains the rapid catalyst deactivation. In this work we focused on the development of catalysts for the second step, namely the ammoxidation of acrolein to acrylonitrile in presence of water. Various multicomponent oxide catalysts were synthesized by a coprecipitation method. The corresponding catalysts were characterized by BET, XRD, UV-DRS, FTIR, EDX, ICP-OES and XPS techniques. Their activity in acrolein ammoxidation reaction was studied in a fixed bed reactor in the gaseous phase in presence of water. The effect of the addition of different elements in the catalyst composition on the catalyst performance is also studied. Furthermore, an optimization of the reaction parameters using a design of experiment has been carried out in order to obtain a high yield of acrylonitrile.

Résumé

Ce travail de thèse a consisté en une étude de la conversion catalytique du glycérol en acrylonitrile par une voie indirecte, c.à.d. via l'acroléine comme intermédiaire. Cette route implique d'abord une étape de déshydratation du glycérol en acroléine suivie par l'ammoxydation de l'acroléine obtenue en acrylonitrile en présence d'oxygène, d'ammoniac et d'eau sur un catalyseur oxyde mixte multi-composant. L'étape de déshydratation du glycérol ayant été déjà très étudiée, ce travail a été focalisé sur le développement de catalyseurs pour l'ammoxydation de l'acroléine en acrylonitrile en presence d'eau. Différents catalyseurs à base de Mo et de Bi ont était synthetisés et caracterisés par BET, DRX, UV-VIS, FT-IR, EDX, ICP et XPS. L'activité catalytique pour l'ammoxydation de l'acroléine a été mesurée dans un lit fixe en phase gaz. Finalement, les conditions opératoires de mise en oeuvre du meilleur catalyseur ont été optimisées par l'utilisation d'un plan d'expérience afin de maximiser le rendement en acrylonitrile.

1. Introduction

1.1 Background

The depletion of fossil fuels, concerns regarding the Green House Gases (GHG) emissions and the rapid increase in the global energy demand are driving our society towards the exploration for renewable resources that can replace fossil fuels. In these regards, oil, natural gas and coal can be substituted by renewable resources like solar, wind, geothermal and hydrothermal energy for heat and electricity production. On the other hand, biomass is considered as a sustainable source of organic carbon, which can perfectly substitute petroleum for the production of chemicals and organic materials and, in some cases of fuels. Biomass holds a remarkable potential in terms of diversity, composition, abundance and, more importantly, it features a closed cycle in which the released CO_2 from combustion or decomposition is recaptured by the existing plants.[1] However, at the current point, the world energy production is still mainly based on petroleum resources, whereas only around 2% of the global energy production are ensured by renewable resources. On the other hand, the global energy consumption is further increasing and - by 2035 - is predicted to be 1.5 times higher than today (Figure 1).

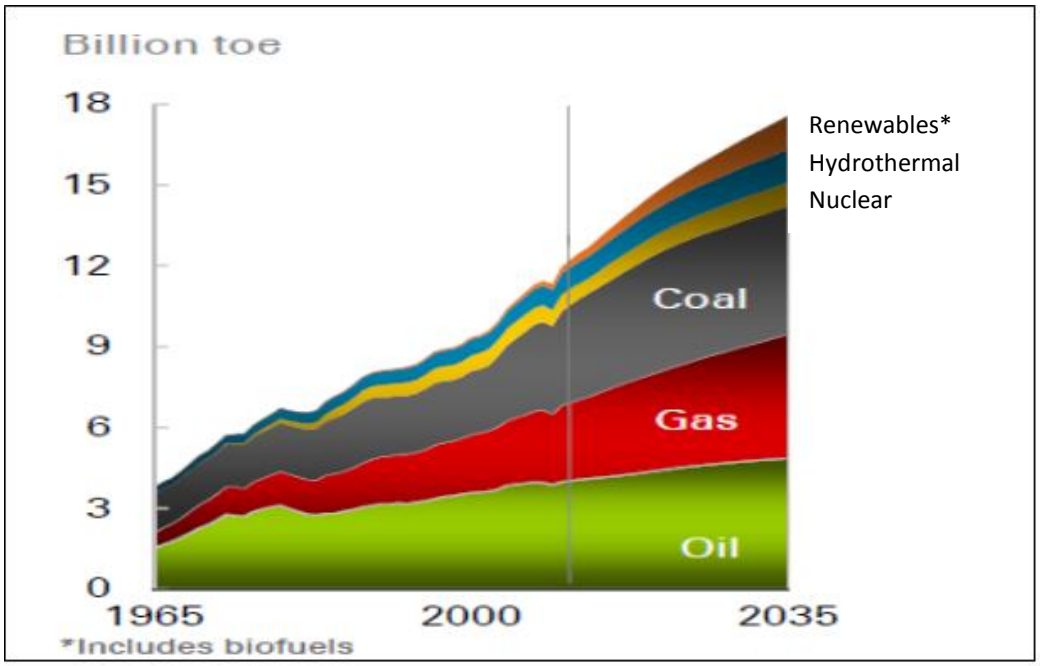

Figure 1: World energy production distribution by source.[2]

During the last century, the oil industry was economically successful because of its efficiency and complete utilization of petroleum resources in highly integrated facilities (refineries).

Following a similar approach, the transformations of bio-feedstock into fuels, valuable chemicals and energy in an integrated facility is currently studied (bio-refinery concept).[1]

In this context, one example for the transformation of a bio-feedstock in energy application is the transesterification of vegetable oils into a transport fuel known as 'biodiesel'. Over the last decade, biodiesel has emerged as a viable fuel with high energy and low sulphur content.[3]

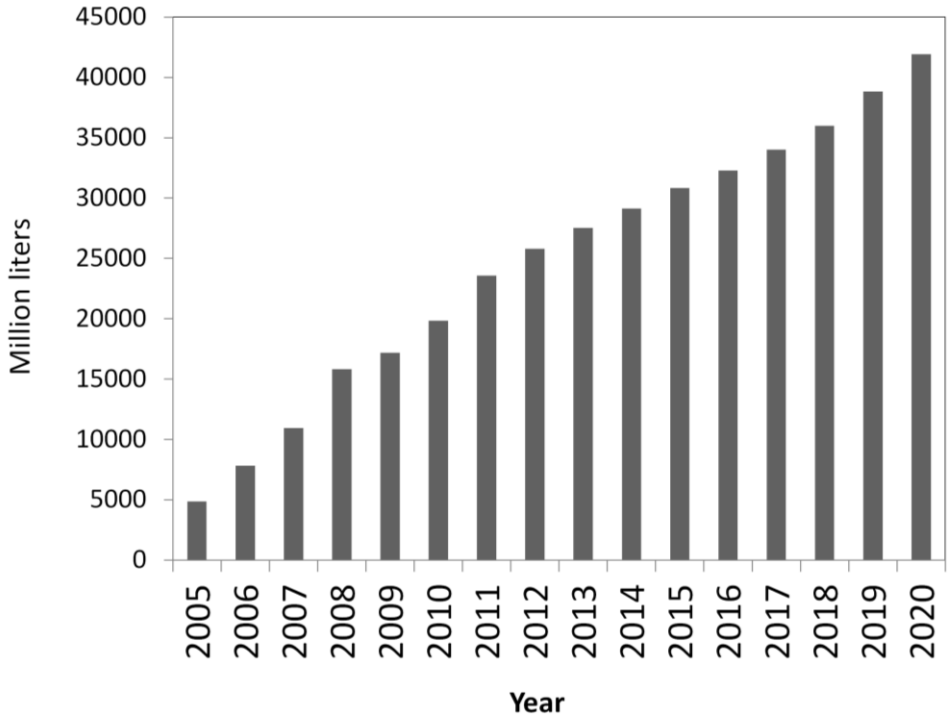

Figure 2: Global biodiesel production.

The rapidly increasing global vehicle fleet – from approximately 1 billion today to 1.6 billion predicted in 2030 – combined with the decreasing fossil fuel sources brought the attention towards the production of biodiesel as alternative renewable fuel.[4] For example, EU has set the target to blend domestic petro-based fuels with 7% (initially it was even 10%) of fuels derived from renewable resources by 2020.[5] As a result, the biodiesel production has increased drastically and even if this prevision could be seen as optimistic considering the recent revision of the EU transportation fuels policy it is predicted to reach about 42 million metric tons in 2020 (as shown in Figure 2).[6]

Consequently, the amount of glycerol, the main byproduct in the production of biodiesel, also increases. For 1 ton of biodiesel produced, about 100 kg of glycerol are obtained in the process of trans-esterification of fatty acids with methanol (Figure 3).

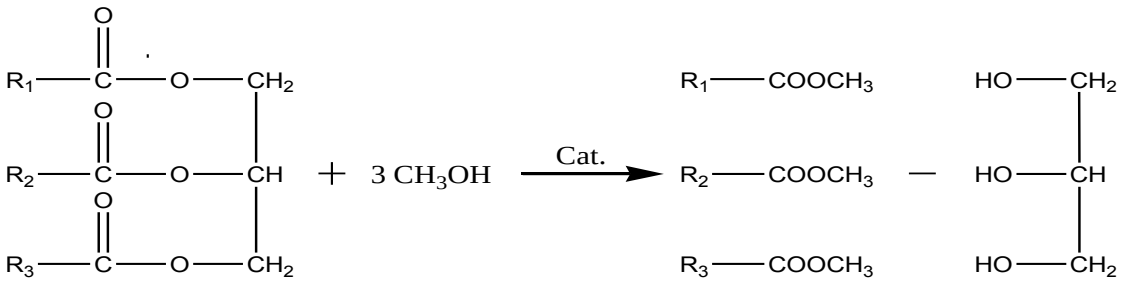

Figure 3: Transesterification reaction of fats and oils (triglycerides) to produce biodiesel and glycerol.

As a matter of fact, the glycerol issued from the biodiesel production is flooding the market (Figure 4). However, the markets addressed by traditional consumers of glycerol (cosmetics, tobacco, etc.) cannot absorb this oversupply of crude glycerol, which substantially decreased the bioglycerol price.[7] Nowadays, refined glycerol (99.7%) is available for around 1600 US$/ton, but crude glycerol (80%) is largely available at the significantly lower price of 190-220 US$/ton.[8]

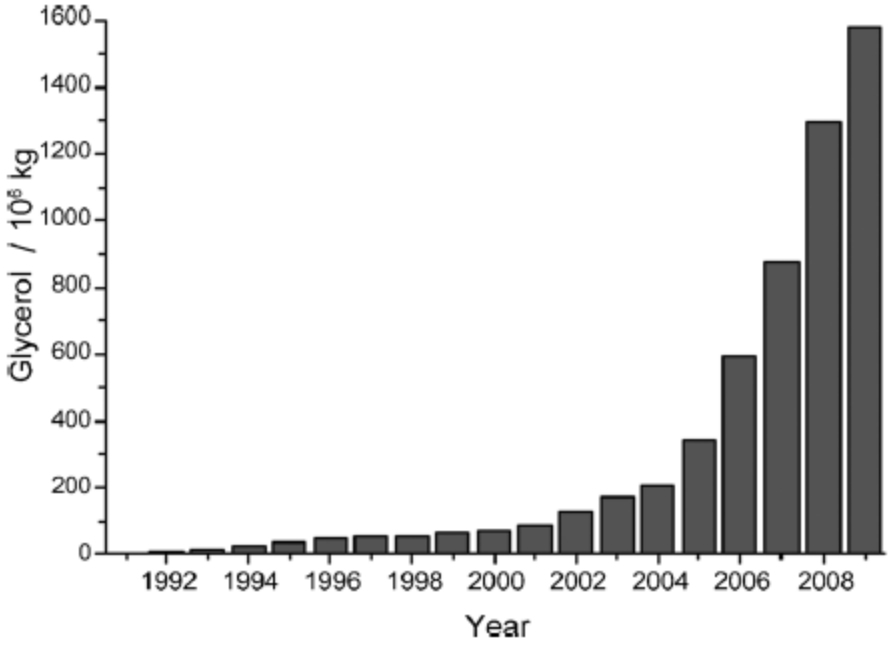

Figure 4: Annual glycerol production resulting from biodiesel production.[9]

The combination of low price and high availability has attracted researchers to propose various valorization reactions. The latter will also help to achieve a sustainable business in biodiesel industry.

1.2 Bioglycerol valorization

There are more than 1500 direct applications of glycerol already known. This highlights its tremendous potential as renewable feedstock for the chemical industries.[10] Due to its non-toxic nature, it is largely used in food, drug and cosmetic industry. The next important application of glycerol is in plastic and tobacco industries, where it is used as a flavoring agent to tobacco, adding sweetness and preventing dehydration. Figure 5 shows the various applications for glycerol.[11]

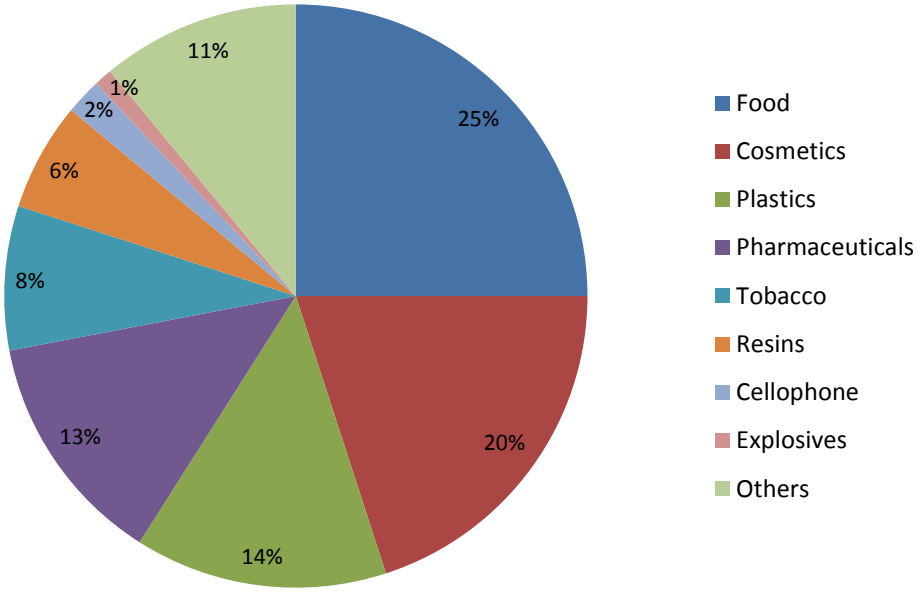

Figure 5: Glycerol utilization in various application fields.

However, these traditional applications of glycerol are significantly restricted for crude glycerol unless previous purification steps. Moreover, as stated earlier, the expansion of the biodiesel industry has led to abundant and cheap glycerol, which needs to find new technologies for the large-scale processing into valuable products. Due to its three hydroxyl groups, glycerol exhibits versatile and high chemical reactivity. Some of the most important and novel routes to upgrade glycerol are shown in Figure 6 and briefly described below.

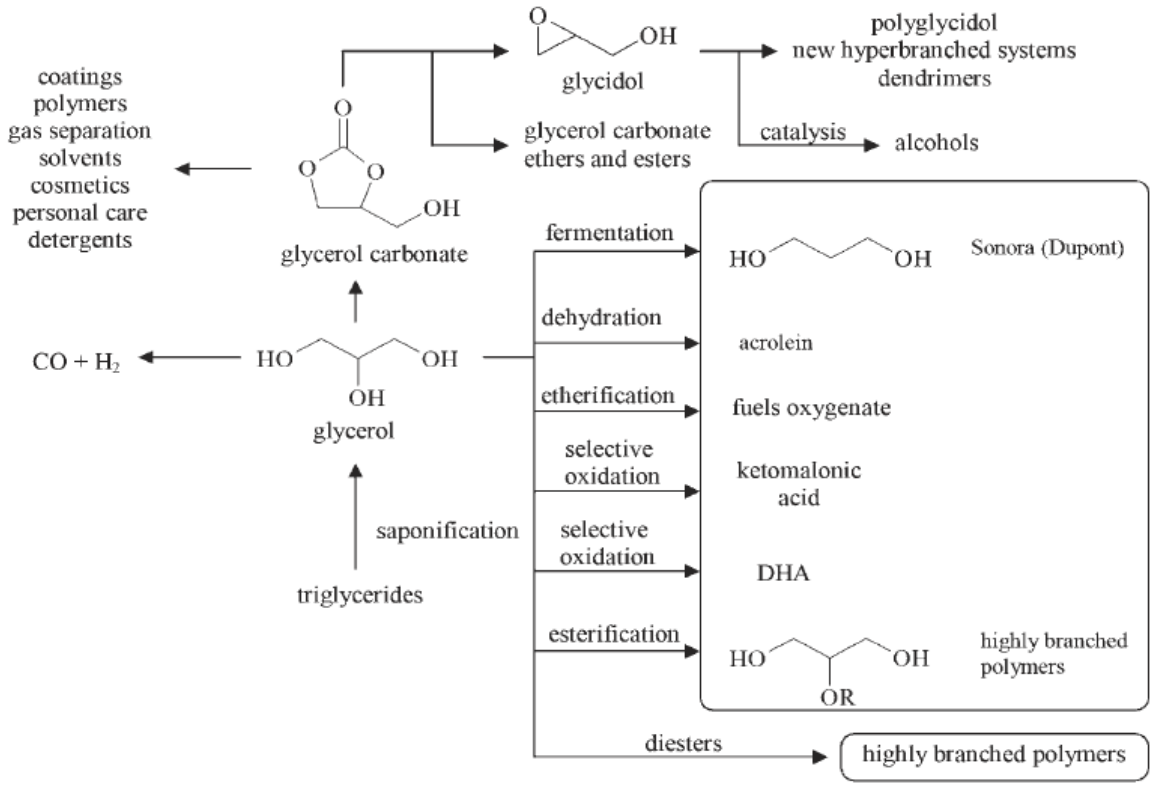

Figure 6: Novel routes of valorization of glycerol.[3]

The different ways of valorizing glycerol are summarized in various review articles.[1, 3, 12] Among the most interesting possibilities, one can mention the hydrogenolysis to produce propylene glycol or *1,3*-propanediol, which are used in the polymer industry.[13] The reforming of glycerol on Pt-Rh catalysts yields syngas, which is used in the Fischer-Tropsch process, and also for hydrogen production.[14] Furthermore, the etherification of glycerol is a possibility to produce glycerol-*tert*-butylether (GBTE), which is used as an additive for diesel blending. Another way of valorizing glycerol is its esterification to monoacylglycerol (MAG) or diacylglycerol (DAG), which are used as emulsifiers in food and cosmetics.[15] The partial oxidation of glycerol leads to variety of possible products such as glyceric, tartronic and ketomalonic acids and glyceraldehyde.[16] Nevertheless, only few processes based on bioglycerol valorization have reached the industrial level so far. One of these process is the halogenation of glycerol to produce epichlorohydrine by SOLVAY, which is currently ran with a capacity of 10 kt/year in Tavaux (France).[17] Another commercial process is the production of biomethanol, which is employed by BioMCN in Delfzijl (Netherland).[18]

However, one of the most promising ways of glycerol valorization is its catalytic dehydration to acrolein, which is an important intermediate for the synthesis of polymers (poly acrylate) and cattle feeding additives (*DL*-methionine). The other major applications of acrolein are shown in Figure 7.[9]

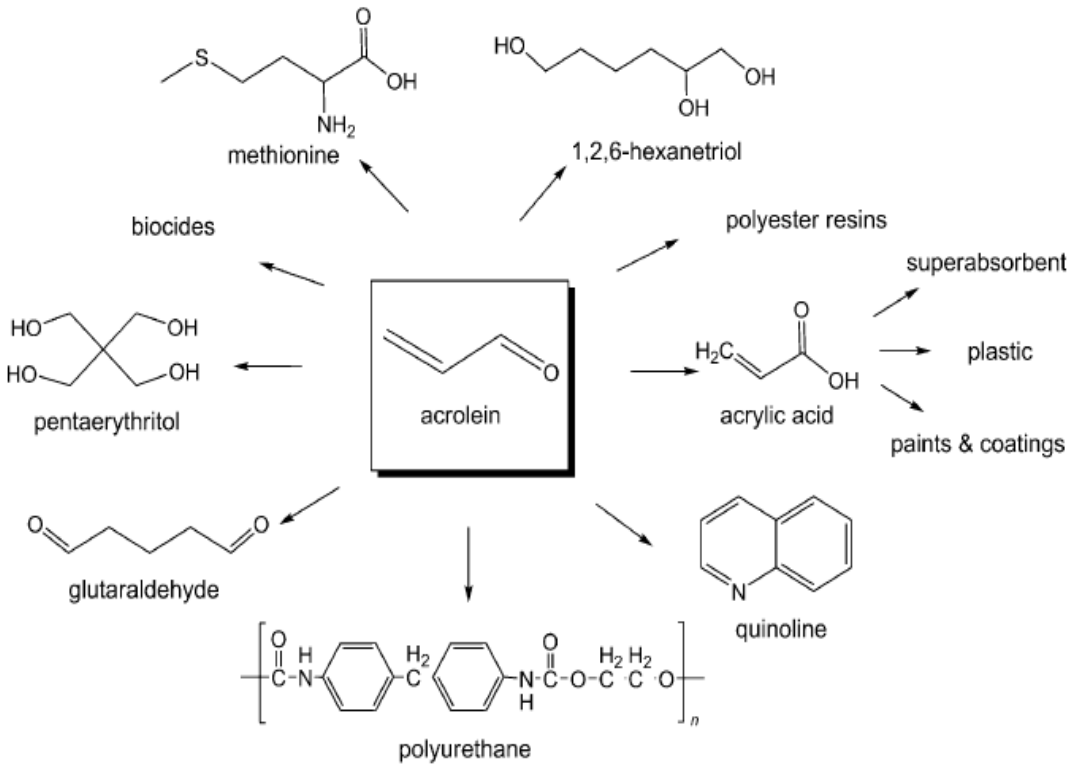

Figure 7: Chemicals derived from acrolein.

The commercial synthesis of acrolein is currently based on the partial oxidation of propene over complex multicomponent BiMoOx-based catalysts. The selectivity obtained in this process is around 85% with 95% of propylene conversion.[19] Propane is also reported as a cheap starting material for the acrolein synthesis, but the reaction suffers from lower yields.[20] However, considering the fossil fuel depletion issues, these processes need to be replaced with bio-renewable resources.

The glycerol dehydration is an intensively studied reaction. A detailed state of art is given in Chapter 2. But still, no commercial application has been launched. Because of its toxicity and

high volatility, acrolein is usually directly converted into its derivatives. Therefore, new glycerol dehydration processes are emerging, where bio-acrolein production is considered as an intermediate step in cascade reaction directly targeting subsequent various final products.

One example of such a process is the production of renewable acrylonitrile starting from glycerol by dehydration to acrolein followed by the ammoxidation of the latter.[21] Acrylonitrile is a very important intermediate in polymer industry and is among the top 50 chemicals produced in US and mainly utilized in the production of acrylic fibers (ABS) and resins (SAN).[22]

1.3 Acrylonitrile - Historical context

Acrylonitrile (ACN) is a clear colorless, toxic liquid. It was firstly synthesized in 1893 by the French chemist Charles Moureu by the dehydration of acrylamide or ethylene cyanohydrin. The presence of two reactive sites at the carbon-carbon double bond and the nitrile functional group makes it chemically reactive especially towards the polymerization reaction. Its potential use in the manufacture of acrylic fibers, introduced by DuPont in the 50s, increased the global demand of acrylonitrile and also spurred efforts to develop improved technologies to fulfill the growing demands.[23]

1.3.1 Acrylonitrile production

The first process for acrylonitrile production at large scale was the ethylene cyanohydrin process, depicted in Figure 8.

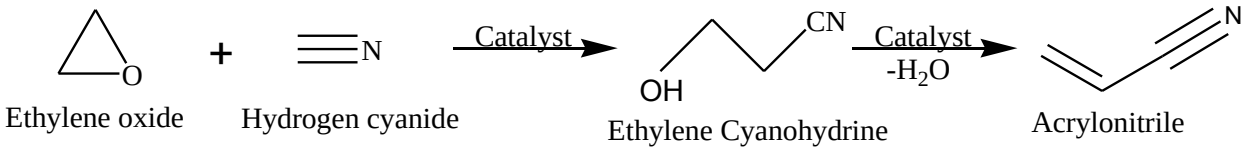

Figure 8: Acrylonitrile synthesis from ethylene oxide and hydrogen cyanide.

This process was reported by American Cyanamid and Union Carbide in the US and by I. G. Farben in Germany. In this process, ethylene oxide is first converted to ethylene cyanohydrin in

the base-catalyzed addition of hydrocyanic acid at 60°C. This step is followed by the dehydration of cyanohydrin to acrylonitrile using an alkali metal catalyst at 200°C.[24]

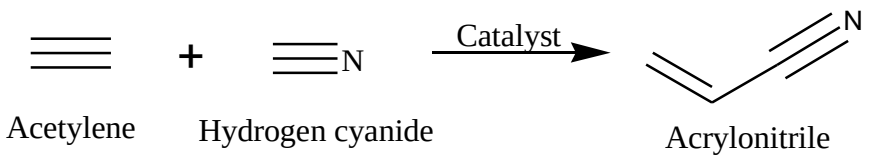

Figure 9: Acrylonitrile synthesis from acetylene and hydrogen cyanide.

DuPont, American Cyanamid and Monsanto applied another route to acrylonitrile based on the catalytic addition of hydrocyanic acid to acetylene (as shown in Figure 9). The catalyst used was cuprous chloride. Nevertheless, the commercial plants using cyanohydrin and acetylene-based processes were shut down in the 70s due to the use of a rather expensive starting material.[22] In fact, cheaper starting materials like propylene were already being introduced.

The other chemical routes to acrylonitrile are:

- **Acetaldehyde and hydrocyanic acid coupling followed by a dehydration:**

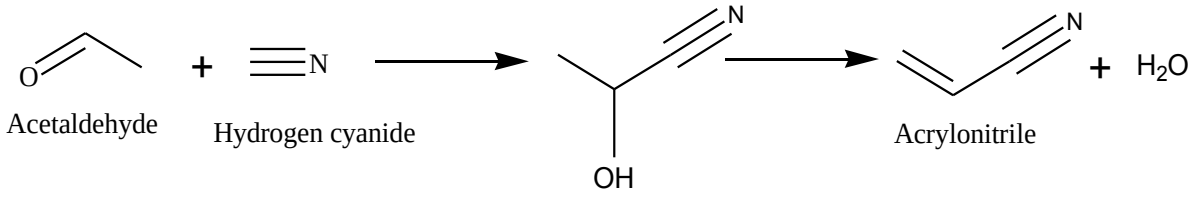

- **Propionitrile dehydrogenation:**

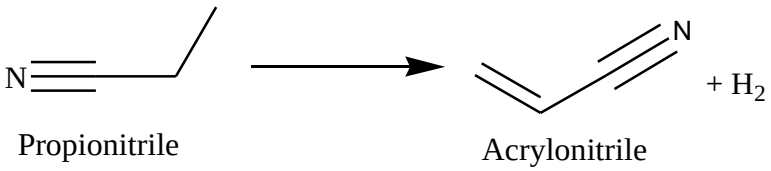

- **Propylene and nitric acid reaction:**

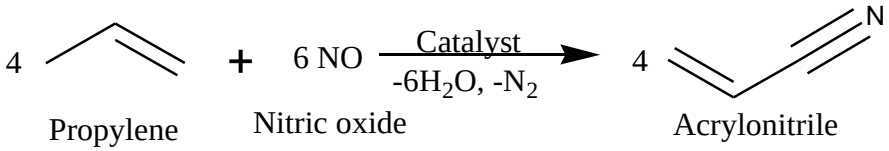

However, none of these routes achieved large-scale commercial application.[23]

The major breakthrough in the acrylonitrile production was the introduction of the propylene ammoxidation process by Standard oil of Ohio (today BP) in 1959, the so called SOHIO process (Figure 10).[25]

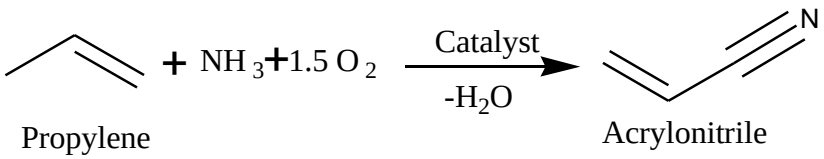

Figure 10: Ammoxidation of propylene to acrylonitrile (SOHIO process).

Almost 90% of the annual worldwide acrylonitrile production is based on this synthesis route nowadays. The process is referred as ammoxidation because the propylene in this process is oxidized in presence of ammonia to produce acrylonitrile.[26] Due to the commercial importance of the propylene ammoxidation process, significant research activities have been employed to develop high selective catalysts. The first commercial production of acrylonitrile by SOHIO used bismuth-phospho-molybdate ($Bi_9PMo_{12}O_{52}$) on silica as a catalyst for the propylene ammoxidation with bismuth molybdate being the active phase.[25] The catalyst was progressively modified by addition of iron, cobalt, nickel and also promoters like alkali metals, in order to achieve higher yields in acrylonitrile.

In the commercial process, the ammoxidation reaction is carried out in a fluidized bed reactor. Indeed, the reaction is highly exothermic whereby water is pumped through pipes in the reactor to recover the heat of the reaction for the production of steam. Propylene and stoichiometric excess of ammonia and oxygen (as air) are injected to the reactor at a temperature from 400 to 510°C and at a pressure between 0.5 to 2 bar. After that, the hot effluents are quenched with water in a countercurrent absorber and unreacted ammonia is neutralized with sulphuric acid (Figure 11). Thereafter, acrylonitrile is separated from the byproducts HCN and acetonitrile in several subsequent rectification columns c-f in Figure 11.

Although the majority of acrylonitrile production uses molybdate-based catalyst, antimonate catalysts are also employed. In fact, processes based on iron-antimony oxide catalysts promoted with vanadium, copper, tellurium and tungsten are also commercialized today.[27]

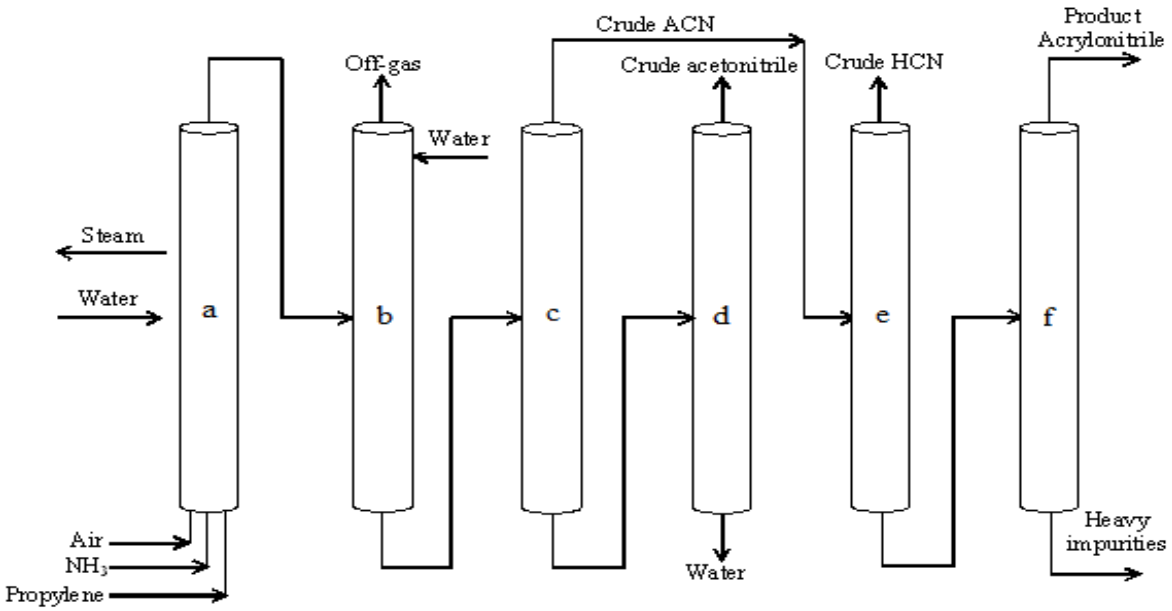

Figure 11: Scheme of SOHIO process- a) Fluidized bed reactor; b) Countercurrent absorber; c) Recovery column; d) Acetonitrile stripping column; e) Light fractionation column and f) Product column.[23]

1.3.2 Uses of acrylonitrile

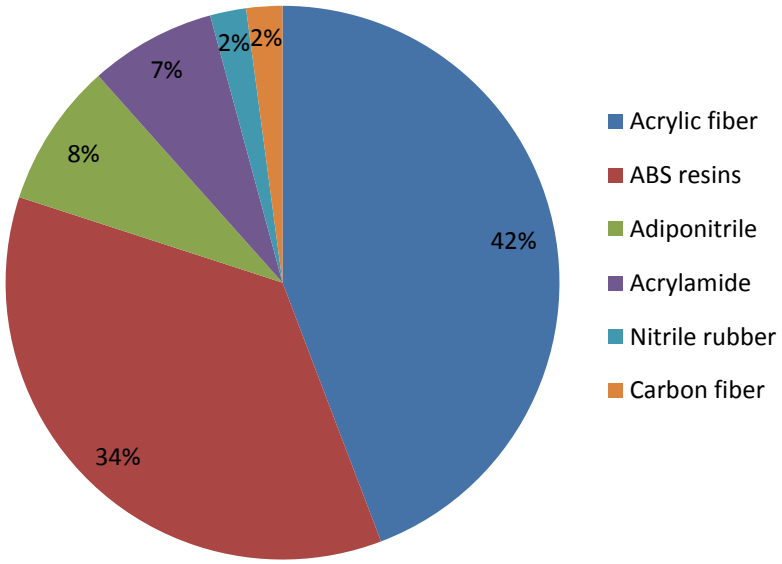

Figure 12: Acrylonitrile consumption in different applications.[23]

Introduction

Acrylonitrile is principally used in the production of acrylic fiber (42%) and acrylonitrile-butadiene-styrene (ABS) resins (32%), as shown in Figure 12. The other uses of acrylonitrile include the production of adiponitrile, acrylamide, nitrile rubber and carbon fiber.

Acrylic fiber – Acrylic fiber have remained the major outlet for acrylonitrile production in the US and Far East countries like Japan. Fibers containing 85% or more acrylonitrile are called acrylics, whereas fibers containing 35 to 85% acrylonitrile are termed modacrylics. Acrylic fibers are primarily used in the manufacture of apparel and home furnishings.

ABS resins/ SAN resins – ABS and SAN resins are the fastest growing application for acrylonitrile. ABS is a high performance polymer mainly because of its high mechanical strength, coloring characteristics and processing ease. These resins normally contain about 25% acrylonitrile. It is used in numerous automotive, construction, appliance and electronics applications. SAN resins contain between 25% and 30% acrylonitrile. They are optically transparent and employed for packaging, optical fibers and food containers among other applications.

Adiponitrile – The largest increase of acrylonitrile consumption has come from adiponitrile, which is used to manufacture hexamethylenediamine (HDMA, $C_6H_{16}N_2$) by electrohydrodimerization. HDMA is used exclusively for the manufacture of Nylon-6,6.

Acrylamide – Acrylamide is manufactured from acrylonitrile by a copper-catalyzed hydration process. Acrylamide is used primarily in the form of a polymer, polyacrylamide, in the paper and pulp industry in waste water treatment, oil production and mineral processing.

Nitrile rubber – The nitrile rubber consists of butadiene-acrylonitrile copolymers with an acrylonitrile content ranging from 15-45%. They are used in the industry because of their chemical, oil and ozone resistance. They are mainly used in the manufacture of gaskets, seals and electrical cable jackets.

Carbon fiber – Carbon fibers are produced by pyrolysis of oriented polyacrylonitrile fibers and used in the aircraft, defense and aerospace industries.

1.4 Aim of this work

The production of acrylonitrile starting from glycerol has been described as a new route by either direct ammoxidation[21a] or *via* acrolein as an intermediate [21b]. This route is promising because it serves two purposes, i) utilization of glycerol by-produced in the transesterification reaction, whereby the economic viability of the biodiesel production increases and ii) use of a renewable feedstock enabling thus a 'green and sustainable' process for the acrylonitrile production.

Therefore, the aim of this work is to study the conversion of glycerol to acrylonitrile through the indirect route *via* acrolein as an intermediate. In the indirect route, glycerol is first dehydrated to acrolein over an acidic catalyst and then the as-formed acrolein is ammoxidized to acrylonitrile over a multicomponent catalyst in the presence of oxygen and air. The glycerol dehydration to acrolein process is widely studied and lot of research efforts has been devoted to the development of catalysts and process technologies. For the moment, the major problem remains the rapid catalyst deactivation.[9, 28] In this work we focused on the development of catalysts for the second step, namely the ammoxidation of acrolein to acrylonitrile. The catalysts were synthesized, characterized and tested for their catalytic performances in the ammoxidation reaction in a fixed bed reactor in the gaseous phase. The effect of different elements in the catalyst composition on the catalyst activity was also studied. Furthermore, the optimization of reaction parameters was carried out to find suitable reaction conditions in order to obtain high yields of acrylonitrile.

1.5 References

[1] J. C. Serrano-Ruiz, R. Luque, A. Sepulveda-Escribano, *Chemical Society reviews* **2011**, *40*, 5266-5281.
[2] B. E. O. 2035, *http://www.bp.com/en/global/corporate/about-bp/energy-economics/energy-outlook/outlook-to-2035.html* **2012**.
[3] M. Pagliaro, R. Ciriminna, H. Kimura, M. Rossi, C. Della Pina, *Angewandte Chemie* **2007**, *46*, 4434-4440.
[4] E. O. BP, *http://www.bp.com/en/global/corporate/about-bp/energy-economics/energy-outlook.html* **2012**.
[5] https://www.agra-net.net/agra/world-ethanol-and-biofuels-report/biofuel-news/biodiesel/european-union---council-approves-7-cap-for-crop-based-biofuels-442927.htm
[6] OECD-FAO Agricultural Outlook 2011-2020.
[7] B. Katryniok, S. Paul, F. Dumeignil, *ACS Catalysis* **2013**, *3*, 1819-1834.
[8] ICIS price report,
[9] L. Liu, X. P. Ye, J. J. Bozell, *ChemSusChem* **2012**, *5*, 1162-1180.
[10] C. S. Callam, S. J. Singer, T. L. Lowary, C. M. Hadad, *Journal of the American Chemical Society* **2001**, *123*, 11743-11754.
[11] R. Christoph, B. Schmidt, U. Steinberner, W. Dilla, R. Karinen, *Ullman's Encyclopedia of Industrial Chemistry* **2006**.
[12] A. Behr, J. Eilting, K. Irawadi, J. Leschinski, F. Lindner, *Green Chemistry* **2008**, *10*, 13.
[13] C. Rode, A. Ghalwadkar, R. Mane, A. Hengne, S. Jadkar, N. Biradar, *Organic Process Research & Dev.* **2010**, *14*, 1385-1392.
[14] D. A. Simonetti, J. Rass-Hansen, E. L. Kunkes, R. R. Soares, J. A. Dumesic, *Green Chemistry* **2007**, *9*, 1073-1083.
[15] N. O. Sonntag, *Journal of the American Oil Chemists Society* **1982**, *59*, 795A-802A.
[16] aH. Kimura, *Applied Catalysis A: General* **1993**, *105*, 147-158; bH. Kimura, K. Tsuto, T. Wakisaka, Y. Kazumi, Y. Inaya, *Applied Catalysis A: General* **1993**, *96*, 217-228.
[17] D. Siano, E. Santacesaria, V. Fiandra, R. Tesser, G. Di Nuzzi, M. Di Serio, M. Nastasi, (ASER), **2006**.
[18] E. Voegele, *Biodiesel Magazine* **2011**, *6*.
[19] G. W. Keulks, L. D. Krenzke, T. M. Notermann, *Advances in Catalysis* **1979**, *27*, 183-225.
[20] M. M. Lin, *Applied Catalysis A: General* **2001**, *207*, 1-16.
[21] aM. O. Guerrero-Perez, M. A. Banares, *ChemSusChem* **2008**, *1*, 511-513; bC. Liebig, S. Paul, B. Katryniok, C. Guillon, J.-L. Couturier, J.-L. Dubois, F. Dumeignil, W. F. Hoelderich, *Applied Catalysis B: Environmental* **2013**, *132-133*, 170-182.
[22] J. F. Bradzil, in *Kirk-Othmer Encyclopedia of Chemical Technology*, John Wiley & Sons, Inc., **2000**.
[23] J. F. Brazdil, in *Ullmann's Encyclopedia of Industrial Chemistry*, Wiley-VCH Verlag GmbH & Co. KGaA, **2000**.
[24] aE. L. Carpenter, (American Cyanamid Co), **1954**; bB. P. H. De, (Stamicarbon), **1956**.
[25] J. J. D. Idol, (Standard Oil Co), **1959**.
[26] P. W. Langvardt, *Ullmann's Encyclopedia of Industrial Chemistry* **1985**.
[27] aI. Nagase, S. Saito, Y. Sasaki, T. Yoshino, (Nitto Chemical Industry Co Ltd), **1970**; bT. Yoshino, S. Saito, Y. Sasaki, K. Moriya, (Nitto Chemical Industry Co Ltd), **1971**.
[28] aB. Katryniok, S. Paul, V. Bellière-Baca, P. Rey, F. Dumeignil, *Green Chemistry* **2010**, *12*, 2079; bB. Katryniok, S. Paul, M. Capron, F. Dumeignil, *ChemSusChem* **2009**, *2*, 719-730.

2. State of the Art

2.1 Direct ammoxidation of glycerol

The direct ammoxidation of glycerol to acrylonitrile has been rarely studied so far. Very few publications and only one patent are available concerning the direct one-step reaction.

The first patent on the direct ammoxidation of glycerol was filed in 2008 by Arkema,[1] claiming both direct glycerol and indirect ammoxidation pathways *via* the intermediate supposed to be acrolein. According to this patent, the direct conversion of glycerol is performed in the vapor phase with ammonia and oxygen in the presence of an acid catalyst. The glycerol is injected under its pure form or as a diluted aqueous solution (10 wt.% minimum concentration) into the reactor. The reaction is carried out at a temperature between 280°C and 550°C and a pressure between 1 and 5 bar. The ammonia/glycerol molar ratio may vary between 1 and 1.5, whereas the oxygen/glycerol molar ratio may be kept between 0.5 and 10. The catalyst used consists of, as aforementioned, an acid catalyst, which may comprise one or more mixed oxides containing elements chosen from Mo, Bi, Fe, Sb, Sn, V, W, Zr, Ti, Cr, Ni, Al, P or Ga. However, the catalyst has to be selected wisely to avoid the blocking of acidic centers by ammonia at the reaction temperature. However, it should be noted that no practical example is given for direct ammoxidation of glycerol in this patent. Therefore, there is no information on the glycerol conversion and acrylonitrile selectivity.

The best results for direct ammoxidation of glycerol were claimed by Guerrero-Perez *et al.* using a one step conversion of glycerol to acrylonitrile in the presence of oxygen and ammonia.[2] The work was focused on the use of alumina-supported catalysts prepared by a slurry method. The active phases were based on V, Sb, Nb oxides or mixed oxides. The reaction conditions were quite harsh with a reaction temperature of 400°C. The gas reaction feed composed of 25% oxygen and 8.6% ammonia was passed over 50 mg of catalyst, which resulted in an extremely short contact time of 10 milliseconds.

The results obtained for different alumina-supported catalysts are reported in Table 1. The supported Sb and Nb oxides are poorly active (10-16% conversion) and show negligible selectivity to acrylonitrile (1%). On the other hand, supported vanadium oxide is the most active (87%), but exhibits no selectivity towards acrylonitrile.

Table 1: Conversion of glycerol and selectivity to main products.[2]

Catalyst	Conversion, %	Selectivity, %				
		Acrylonitrile	Acrolein	*1,2*-propanediol	Acetonitrile	Propanal
Sb/Al	10	1	29	28	19	14
Nb/Al	16	1	27	29	2	35
V/Al	87	-	7	27	1	54
VSb/Al	72	56	29	6	1	4
VSbNb/Al	83	58	26	7	1	2

Where Sb states for Sb_2O_3, Nb for Nb_2O_5,and V for V_2O_5 dispersed on an alumina support.

However, the addition of Sb and Nb to supported vanadium oxide catalysts increases the acrylonitrile selectivity above 55%. The authors claimed that $VSbO_4$ is the active species in the VSb/Al catalyst. The 'V species' provide good catalytic activity, whereas the Sb-based sites endow the catalyst with the capacity to form C-N triple bonds. Furthermore, the presence of Nb increases the acidity, which enhances the activation of ammonia resulting to an increased conversion (83 vs. 72%).

However, it was recently stated that the aforementioned results are definitely not reproducible. Contrary to the results claimed by Guerrero-Perez *et al.*, Guillon *et al.* observed full conversion of glycerol with only traces of the acrylonitrile (2% selectivity), and CO_2 as main product (50% yield).[3] This is still controversial and by both teams recently detailed their views on the subject.[4] [3]

Calvino-Casilda *et al.* reported in 2009 the microwave-assisted synthesis of acrylonitrile using direct ammoxidation of glycerol in a batch reactor.[5] The alumina-supported V-Sb catalysts were prepared using different antimony precursors such as Sb_2O_3 and Sb tartrate. The reaction was carried out using hydrogen peroxide as an oxidizing agent in solvent free conditions. The blank reaction under microwave condition showed *ca.* 38% conversion within one hour at 100°C and produced mainly acrolein, confirming that, under these conditions, the dehydration of glycerol to acrolein can occur without any catalyst. The presence of alumina moderately shifted the selectivity to acrylonitrile (14%) and propanal (13%). Further, the author stated that none of the single oxides of V and Sb supported on alumina were selective to acrylonitrile, but rather to oxygenates. On the other hand, the addition of antimony to alumina-supported vanadium oxide

modulated the selectivity to acrylonitrile similarly to the reaction under conventional thermal activation. However, it was also shown that the antimony precursor used during the catalysts preparation plays a significant role on activity. The authors claimed that the formation of the rutile $VSbO_4$ phase in the VSb/Al catalyst was promoted when using dissolved tartrate complex, which also yielded a positive impact on the catalytic performances, reaching more than 80% of acrylonitrile selectivity with 47% conversion of glycerol. It is noteworthy that $VSbO_4$ was already claimed being the active phase in the propane ammoxidation to acrylonitrile[6] suggesting thus a similar mechanism between propane and glycerol ammoxidations to acrylonitrile.

In continuation of this work, in 2010 Calvino-Casilda *et al.* studied the effect of niobium doping on the performance of VSb/Al catalysts in the microwave activated-direct glycerol ammoxidation. The authors reported that the niobium doping of alumina-supported VSb oxide catalyst is detrimental to the acrylonitrile selectivity and favors the formation of acrolein or *1,2*-propanediol. This was ascribed to the formation of a well-defined niobium-containing $SbNbO_4$ phase, which is inactive for acrylonitrile formation in contrast to the $VSbO_4$ phase.

It should be noted that the direct ammoxidation is based on a simultaneous dehydration and ammoxidation. While the dehydration is generally considered to be catalyzed by acid catalysts, the ammoxidation requires a classical oxidation catalyst. Hence, the acidic catalyst can be easily inhibited by the ammonia when co-fed in the single step process.[1] Furthermore, both reactions require rather different conditions: Whereas the dehydration is generally reported for temperatures around 300°C,[7] the ammoxidation is generally referred to higher temperatures (> 350°C), making thus these two reactions not easily combinable. As a conclusion, the direct route is quite challenging in terms of catalyst design and process development and the few experimental results published by the Spanish team of Guerrero-Perez and Calvino-Casilda *et al.* are in the center of a controversy.[4] [3]

2.2 Indirect ammoxidation of glycerol

The indirect ammoxidation of glycerol *via* the intermediate formation of acrolein has also been rarely studied until now. There is only one patent filed by Arkema in 2008.[1] Figure 1 shows the reaction scheme of the indirect route of glycerol ammoxidation to acrylonitrile *via* intermediate acrolein synthesis.

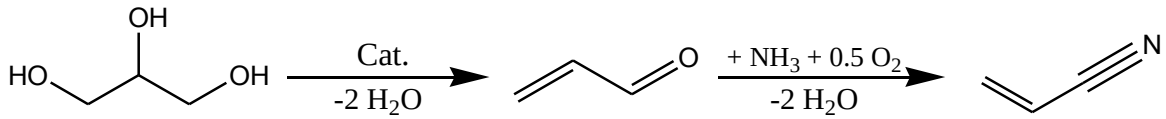

Figure 1: Indirect ammoxidation of glycerol *via* intermediate synthesis of acrolein.

In a typical example of the aforementioned patent, glycerol was dehydrated to acrolein in a tubular reactor over a 9.3% WO_3/ZrO_2 catalyst at 300°C. The reaction in the presence of oxygen 53% yield in acrolein at total conversion of glycerol. The product stream issued from the first reactor an acrolein/water mixture, which, after partial condensation and separation of heavy byproducts, was introduced into the second reactor.

The corresponding reactant mixture molar composition for the ammoxidation was 4.5/8.7/5.4/66.4/15 ($Acro/O_2/NH_3/inert/H_2O$). The latter was reacted over a commercial BiMo catalyst labeled ACF4 (initially developed for the propylene oxidation by Nippon Shokubai) at 420°C and at 1200 h^{-1} GHSV. The yield obtained for acrylonitrile was 60%. The reaction conditions and results are summarized in Table 2 below.

Table 2: Indirect ammoxidation of glycerol to acrylonitrile

Reaction	Catalyst	Feed composition (contact time or GHSV h^{-1})	Conditions	Yield (%)
Dehydration of glycerol	WO_3/ZrO_2	6.0/4.5/89.5 $GLY/O_2/H_2O$ (2.9 s contact time)	250-350°C, Pressure 1-5 bar	55% acrolein
Ammoxidation of acrolein	$BiMoO_x$	4.5 /8.7/5.4/66.4/15 $Acro/O_2/NH_3/N_2/H_2O$ (1200 h^{-1})	400-500° C, 1-5 bar	60% Acrylonitrile

Nevertheless, one must be aware that both reaction steps, namely the glycerol dehydration and the acrolein ammoxidation, were studied independently. However, no further publications or patents on the two step conversion of glycerol to acrylonitrile are available to date. Therefore, the scientific state of the art for each reaction step will be presented independently in the followings.

2.2.1 Dehydration of glycerol to acrolein

Glycerol dehydration has been an extensively studied reaction during the last decade. Figure 2 shows that the number of publications per year dealing with this subject has significantly increased.

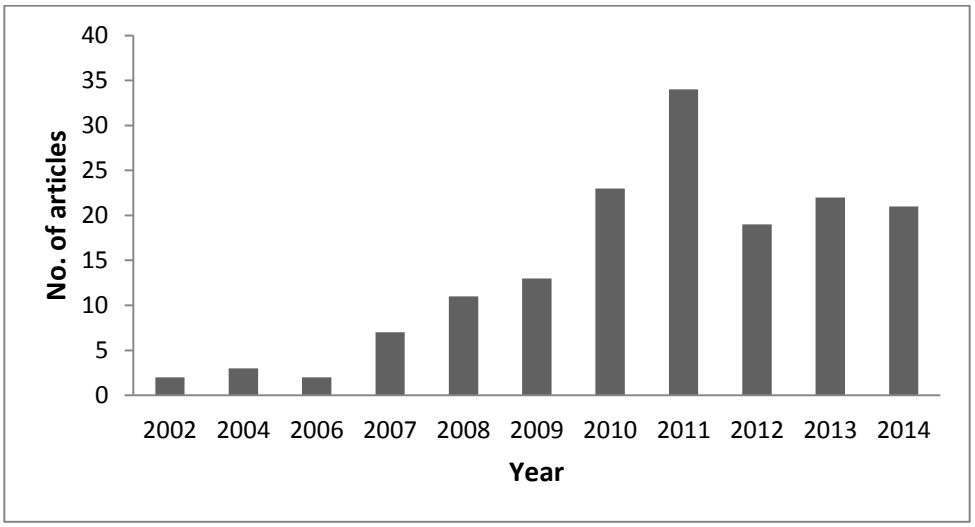

Figure 2: Evolution of the number of articles on 'glycerol dehydration to acrolein'.[8]

It is well known since the 19th century that glycerol decomposes into acrolein and water upon heating. However, an acid catalyst is needed to obtain significant selectivity to acrolein at moderate temperature.

The early work includes the patent published in 1930 by Schering, where the reaction was carried out in the gas phase over supported lithium catalyst yielding 75% in acrolein.[9] In another patent by Groll and Hearne filed by the Shell company, the dehydration was performed in the liquid phase in the presence of sulphuric acid as a catalyst at 190°C yielding nearly 50% in acrolein.[10] Hoyt and Manninen further studied the liquid phase dehydration using clay-supported phosphorus acid catalyst.[11] The reaction was carried out in petroleum oil as a reaction medium, which was chosen due to its high boiling point, resulting in an acrolein yield of 72.3%.

However, these early works remained un-followed until cheaper glycerol from the biodiesel production became available. It rapidly became clear that the key factor that influences the catalyst activity and stability is the acidity of the catalyst. In 2006, Dubois *et al.* studied the influence of the acidity quantitatively carrying out the reaction over catalysts with different Hammett Acidities (HA) ranging from -9 to -18.[12] The Nafion catalysts (HA = -12) and tungsten oxide supported on zirconium oxide (HA = -14.5) gave around 70% selectivity to acrolein with full glycerol conversion, while the zeolite catalysts with an HA < +2 did not exceed 60% of selectivity. The authors concluded that catalysts with an HA between -10 to -16 were the best candidates for the selective dehydration of glycerol to acrolein.

Inspired from these results, Chai *et al.* studied the influence of the catalyst acidity of niobium oxide catalyst.[13] As the acidity of niobium oxide is inversely related to the calcination temperature, the latter allowed tuning the acidity. From the results, one can see that the catalyst calcined at low temperature (*i.e.*, 350°C) showed the best results with 50% selectivity to acrolein with 90% conversion in glycerol. However, the catalyst suffered from high carbon deposition and thus quick deactivation, which finally suggests that the acid strength of the catalyst must be carefully tuned in a narrow range to find a compromise between performances and long-term stability.

Furthermore, the same author studied the influence of the acidity by classifying the catalysts into four groups according to their acidity.[14] Group 1 containing basic catalyst with HA > +7 did not show any selectivity to acrolein. On the other hand, the selectivity for the catalysts from Group 2 (HA between -3 and +7) was in the range of 30%. Group 3 with an HA between -8 and -3 contained catalysts such as alumina supported-phosphorus acid, alumina supported HPAs, niobium oxide (calcined at 400-500°C), HZSM zeolite and pure alumina. The results were promising for alumina-supported phosphotungstic acid and mixed tungsten oxide/zirconium oxide with around 70% selectivity to acrolein at 70% conversion. However, again, these catalysts showed poor stability and their performance decreased significantly with time on stream. Group 4 includes strong acid catalysts such as Hβ-zeolite, alumina silicate and sulfonated zirconium oxide with HA < -8. These catalysts were less selective than group 3, but were more stable showing glycerol conversion of 75% even after 10 h under stream.

In addition to this, Chai *et al.* showed that the type of the acid sites, *i.e.*, Brønsted and Lewis sites also influences the catalytic performances.[14] The obtained catalytic results showed that the

reaction does not follow the same pathway over these two different types of acids. Alhanash *et al.*[15] further studied in details the mechanism of glycerol dehydration over Brønsted and Lewis acid sites. They concluded that Lewis acid sites need higher reaction temperatures due to their higher activation energy compared to Brønsted sites. Moreover, Lewis acid sites are more selective to acetol, which is the major by-product in glycerol dehydration.

In the followings, the most widely used catalysts will be discussed in more details, notably supported HPAs, zeolites and the family of the metal oxide, phosphates and pyrophosphates.

Chai *et al.* studied zirconia[16] and silica supported HPA catalysts[17]. The authors showed that the nature of the catalyst support has a significant effect on the thermal stability and the dispersion of the active phase. Zirconia as a support shows better stability against the deactivation of the catalyst.

Katryniok *et al.*[18] also studied the aforementioned silica and zirconia supported HPA catalyst. By using a zirconia grafted (20%) SBA-15 as a support for silicotungstic acid, the stability of the catalyst was remarkably improved [13] and a 71% yield to acrolein after 5 hours on stream and 69% yield after 24 hours on stream at 275°C were obtained.

The influence of textural properties of the porous support was studied by Tsukuda *et al.* using three commercial silica with pore sizes of 3, 6 and 10 nm.[19] The best results were obtained over silicotungstic acid supported on a silica with 10 nm pore diameter showing 86% selectivity at full conversion of glycerol at 275°C. The author claimed that the small pore size of 3 nm induces coking due to the steric limitations within the porous framework.

Similar effect were observed by Atia *et al.* for silicotungstic acid supported on alumina with 5 and 12 nm pore size.[20] The selectivity to acrolein increased from 65% for the alumina with 5 nm pore size to over 85% for the alumina with 12 nm pore size at full glycerol conversion.

Dubois *et al.* introduced the idea of partial or complete substitution of the protons of HPAs by metal cations.[21] The authors claimed that the partially caesium-neutralized HPAs ($Cs_{2.5}H_{0.5}PW_{12}O_{40}$ and $Cs_{2.5}H_{3.5}SiW_{12}O_{40}$) and rubidium-neutralized HPA ($Rb_{2.5}H_{0.5}PW_{12}O_{40}$) required significantly lower reaction temperatures (260–280°C *vs.* 300–350°C) than the totally neutralized compounds. Furthermore, these partially neutralized HPAs showed higher selectivity to acrolein with the best results reported for $Cs_{2.5}H_{1.5}SiW_{12}O_{40}$ exhibiting a 93% yield in acrolein.

Zeolitic structured materials are also reported to be highly active in dehydration reactions. Li and Zhuang *et al.*[22] studied zeolites like MCM-49, MCM-22, MCM-56 and ZSM-11. The obtained acrolein yields were in the range of 70-85% for all the catalysts, with nearly no decrease in the catalytic performance during 400 h of reaction.

In 2007, Okuno and coworkers published a patent on metallosilicate catalysts with MFI structures.[23] They prepared aluminosilicates, gallosilicates and ferrosilicates. Hereby, aluminosilicates offered the most stable performance without any ion exchange with a selectivity of 65% to acrolein. Furthermore, the same group reported the possibility of tuning the acidity by modifying the Si/Al ratio whereby the best results were obtained for ratio of 28, which resulted in a yield to acrolein of 63%.[24]

Kim *et al.* published the results on their investigations on the effect of silica/alumina ratio in zeolites of the HZSM-5 type.[25] The author claimed that the catalyst with lower silica/alumina ratio exhibited a higher number of strong acid sites. However, the presence of Lewis acid sites in the catalysts with low silica/alumina ratio results in a poor selectivity to acrolein (41.6% for the silica/alumina ratio 30). They concluded that a high number of Brønsted acid sites, such as in a HZSM-5 with silica/alumina ratio of 150, was more efficient to boost the performances, since it yielded a 63.8% selectivity at 75.8% glycerol conversion.

Zhou and coworkers synthesized a micro- and mesoporous ZSM-5 composites.[26] The best results achieved with these catalysts was a 73.6% selectivity in acrolein at 98.3% glycerol conversion. Furthermore, Pathak *et al.*[27] showed that the selectivity of acrolein increases with the pore size of ZSM-5, whereas the selectivities to by-products like acetaldehyde, formaldehyde and acetol decrease in the same time.

A final group of catalysts consisting of metal oxides, phosphates and pyrophosphates was also widely studied for the dehydration of glycerol. Chai *et al.*[28] studied binary mixtures of zinc oxide, tin oxide, zirconia, titania and silica. However, low acrolein yield of only 36% over these catalysts was due to their low acidity and also to their small pore diameter.

Phosphate-modified titania, alumina and silica/alumina (SAPO) were studied by Suprun *et al.*[29] The authors reported that the acidic and textural parameters have a strong influence on the performance, whereby the most acidic silica-alumina phosphate catalyst showed a selectivity of 72% to acrolein.

The glycerol dehydration over rare earth pyro phosphates was reported by Liu *et al.* in 2009.[30] The authors were able to achieve yields of 70% towards the desired product acrolein over several rare earth pyrophosphates, like, for example, over $Nd_4(P_2O_7)_3$ or $Sm_4(P_2O_7)_3$. The experiments were carried out at 320°C for 8 hours.

One of the best performance reported so far for the glycerol dehydration to acrolein in the gas phase was obtained by Deleplanque *et al.*[31] They studied the dehydration over iron phosphates, which were prepared by different synthesis methods. The reaction was carried out at 280°C and the highest yield in acrolein of 92% was observed for a $FePO_4$ solid prepared by an hydrothermal synthesis method. However, in long term runs, the experiment suffered from significant deactivation due to the increasing carbon deposition with time on stream. Nevertheless, this issue could be tackled using co-feeding of oxygen, which not only decreased the deactivation, but also had a positive effect by suppressing the by-product formation like acetol.

In 2006, Dubois *et al.* proposed the use of tungsten oxide on zirconia as a catalyst for glycerol dehydration.[12a] Over the 9 wt.% tungsten oxide catalyst, they achieved total conversion of glycerol with 74% of acrolein yield at 300°C. Redlingshofer *et al.* further reported in a 2008 patent this binary metal oxide system further doped with promoters.[32] The highest acrolein selectivity (79%) was achieved over tungstic acid at 260°C. Nevertheless, the catalyst deactivated with time on stream with an acrolein yield decreasing at a rate of 5% every 10 h. The authors claimed about the possibility of a catalyst regeneration by oxygen treatment at 350°C for 5 h. Furthermore, doping of the catalyst by Pd reduced the deactivation.

Hoelderich *et al.* investigated the glycerol dehydration over tungstated zirconia catalysts.[33] The best performance was observed with 88.7% glycerol conversion and 72.1% acrolein selectivity after 8 h on stream at 280°C. The authors showed that the co-feeding of oxygen reduces the by-product formation like acetol.

Furthermore, Ulgen *et al.*[34] reported that the use of a titania support had an advantage over zirconia, since the latter contains basic sites that caused increased selectivity to by-product acetol. A selectivity of 74% to acrolein was reported at almost full conversion of glycerol (98%) at 280°C after 8 hours on stream. Again, the positive effect of oxygen co-feeding in terms of reducing the by-products formation was reported together with an increase in the long-term stability of the catalytic system.

The aforementioned results for the gas phase dehydration of glycerol to acrolein are gathered and summarized in Table 3.

Table 3: Catalytic performance of different catalytic systems for glycerol dehydration.

Active phase	Support	***T*** °C	TOS (h)	Glycerol Conversion	Acrolein Selectivity	Feed information	Ref.
$FePO_4$	-	280	5	100	92.1	600[1]	[31]
30% $H_4SiW_{12}O_{40}$	SiO_2	275	5	98.3	86.2	0.587[2]	[19]
H_2WO_4	-	260	5	100	79	2.4[3]	[32]
H_2WO_4+ 1% Pd	-	260	5	100	77	2.4[3]	[32]
0.5% Pd/Cs/PW	-	275	5	79	96	2.8[2]	[15]
20% $H_4SiW_{12}O_{40}$	AS4[4]	275	n.a.	100	75	0.574[2]	[20]
13.9% WO_3	TiO_2	280	8	98	74	0.36[3]	[33b, 34]
20% STA	20%ZrO_2/SBA-15	275	5	96	74	0.18[3]	[18]
$Nd_4(P_2O_7)_3$	-	320	8	87.2	79.9	227[1]	[30]
$Sm_4(P_2O_7)_3$	-	320	8	89.7	77.8	227[1]	[30]
$Gd_4(P_2O_7)_3$	-	320	8	88.2	78.9	227[1]	[30]
Er4(P2O7)3	-	320	8	86.7	79.7	227[1]	[30]
15.43% WO_3	ZrO_2	280	8	88.7	72.1	0.37[3]	[33a]
HZSM-5	-	320	10	100	60	155[1]	[35]
$Cs_{2.5}H_{1.5}SiW_{12}O_{40}$	-	280	n.a.	100	93	2445[1]	[21b]

[1]: GHSV [h^{-1}]; [2]: WHSV [h^{-1}]; [3]: contact time [s]; [4]: AS4 stands for 'aluminosilicate'.

2.2.2 Ammoxidation of acrolein to acrylonitrile

The production of acrylonitrile starting from acrolein was first reported in a patent filed by Wagner *et al.* from Philips Petroleum Company in 1946. The process was carried out in a fixed bed reactor using Cr_2O_3 (30 wt.%) supported on alumina as a catalyst. Acrolein and ammonia were fed using a 1:2 molar ratio at 510°C with a contact time of 0.5 s. It is interesting to note that in that work no oxygen was added to the feed. However, no exact yield is reported for acrylonitrile, but only qualified as "good".[36]

In 1954, Bellringer *et al.* from Distillers Company Ltd. claimed a process for manufacturing *α,β* unsaturated nitriles by reaction of *α,β* unsaturated aldehydes and ammonia in the presence of oxygen in the vapor phase.[37] The catalysts used were prepared with several metals (*e.g.*, Fe,

Mo, P, Co, Ni, V or Pd). The active metal compound was supported on silica or alumina. It was described that the addition of oxygen improved the yield of nitrile and also the catalyst lifetime. Besides acrolein and ammonia, diluents were used such as nitrogen, carbon dioxide and steam. The use of diluents contributes towards a longer catalyst lifetime and also enables the reaction to be carried out outside the explosive range. The best performance was reported over the pure MoO_3 catalyst. This catalyst yielded up to 78% in acrylonitrile at temperatures from 365-405°C, ammonia/acrolein molar ratio 1.1 and contact time of 2.7 s. The silica-supported MoO_3 catalyst gave almost similar yield of 77.2% for acrylonitrile, but at lower temperature (334-354°C). Furthermore, the addition of phosphoric acid was claimed to promote the efficiency of the silica-supported MoO_3 catalyst with improved yield of 80% to acrylonitrile.

Another patent filed by Wood *et al.* from Distillers Company Ltd. in 1959 describes a process for acrylonitrile production by vapor phase ammoxidation of acrolein over oxidation catalysts containing tin and antimony oxides. A gas mixture with a molar composition of Acrolein:Air:N_2:NH_3 of 2:87:8:3 was passed through the catalytic bed using a contact time of 2 s at 421°C. An acrylonitrile yield of 74.3% was reported. However, no water was introduced in the feed.[38]

Arsenic-based catalysts were claimed in 1963 by Vanderborght *et al.* from UCB (Union Chimique Belge) for the ammoxidation of acrolein to acrylonitrile.[39] The AsFe mixed oxide catalyst were studied in a fixed bed reactor at 400°C with a contact time of 1.2 s, yielding 87.1% of acrylonitrile. Hereby, the reaction feed contains also water in a ratio of 8.3 (water:acrolein). In another example with the same catalyst under slightly different reaction conditions (380°C, 0.5 s contact time) and in the absence of water, the yield of acrylonitrile was higher than 90%. The best yield was observed over the AsFeCo mixed oxide catalyst at 350°C with 0.5 s contact time (94.5%), but in the absence of water. However, due to high toxicity, the use of arsenic is obviously not feasible in industrial processes.

Cathala *et al.* studied the acrolein ammoxidation on Bi-Mo-O catalysts at 460°C with an acrolein:ammonia molar ratio of 2.4. The yield obtained for acrylonitrile was 67.5%. According to the authors, the selectivity to acrylonitrile was higher when acrolein was used as a starting material instead of propylene over the same catalyst.[40]

Oka *et al.* have studied the conversion rates of acrolein and propylene in ammoxidation reaction over a Fe_2O_3-Bi_2O_3-P_2O_5 catalyst.[41] Hereby, the authors claim that the acrolein ammoxidation

rate is about 1000 times faster than for propylene at 400°C assuming that the reaction can be in the chemical regime at 400°C.

Recently, Liebig *et al.* reported the indirect ammoxidation of glycerol to acrylonitrile *via* the intermediate formation of acrolein using a tandem reactor coupling a dehydration step with an ammoxidation step.[42] Sb-V-O and Fe-Sb-O catalysts were applied for the ammoxidation of acrolein. The Fe-Sb-O catalyst was found more selective due to the *in situ* formation of a $FeSbO_4$ mixed oxide phase on the surface (36% yield). The reaction conditions were as follows: 400°C, gas composition: 86.8% water, 7.7% O_2, 3.3% NH_3 and 2.2% acrolein, 0.12 s contact time.

The aforementioned results obtained for the acrolein ammoxidation to acrylonitrile are summarized in Table 4.

Table 4: Catalytic performances observed for acrolein ammoxidation.

Catalyst	Temp °C	Feed composition- molar ratio Acro/O_2/NH_3/inert/H_2O	Yield %	Ref.
30% Cr_2O_3/Alumina	510°C	0.5[1]	'good'	[36]
20-70 wt.% MoO_3/SiO_2	440°C	2.8/1.9/4.6/11/79.7 1138[2]	25-60%	[37]
Sb-SnO_x	421°C	2.0/17.4/3/77.6 2[1]	70%	[38]
As_2O_5 based catalyst	380-400°C	2.0/19.0/2.6/76.3 0.3[1]	87-92%	[39]
Bi-Mo-O	460°C	-	87%	[40]
Fe_2O_3-Bi_2O_3-P_2O_5	400°C	11.4/7/20.3/10/51.2 1.8[1]	40%	[41]
ACF4 ($BiMoO_x$)	420°C	4.5/8.7/5.4/66.4/15 1200[2]	60%	[1]
Fe-Sb-O	400°C	2.2/7.7/3.3/86.8 0.12[1]	36%	[42]

[1]: contact time [s]; [2]: GHSV [h^{-1}]

2.3 Multicomponent Bi-Mo-O*x* catalysts

According to the literature, the ammoxidation reaction requires active and selective catalysts, which are complex under the form of multifunctional mixed oxides. In this context, it is worthwhile to discuss about multicomponent Bi-Mo-O*x* catalysts, which are also reported as very efficient in the oxidation and ammoxidation of olefins.[43]

The multicomponent BiMoOx catalysts containing bivalent (*i.e.*, Co^{II}) and trivalent (*i.e.*, Fe^{III}) metals, exhibit several mixed phases of metal molybdates. These catalysts show high activity compared to the pure bismuth molybdates mainly due to the high oxygen mobility and redox character.[44] [45]

The bismuth phosphomolybdate ($Bi_9PMo_{12}O_{52}$) supported on silica was the first commercialized catalyst by SOHIO for propylene ammoxidation.[46] Bismuth molybdate was reported to be the active and selective component in the catalyst. Silica was added to provide mechanical strength and attrition resistance to the catalyst. In a typical reaction, carried out in a fluidized bed reactor to evacuate the reaction heat, the acrylonitrile yield reaches 65% at complete conversion of propylene at 470°C.

Since the initial commercialization of the bismuth molybdate-based ammoxidation catalyst, several generations of improved catalysts with higher yields were developed. These improved catalysts are termed as 'multicomponent catalysts', as they consist of numerous elemental components along with bismuth and molybdenum.

The first and important development in multicomponent bismuth molybdate catalyst was reported by Knapsack-Griensheim when they incorporated iron into the $Bi_9PMo_{12}O_{52}$ catalyst of SOHIO.[47] The addition of iron resulted in an increase in productivity of acrylonitrile per gram of catalyst compared to the initial $Bi_9PMo_{12}O_{52}$ ammoxidation catalyst. At 450°C, an overall acrylonitrile yield of 68% was obtained at 91% propylene conversion. This higher activity shows that iron increases the specific activity of bismuth molybdate catalyst, which arises from an increase in turnover number.

The next major improvement in multicomponent Bi-Mo catalyst was reported by Yamguchi *et al.* from Nippon Kayaku Co. in 1969 by incorporation of bivalent transition metals such as Co and Ni to the iron bismuth molybdate catalyst.[48] They claimed that the oxidation of propylene with catalysts containing Ni, Co, Fe, P, Bi, and Mo reached higher yield in acrolein than the

previously reported simple bismuth phosphomolybdate catalysts. Typically, the catalyst was prepared by adding an aqueous solution of water-soluble salts of bismuth, iron, nickel and cobalt to the molybdenum precursor. In a typical example, the oxidation of propylene over a $Ni_{10}Co_{0.3}FeBiPMo_{12}O_{61}$ catalyst gave an acrolein yield of 71% with 95% conversion of propylene.

This discovery was soon exploited by others, particularly by SOHIO in 1973 for the selective ammoxidation of propylene for acrylonitrile production in the presence of ammonia and oxygen.[49] The key modification introduced by SOHIO was the incorporation of an alkali metal element, notably potassium. The catalyst showed a high activity for nitrile production and also an excellent redox stability and efficient ammonia utilization under the reaction conditions. For example, the catalyst with the composition $Co_{4.5}Ni_{2.5}Fe_3BiK_{0.07}P_{0.5}Mo_{12}O_{55}$ using silica (17.5 wt.%) as a binder, gave a 80% yield to acrylonitrile at 400°C at a 2.9 s contact time.

Rao *et al.* studied the Co-Ni-Fe-Bi-P-Mo catalyst supported on silica for propylene ammoxidation.[50] The catalyst having a composition of 50% $Ni_3Co_5Fe_3BiPK_{0.1}Mo_{12}O_{52.5}$ / 50% SiO_2 was examined in a continuous reactor at 480°C with a feed ratio of $C_3H_6/NH_3/air = 1/1.5/11$. The best performance of 85% propylene conversion and 75% selectivity to acrylonitrile was achieved after 10 h on stream.

Due to its improved activity in oxidation reaction, the multicomponent bismuth molybdate catalyst was also used for several other oxidation processes such as propylene oxidation[48], oxidative dehydrogenation of *n*-butene to *1,3*-butadiene[45] [51] [52], oxidation of *iso*butene to methacrolein[53] and production of *iso*prene from *iso*amylene.[54]

In spite of its excellent catalytic activity and selectivity in the industrial oxidation/ammoxidation processes, the reason why multicomponent bismuth molybdate catalysts show high performance has not been elucidated because the structure of the multicomponent catalyst was too complex.
The practical multicomponent bismuth molybdate catalyst consists of three parts: one is pure bismuth molybdate, other is trivalent metal molybdate (Fe^{3+}, Cr^{3+}), and the third one is a mixture or solid solution of divalent metal molybdates (Co^{2+}, Ni^{2+}, Mg^{2+}). Wolf *et al.* proposed a core and shell model structure of unsupported multicomponent catalyst based on a XPS study, as shown in figure 3A. Bi is present as a thin shell of bismuth molybdate on the surface of the

catalyst particle whereas the core consists of $Fe_2(MoO_4)_3$ and $Me^{II}MoO_4$ (Me^{II} = Co, Ni or Mg).[51] The activity and selectivity of the catalyst were ascribed exclusively to Bi_2MoO_6 and $Bi_2Mo_3O_{12}$, which were present on the surface.

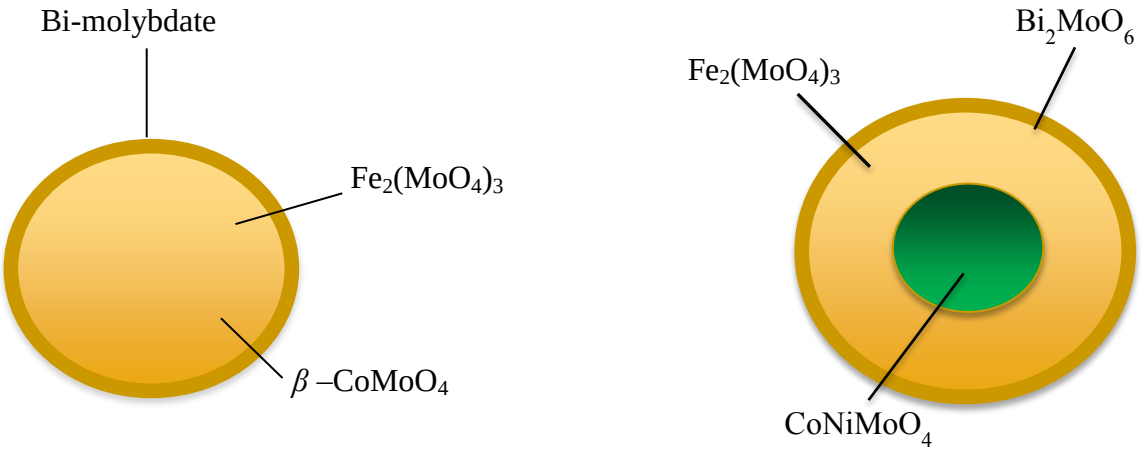

Figure 3: Structure of multicomponent catalyst by Wolf *et al.* (A) and Prof. P. Gaucher (B).

The similar structure of multicomponent catalyst was reported by Prof. P. Gaucher in his PhD thesis, where he proposed a three-layered structure, as shown in Figure 3B, where the inner core of the catalyst is composed of bivalent metal molybdate (Co or Ni), which is covered by trivalent iron molybdate, and, finally, the surface is made of bismuth molybdate active phase.

However, the studies by Rao *et al.*[50] on silica-supported multicomponent catalyst contradicts with Wolf's core and shell model structure. The XPS studies on 50% $Ni_3Co_5Fe_3BiPK_{0.1}Mo_{12}O_{52.5}$ / 50% SiO_2 catalyst showed that these catalysts were still active even when elements such as Co, Ni, Fe and Si were present on the surface along with bismuth and molybdenum.

Therefore, it is difficult to derive an exact structure of the multicomponent catalyst. Nevertheless, despite the contradiction in the structural revelations, the basic composition of multicomponent catalyst is common. They require at least four elements, divalent and trivalent metal cations as well as bismuth and molybdenum. It is necessary that both divalent and trivalent metal cations have almost the same ionic radius and form a solid solutions of $Me^{II}MoO_4$ and $Me_2^{III}(MoO_4)_3$.[55] Each element contained within these combinations has its designated function. The active site of the catalyst is the bismuth molybdate, which activates and adsorbs the olefin molecule. Bismuth molybdate exists crystallographically, as one of the three phases. They are

commonly denoted as α-$Bi_2Mo_3O_{12}$, β-$Bi_2Mo_2O_9$, and γ-Bi_2MoO_6. However, there is no agreement as to which phase is the most active and selective for the oxidation reaction. Kolchin *et al.*[56] and German *et al.*[57] stated that the activity follows the sequence $\beta > \alpha > \gamma$ for propene oxidation and ammoxidation, while Monnier and Keulks[58] claimed the order is $\gamma > \beta > \alpha$, whereas Burrington and Grasselli[59] found that order is $\beta = \alpha > \gamma$ for selective oxidation of propene. For oxidative dehydrogenation Batist *et al.*[60] found that the activity follows the sequence $\gamma > \beta > \alpha$ and Matsuura *et al.* stated that the order is $\beta > \alpha > \gamma$. Furthermore, Carson *et al.*[61] stated that there is a synergy effect between the α and γ phases leading to an enhancement in activity and selectivity for an intimate equimolar mixture.

Iron works as an efficient redox couple Fe^{3+}/Fe^{2+}, where Fe^{3+} transfers lattice oxygen to Bi-Mo-O active sites and Fe^{2+} enables dioxygen chemisorption and incorporation of lattice oxygen into the lattice. Co, Ni, Mg and Mn forms isostructural molybdates with Fe^{2+} molybdate and eventually stabilize it by providing the host structure to Fe^{2+}.

The overall functioning of the multicomponent catalyst is reported to be based on the principal of phase cooperation, where the two phases cooperate with each other for which they must be in utmost proximity one to another.

2.4 Present study on catalytic ammoxidation of acrolein to acrylonitrile

As we have seen in the previous paragraph, multicomponent bismuth molybdate catalysts became the favorite candidates in the industrial oxidation/ammoxidation processes due to their proven efficiency. However, their application in acrolein ammoxidation has not been explored yet. The literature survey shows that very few processes have been reported on the acrolein ammoxidation reaction, and that most of the time, no water is present in the feed, which cannot be the case in a tandem reaction starting from glycerol (Table 4). Therefore, there is a wide scope to study the multicomponent bismuth molybdate catalyst for the ammoxidation of acrolein in the presence of water.

Therefore, with respect to our work, we focused on the synthesis of the multicomponent bismuth molybdate catalyst with the composition $Co_{4.5}Ni_{2.5}Fe_3BiK_{0.07}P_{0.5}Mo_{12}O_{55}$ using silica (17.5 wt.%)

as a binder, which was reported to be highly active in propylene ammoxidation reaction with 80% yield to acrylonitrile.[49] Furthermore, effect of different elements in the composition was systematically investigated by preparing and testing series of catalyst prepared by coprecipitation method. The textural properties, identification of metal molybdates, the bulk and surface composition of the catalysts were studied and their correlation with the catalytic performances was established to find out the determining factors for selective ammoxidation reaction.

Finally, a design of experiment was carried out to find out the optimized reaction conditions for the ammoxidation reaction.

2.5 References

[1] J.-L. Dubois, (Arkema), US20100048850, **2008**.
[2] M. O. Guerrero-Perez, M. A. Banares, *ChemSusChem* **2008**, *1*, 511-513.
[3] C. Liebig, S. Paul, B. Katryniok, C. Guillon, J.-L. Couturier, J.-L. Dubois, F. Dumeignil, W. F. Hoelderich, *Applied Catalysis B: Environmental* **2014**, *148–149*, 604-605.
[4] M. A. Bañares, M. O. Guerrero-Pérez, *Applied Catalysis B: Environmental* **2014**, *148–149*, 601-603.
[5] V. Calvino-Casilda, M. O. Guerrero-Pérez, M. A. Bañares, *Green Chemistry* **2009**, *11*, 939-941.
[6] M. Guerrero-Pérez, M. Banares, *Chemical Communications* **2002**, 1292-1293.
[7] aB. Katryniok, S. Paul, M. Capron, F. Dumeignil, *ChemSusChem* **2009**, *2*, 719-730; bB. Katryniok, S. Paul, V. Bellière-Baca, P. Rey, F. Dumeignil, *Green Chemistry* **2010**, *12*, 2079.
[8] Scopus.com accessed on July 14, 2014 with keywords "glycerol dehydration acrolein".
[9] (SCHERING KAHLBAUM), FR695931(A), **1930**.
[10] G. Hearne, H. Groll, (Shell Dev), US2042224 A, **1936**.
[11] H. E. Hoyt, T. H. Manninen, (U S Ind Chemicals Inc), US2558520 A, **1951**.
[12] aJ.-L. Dubois, C. Duquenne, W. Holderich, J. Kervennal, (ARKEMA FRANCE), WO2006087084, **2006**; bJ.-l. Dubois, C. Duquenne, W. Hölderlich, (Arkema, France), WO2006087083, **2006**.
[13] S.-H. Chai, H.-P. Wang, Y. Liang, B.-Q. Xu, *Journal of Catalysis* **2007**, *250*, 342-349.
[14] S.-H. Chai, H.-P. Wang, Y. Liang, B.-Q. Xu, *Green Chemistry* **2007**, *9*, 1130-1136.
[15] A. Alhanash, E. F. Kozhevnikova, I. V. Kozhevnikov, *Applied Catalysis A: General* **2010**, *378*, 11-18.
[16] S.-H. Chai, H.-P. Wang, Y. Liang, B.-Q. Xu, *Applied Catalysis A: General* **2009**, *353*, 213-222.
[17] S.-H. Chai, H.-P. Wang, Y. Liang, B.-Q. Xu, *Green Chemistry* **2008**, *10*, 1087-1093.
[18] B. Katryniok, S. Paul, M. Capron, C. Lancelot, V. Bellière-Baca, P. Rey, F. Dumeignil, *Green chemistry* **2010**, *12*, 1922-1925.
[19] E. Tsukuda, S. Sato, R. Takahashi, T. Sodesawa, *Catalysis Communications* **2007**, *8*, 1349-1353.
[20] H. Atia, U. Armbruster, A. Martin, *Journal of Catalysis* **2008**, *258*, 71-82.
[21] aJ.-L. Dubois, Y. Magatani, K. Okumura, (ARKEMA FRANCE), WO2009127889, **2009**; bJ.-L. Dubios, Y. Magatani, K. Okumura, (ARKEMA FRANCE), WO2009128555, **2009**.
[22] aX.-Z. Li, (Shanghai Huayi Acrylic Acid Co), CN 101070276, **2007**; bA. Zhuang, C. Zhang, S. Wen, X. Zhao, T.Wu, (Shanghai Huayi Acrylic Acid Co), CN101225039, **2008**.
[23] M. Okuno, E. Matsunami, T. Takahashi, H. Kasuga, M. Okada, M. Kirishiki, (NIPPON SHOKUBAI CO., LTD.), WO2007132926, **2007**.
[24] M. Okuno, E. Matsunami, T. Takahashi, H. Kasuga, (Nippon Catalytic Chem. Ind.), JP2007301506, **2007**.
[25] Y. T. Kim, K.-D. Jung, E. D. Park, *Microporous and Mesoporous Materials* **2010**, *131*, 28-36.
[26] C.-J. Zhou, C.-J. Huang, W.-G. Zhang, H.-S. Zhai, H.-L. Wu, Z.-S. Chao, *Studies in Surface Science and Catalysis* **2007**, *165*, 527-530.
[27] K. Pathak, K. M. Reddy, N. N. Bakhshi, A. K. Dalai, *Applied Catalysis A: General* **2010**, *372*, 224-238.
[28] L.-Z. Tao, S.-H. Chai, Y. Zuo, W.-T. Zheng, Y. Liang, B.-Q. Xu, *Catalysis Today* **2010**, *158*, 310-316.
[29] W. Suprun, M. Lutecki, T. Haber, H. Papp, *Journal of Molecular Catalysis A: Chemical* **2009**, *309*, 71-78.
[30] Q. Liu, Z. Zhang, Y. Du, J. Li, X. Yang, *Catalysis Letters* **2009**, *127*, 419-428.
[31] J. Deleplanque, J. L. Dubois, J. F. Devaux, W. Ueda, *Catalysis Today* **2010**, *157*, 351-358.
[32] H. Redlingshofer, C. Weckbecker, K. Huthmacher, A. Dorflein, (EVONIK DEGUSSA GMBH), WO2008092533, **2008**.
[33] aA. Ulgen, W. Hoelderich, *Catalysis Letters* **2009**, *131*, 122-128; bW. Hölderich, A. Ülgen, (Hölderich Wolfgang), DE102008027350A1, **2008**.
[34] A. Ulgen, W. F. Hoelderich, *Applied Catalysis A: General* **2011**, *400*, 34-38.
[35] C.-J. Jia, Y. Liu, W. Schmidt, A.-H. Lu, F. Schüth, *Journal of Catalysis* **2010**, *269*, 71-79.
[36] C. R. Wagner, (Phillips Petroleum Company), US2412437, **1946**.
[37] F. J. Bellringer, T. Bewley, H. M. Stanley, (The Distillers Co. Ltd.), GB709337, **1954**.
[38] B. Wood, (The Distillers Co. Ltd.), GB897226, **1962**.
[39] H. Vanderborght, (Union Chimique Belge), BE628287, **1963**.
[40] M. Cathala, J. Germain, *Bull. Chem. Soc.* **1971**, *6*, 2167-2174.
[41] H. Oka, K. Miyake, Y. Haranoa, T. Imoto, *J. Appl. Chem. Biotechnol.* **1975**, *25*, 663-670.
[42] C. Liebig, S. Paul, B. Katryniok, C. Guillon, J.-L. Couturier, J.-L. Dubois, F. Dumeignil, W. F. Hoelderich, *Applied Catalysis B: Environmental* **2013**, *132-133*, 170-182.

[43] R. K. Grasselli, *Catalysis Today* **1999**, *49*, 141-153.
[44] H. H. Kung, M. C. Kung, in *Advances in Catalysis, Vol. Volume 33* (Eds.: H. P. D.D. Eley, B. W. Paul), Academic Press, **1985**, pp. 159-198.
[45] Y. Moro-Oka, W. Ueda, in *Advances in Catalysis, Vol. Volume 40* (Eds.: H. P. D.D. Eley, O. H. Werner), Academic Press, **1994**, pp. 233-273.
[46] J. L. Callahan, R. K. Grasselli, E. C. Milberger, H. A. Strecker, *Product R&D* **1970**, *9*, 134-142.
[47] S. Kurt, V. Wilhelm, K. Joachim, S. Rolf, S. Gunter, (KNAPSACK AG), US3226422, **1965**.
[48] G. Yamaguchi, S. Takenaka, (NIPPON KAYAKU KK), US3454630, **1969**.
[49] (The Standard Oil Co.), GB1319190, **1973**.
[50] T. S. R. P. Rao, P. G. Menon, *Journal of Catalysis* **1978**, *51*, 64-71.
[51] M. W. J. Wolfs, P. H. A. Batist, *Journal of Catalysis* **1974**, *32*, 25-36.
[52] J. C. Jung, H. Lee, H. Kim, Y.-M. Chung, T. J. Kim, S. J. Lee, S.-H. Oh, Y. S. Kim, I. K. Song, *Catalysis Letters* **2008**, *124*, 262-267.
[53] N. Song, C. Rhodes, J. K. Bartley, S. H. Taylor, D. Chadwick, G. J. Hutchings, *Journal of Catalysis* **2005**, *236*, 282-291.
[54] R. K. Grasselli, G. Heights, H. F Hardman, Lyndhurst, (STANDARD OIL CO.), US3642930, **1972**.
[55] Y. Moro-oka, W. Ueda, K.-H. Lee, *Journal of Molecular Catalysis A: Chemical* **2003**, *199*, 139-148.
[56] I. K. Kolchin, E. L. Galperin, S. S. Babkov, L. Y. Margolis, *Kine. katal* **1965**, *6*, 878.
[57] K. German, B. Grzybowka, J. Haber, *Bull. Acud. Pol. Sci., Ser. Sci. Chim.* **1973**, *21*, 319.
[58] J. R. Monnier, G. W. Keulks, *Preps. Div. Pet. Chem.*, **1979**, *24*, 19.
[59] J. D. Burrington, R. K. Grasselli, *Journal of Catalysis* **1979**, *59*, 79-99.
[60] P. A. Batist, J. F. H. Bouwens, G. C. A. Schuit, *Journal of Catalysis* **1972**, *25*, 1-11.
[61] D. Carson, G. Coudurier, M. Forissier, J. C. Vedrine, A. Laarif, F. Theobald, *Journal of the Chemical Society, Faraday Transactions 1: Physical Chemistry in Condensed Phases* **1983**, *79*, 1921-1929.

3. Experimental

The detailed descriptions of the reactor setup used for the ammoxidation reaction, of the catalysts synthesis procedure, and of the different characterization techniques we used are given in the following sections.

3.1 Catalytic test rig – main characteristics

The continuous gaseous phase ammoxidation of acrolein was carried out in a tubular fixed bed reactor. The scheme of the setup is represented in Figure 1.

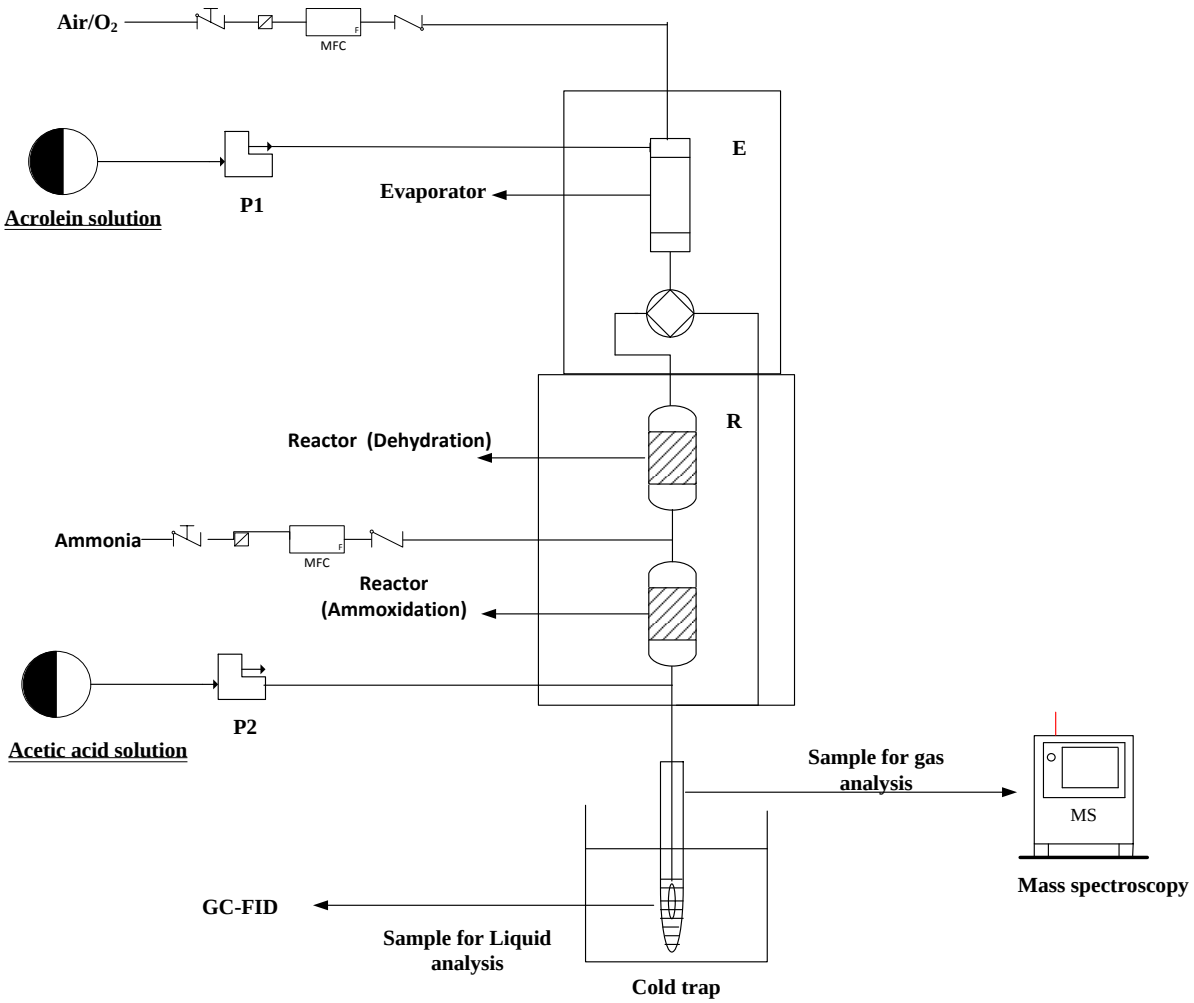

Figure 1: Schematics of the reactor setup for acrolein ammoxidation.

The vertical downflow tandem-reactor set-up was designed and built for carrying out the integrated process of indirect ammoxidation of glycerol. It comprises two reactors, placed one on top of the other. The first reactor on top is used for glycerol dehydration to acrolein and the

second one is used for subsequent ammoxidation of the as-formed acrolein to acrylonitrile. Ammonia is introduced in between the two reactors for completing the feed for the ammoxidation reaction. However, the second reactor can be independently used to specifically study the acrolein ammoxidation reaction:

A picture of the reactor setup used for the ammoxidation reaction is displayed in Figure 2.

Figure 2: Picture of the reactor setup used for acrolein ammoxidation.

The aqueous solution of acrolein is introduced by means of a GILSON HPLC pump 408 in the evaporator (E), where it is firstly vaporized and before being mixed with the second reactant

flow, namely oxygen or air, which is controlled by a mass-flow controller (BROOKS TR5400). The flow of the reactants gas phase mixture is first stabilized bypassing the reactor for 12 hours before introducing it to the pre-heated reactor. The ammonia is added just before the gas mixture enters the catalyst bed to avoid any undesired polymerization of acrolein. The gas mixture is passed through the fixed bed reactor (20 cm length, 1.5 cm ID) in the reaction box (R), which is kept at 205 °C to avoid condensation on cold spots. The reaction products are collected in a cold trap containing a 5% aqueous acetic acid solution (in order to neutralize unreacted ammonia) at -5 °C. Additionally, an aqueous acetic acid solution (10 wt.%) is injected directly after the catalytic bed to inhibit the polymerization of acrolein and acrylonitrile in the tubing.

3.2 Catalytic ammoxidation of acrolein

3.2.1 Catalytic performances evaluation

The detailed reaction parameters for a typical ammoxidation reaction are summarized in Table 1 and described below.

Table 1: Reaction parameters for the acrolein ammoxidation reaction.

Parameter	Value
Evaporator temperature	210 °C
Reaction box temperature	205 °C
Reaction temperature	350 °C – 450 °C
Acrolein (AC) solution feed	0.42 g/h
NH_3/AC molar ratio	1 – 2.5
O_2/AC molar ratio	2.7
Catalyst amount	3.5 g – 10 g
Pressure	Atmospheric

The catalyst with a particle size comprised between 50 and 200 µm is loaded in the middle of the fixed bed reactor. The catalyst is sandwiched between two layers of SiC (200 µm particle size). Quartz wool is placed above and below the catalyst in order to avoid the loss of catalyst from the reactor by flow-discharge. The products are starting to be collected after 1 hour under stream, and analyzed using a GC-FID and a mass spectrometer, as described in the following section.

3.2.2 Quantification of the products

The quantification of the condensed products was performed on a GC, whereas the gaseous products were analyzed by a mass spectrometer. The gas chromatography measurements were performed on an AlphaMOS PR2100 apparatus equipped with a flame ionization detector (FID) and an Alltech EC-1000 semi-capillary column (length: 30 m; diameter: 0.53 mm; film thickness: 1.2 µm) using helium as a carrier gas (Air Liquide, 99.999%). The temperature program was as follows: 40 °C for 7 min before heating to 240 °C with a ramp of 20 °C/min and hold at 240 °C for 1 minute. The injector and the detector temperatures were set at 200 °C and 240 °C, respectively.

The chemical equation of acrolein ammoxidation is shown hereafter:

$$CH_2 = CH - CHO + NH_3 + \tfrac{1}{2}\, O_2 \longrightarrow CH_2 = CH - CN + 2H_2O$$

The acrolein conversion (C_X) was calculated using the following formula:

$$C_X = \frac{n_{X,\,in} - n_{X,\,out}}{n_{X,\,in}} X100$$

Where X is the reactant, namely acrolein, n_{in} is the number of moles of acrolein injected in the reactor inlet, and n_{out} the number of moles of acrolein recovered at the reactor outlet.

The selectivity (Sy) to acrylonitrile was calculated as follows:

$$S_y = \frac{n_{y,\,out}}{n_{x,\,in} - n_{x,\,out}} X\,100$$

Where X is the reactant, namely acrolein, *y* is the formed product (acrylonitrile), n_{in} is the number of moles injected in the reactor inlet, and n_{out} is the number of moles recovered at the reactor outlet.

Carbon balance (CB) was calculated using the following equation:

$$CB = \frac{\sum C_{y,\,out} + C_{x,\,out}}{C_{x,\,in}} \; X\,100$$

Where, $C_{y,out}$ is the total number of carbons in the formed products, $C_{x,\,in}$ is the number of carbons in the reactant injected in the reactor inlet, and $C_{x,\,out}$ is the number of carbons in the reactant recovered at the reactor outlet.

3.3 Catalysts synthesis

3.3.1 Synthesis of γ-Bi_2MoO_6

The γ-Bi_2MoO_6 catalyst was prepared according to the procedure described in the literature.[1],[2]

15.9 g of bismuth nitrate [$Bi(NO_3)_3.5H_2O$, Sigma Aldrich] were dissolved in 20 mL of a 5 M nitric acid solution. In another flask, 2.9 g of ammonium molybdate [$(NH_4)_6Mo_7O_{24}.4H_2O$, Sigma Aldrich] were dissolved in 60 mL of water. Afterwards, the bismuth nitrate solution was added dropwise into the molybdenum solution while maintaining the pH of the mixed solution at 3 during the co-precipitation using an aqueous ammonia solution. The resulting solution was stirred vigorously at room temperature for 1 h. Then, the precipitate was filtered and the solid product was dried overnight at 110 °C. Finally, the catalyst was calcined at 475°C for 5 hours under static air.

3.3.2 Synthesis of multicomponent (MC) Bi-Mo-Ox catalysts

Two catalysts with identical theoretical composition of $Co_{4.5}Ni_{2.5}Fe_3BiK_{0.07}P_{0.5}Mo_{12}O_{55}$ were prepared using silica (17.5 wt.%) as a binder. The difference in the two syntheses is notably the sequential addition of the nitrate precursors in the case of the second synthesis. The two catalysts are labeled MC-1 and MC-2.

The typical synthesis of MC-1 was as follows: 24.075 g of $Bi(NO_3)_3.5H_2O$ (Sigma Aldrich) were dissolved in a 5 M nitric acid solution at room temperature. When all the bismuth nitrate was dissolved, 33.577 g of $Ni(NO_3)_2.6H_2O$ (Fluka), 65 g of $Co(NO_3)_2.6H_2O$ (Sigma Aldrich), and 59.3865 g of $Fe(NO_3)_2.9H_2O$ (Acros Organics) were added to the solution. In a second flask, 105.083 g of $(NH_4)_6Mo_7O_{27}.4H_2O$ (Sigma Aldrich) were dissolved in 80 mL of water with minimum heating at 50 ^oC before 0.3510 g of KNO_3 (Sigma Aldrich) and 2.859 g of H_3PO_4 acid (85%, Sigma Aldrich) were added to obtain a clear solution. Then, the initially prepared solution containing the nitrate precursors was added dropwise under continuous stirring to the second solution, whereby a precipitate formed. Finally, 68.59 g of 30% colloidal silica suspension in water (Ludox AM-30, Aldrich) were added to the precipitate as a binder before the solvent was evaporated at 80 °C. After drying at 150 °C for 24 h, the catalyst was calcined at 540 °C for 24 h under static air.

Catalyst MC-2

The MC-2 catalyst was prepared with sequential addition of nitrate solutions of Ni, Co, Fe and Bi, respectively, to the ammonium heptamolybdate initial solution, using the same theoretical composition as that of MC-1. The typical synthesis of MC-2 was as follows: 35.03 g of ammonium heptamolybdate were dissolved in water. 0.96 g of 85% phosphoric acid and 22.88 g of colloidal silica were successively dissolved under stirring. 11.19 g of $Ni(NO_3)_2.6H_2O$ and 21.688 g of $Co(NO_3)_2.6H_2O$ were dissolved in water and added to the molybdate solution and stirred for 15 min. A $Fe(NO_3)_3.9H_2O$ solution was prepared by dissolving 19.8 g in water and added to the above-described molybdate solution. Finally, a $Bi(NO_3)_3.5H_2O$ solution in 5 M nitric acid was added to the molybdate solution and stirred for 15 min.

The catalyst was heated at 80 °C to remove water and then dried at 110 °C for 16 hours. It was subsequently calcined at 230 °C during 5 h under static air to remove the nitrates and then for another 20 h at 540°C.

Synthesis of series of MC Bi-Mo catalysts with various compositions

The basic procedure used for the preparation of MC-1 catalyst was followed for preparing all the other catalysts. The elements and precursors used for the preparation of the catalysts are $Cr(NO_3)_2.9H_2O$ (Sigma Aldrich) for chromium, $Al(NO_3)_2.9H_2O$ (Fluka) for aluminium, $Mg(NO_3)_2.6H_2O$ (Fluka) for magnesium and $Cu(NO_3)_2.6H_2O$ (Sigma Aldrich) for copper. The catalysts names and their theoretical compositions are summarized in Table 2.

Table 2: Series of MC catalysts and their theoretical compositions.

Catalyst	Composition	Silica (Binder) wt.%*
MC-5	$Co_{4.5}Ni_{2.5}Fe_3BiK_{0.07}P_{0.5}Mo_{12}O_{55}$	0
MC-6	$Co_{4.5}Ni_{2.5}Fe_3BiK_{0.07}P_{0.5}Mo_{12}O_{55}$	50
MC-7	$Co_{4.5}Ni_{2.5}BiMo_8O_{33}$	17.5
MC-8	$Co_{4.5}Ni_{2.5}Fe_3BiMo_{12}O_{49}$	17.5
MC-11	$Co_7Fe_3Bi\ K_{0.07}P_{0.5}Mo_{12}O_{55}$	17.5
MC-12	$Ni_7Fe_3Bi\ K_{0.07}P_{0.5}Mo_{12}O_{55}$	17.5
MC-14	$Co_{4.5}Ni_{2.5}Fe_3Mo_{10}O_{42}$	17.5
MC-15	$Cu_7Fe_3BiK_{0.07}P_{0.5}Mo_{12}O_{55}$	17.5
MC-16	$Mg_7Fe_3BiK_{0.07}P_{0.5}Mo_{12}O_{55}$	17.5
MC-17	$Co_{4.5}Ni_{2.5}Cr_3BiK_{0.07}P_{0.5}Mo_{12}O_{55}$	17.5
MC-18	$Co_{4.5}Ni_{2.5}Al_3BiK_{0.07}P_{0.5}Mo_{12}O_{55}$	17.5

*Silica added in wt% of total composition

3.4 Methods of characterization of the catalysts

3.4.1 Nitrogen adsorption/desorption

The specific surface areas and pore volumes of the catalysts were measured by nitrogen adsorption at liquid nitrogen temperature (-196 °C) using a Micrometrics ASAP 2010 instrument. The specific surface area (S_{BET}) was evaluated by using the multi-point BET method. The total pore volume (Vp) was calculated using the isotherms at the relative pressure (P/P_0) of 0.98.

3.4.2 Thermogravimetric analysis

Thermogravimetry (TG) analyses were performed using a thermo balance (SETARAM) to study the thermal decomposition behaviour of the non-calcined catalyst. The catalysts were heated from room temperature to 550 °C with a heating rate of 5 °C/min under air flow (50 mL/min STP).

3.4.3 Energy Dispersive X-ray analysis (EDAX)

Elemental analysis was performed by energy dispersive X-ray spectroscopy on a Hitachi S3600N electron microscope equipped with a Thermo Ultradry EDS detector using an acceleration voltage of 25 kV.

3.4.4 Inductively Coupled Plasma – Optical emission spectra (ICP-OES)

The bulk composition of the catalyst was determined by Inductively Coupled Plasma spectroscopy on an Agilent Technologies 720 series instrument coupled with an optical emission spectra detector. Prior to analysis, all the catalysts were first dissolved in aqua regia and, then, a very small amount of HF acid was added in order to dissolve silica. Further dilution was done by addition of deionized water.

3.4.5 Fourier transformed infrared spectroscopy

Infrared spectra (FT-IR) were recorded on a Thermo Nicolet 480 apparatus equipped with a MCT detector. The samples (1 wt.%) were pressed to form KBr pellets for analysis, and the spectra were recorded from 400 to 4000 cm^{-1} with a spectral resolution of 4 cm^{-1} and using 256 scans.

3.4.6 X-ray diffraction

Powder X-ray diffractograms were recorded on a Bruker D8 advance diffractometer, using the CuKα radiation (λ = 1.5506 Å) as an X-ray source, in the 2θ range of 10-80° with integration steps of 0.02° (2θ) per second.

XRD measurement employing a temperature program was carried out on a D8 Advance equipment (Bruker AXS) under air flow. The sample was heated from ambient temperature to 800 °C using a heating rate of 10 °C/min.

3.4.7 X-ray photoelectron spectroscopy

X-ray photoelectron spectroscopy (XPS) for surface analyses was carried out using a Kratos Axis Ultra DLD apparatus equipped with a hemispherical analyser and a delay line detector. The spectra were recorded using an Al mono-chromated X-ray source (10 kV, 15 mA) with a pass energy of 40 eV (0.1 eV/step) for high resolution spectra, and a pass energy of 160 eV (1 eV/step) for survey spectrum in hybrid mode and slot lens mode respectively.

3.4.8 UV/Diffuse reflectance spectroscopy

UV/Vis DRS analysis of solid catalysts was performed on a Perkin Elmer-Lambda 650S spectrometer.

3.5 References

[1] J. C. Jung, H. Kim, Y. S. Kim, Y.-M. Chung, T. J. Kim, S. J. Lee, S.-H. Oh, I. K. Song, *Applied Catalysis A: General* **2007**, *317*, 244-249.

[2] J. C. Jung, H. Lee, H. Kim, Y.-M. Chung, T. J. Kim, S. J. Lee, S.-H. Oh, Y. S. Kim, I. K. Song, *Catalysis Letters* **2008**, *124*, 262-267.

4. Characterization Results

4.1 Textural properties

The specific surface areas (SSAs), pore volumes and mean pore diameters of the catalysts, obtained by nitrogen physisorption, are gathered in Table 1.

Table 1: Textural properties of the catalysts

Catalyst reference	Theoretical composition of the active phase	Silica wt.%	SSA, m^2/g	Mean pore diameter, nm	Pore volume, cm^3/g
MC-1	$Co_{4.5}Ni_{2.5}Fe_3BiK_{0.07}P_{0.5}Mo_{12}O_{55}$	17.5	15	16	0.077
MC-2	$Co_{4.5}Ni_{2.5}Fe_3BiK_{0.07}P_{0.5}Mo_{12}O_{55}$	17.5	16	14	0.059
MC-5	$Co_{4.5}Ni_{2.5}Fe_3BiK_{0.07}P_{0.5}Mo_{12}O_{55}$	0	4.5	11.6	0.012
MC-6	$Co_{4.5}Ni_{2.5}Fe_3BiK_{0.07}P_{0.5}Mo_{12}O_{55}$	50	55	13.6	0.198
MC-7	$Co_{4.5}Ni_{2.5}BiMo_8O_{33}$	17.5	19	17.1	0.091
MC-8	$Co_{4.5}Ni_{2.5}Fe_3BiMo_{12}O_{49}$	17.5	10	24.4	0.07
MC-9	γ-Bi_2MoO_6	0	4.9	12.8	0.01
MC-11	$Co_7Fe_3BiK_{0.07}P_{0.5}Mo_{12}O_{55}$	17.5	18	17.8	0.08
MC-12	$Ni_7Fe_3BiK_{0.07}P_{0.5}Mo_{12}O_{55}$	17.5	20	18.7	0.10
MC-14	$Co_{4.5}Ni_{2.5}Fe_3K_{0.07}P_{0.5}Mo_{12}O_{42}$	17.5	21	16.0	0.10
MC-15	$Cu_7Fe_3BiK_{0.07}P_{0.5}Mo_{12}O_{55}$	17.5	12	29.3	0.08
MC-16	$Mg_7Fe_3BiK_{0.07}P_{0.5}Mo_{12}O_{55}$	17.5	13	20.9	0.07
MC-17	$Co_{4.5}Ni_{2.5}Cr_3BiK_{0.07}P_{0.5}Mo_{12}O_{55}$	17.5	10	24.4	0.065
MC-18	$Co_{4.5}Ni_{2.5}Al_3BiK_{0.07}P_{0.5}Mo_{12}O_{55}$	17.5	19	14.5	0.041

All the catalysts containing 17.5 wt.% of silica exhibit a surface area in the range of 13-20 m^2/g except MC-8 and MC-17 catalysts. In contrast, MC-5 and MC-9 the catalysts – silica-free – have lower SSAs of 4.5 and 4.9 m^2/g, respectively. On the other hand, the increased amount of silica (50 wt.%) in catalyst MC-6 resulted in an obvious higher surface area of 55 m^2/g. It is noteworthy that the absence of P and K (MC-8) decreased the surface area of the catalyst from 15 to 10 m^2/g. However, the mean pore diameter was increased from 16 to 24.4 nm in that case.

4.2 Thermal stability of the multicomponent catalyst (TGA)

In order to determine the thermal stability of the multicomponent catalyst, the freshly prepared (dried but non-calcined) MC-1 with composition ($Co_{4.5}Ni_{2.5}Fe_3BiK_{0.07}P_{0.5}Mo_{12}O_{55}$/17.5 Si) was analyzed by thermogravimetry. From the results (Figure 1), one can clearly identify two regions of weight loss (blue line). The first region from 50 to 150°C is mainly due to the loss of water. The 2nd region, which shows a sharp decrease in mass from 200 to 300°C, corresponds to the decomposition of the different nitrates in the catalysts' precursors. Above 300°C, no further weight loss is observed up to 800°C, indicating that the catalyst is thermally stable. Thus, a minimum calcination temperature of 300°C is required for the catalyst. However, with respect to the reaction temperature required for the ammoxidation reaction, the calcinations were finally performed at 540°C in static air in order to avoid eventual *in-operando* sintering of the catalyst.

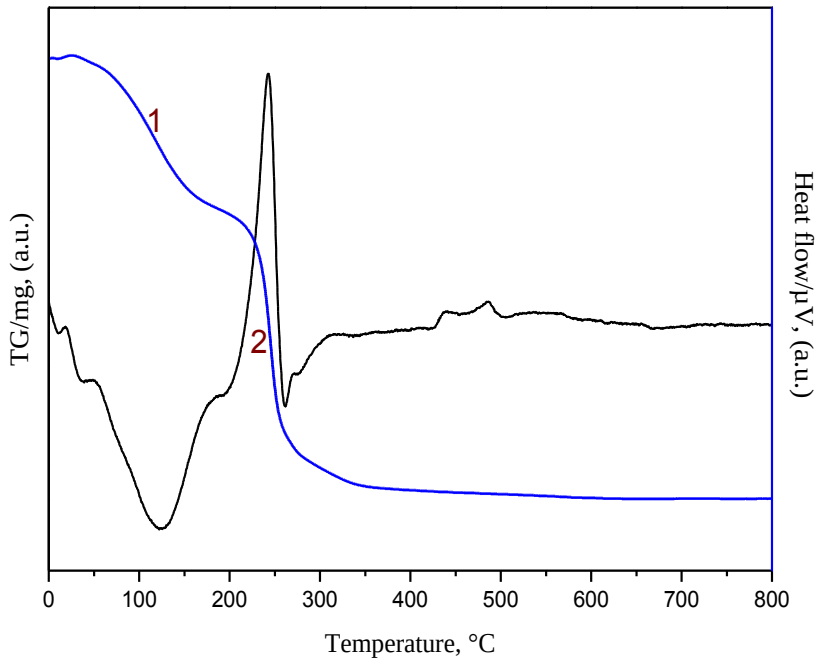

Figure 1: TGA plot of catalyst MC-1

4.3 X-ray diffraction results

The X-ray diffraction pattern of the binary mixed oxide MC-9 catalyst confirms the successful formation of a pure γ-Bi_2MoO_6 phase (Figure 2). The obtained *d* values of 1.63, 1.65, 1.92, 2.70, 2.75 and 3.15 Å (major) are in good agreement with the literature.[1]

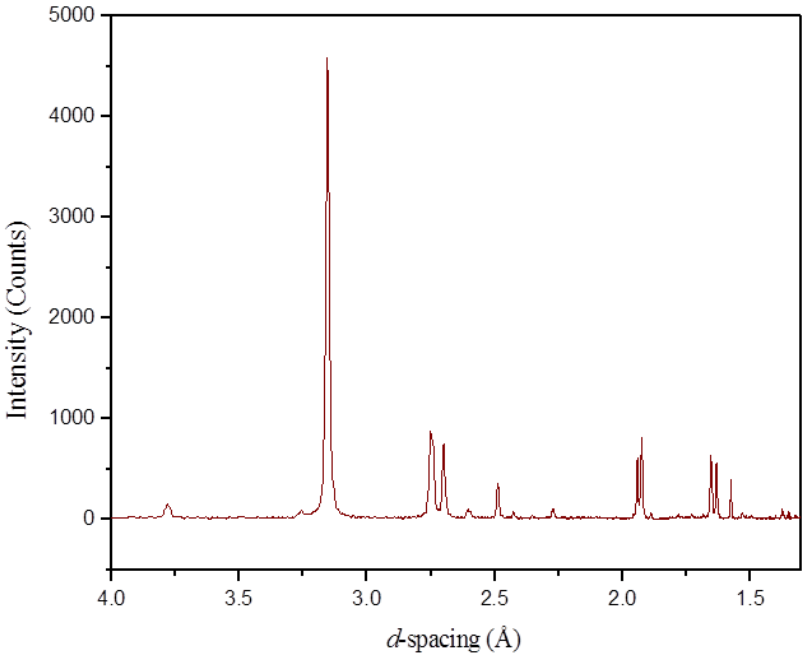

Figure 2: X-ray diffraction pattern of MC-9 catalyst (γ-Bi_2MoO_6)

Concerning the multicomponent catalysts, the XRD results are summarized in Table 2. All the multicomponent catalysts exhibit very complex diffraction patterns.

MC-1 and MC-2 catalysts containing a Co-Ni-Fe-Bi combination show the presence of the β-$CoMoO_4$ phase with *d* values of 2.24, 2.31, 2.44, 2.79 and 3.36 Å (JC-PDS 21-868). [2,3] The formation of α-$CoMoO_4$ phase can be ruled out, since the catalysts were calcined previously: In fact, the β-$CoMoO_4$ phase is stable at high temperature (above 678 K) and exists in a metastable state at room temperature, whereas α-$CoMoO_4$ is stable at low temperature (below 678 K).[5] The main difference between β-$CoMoO_4$ and α-$CoMoO_4$ is the oxygen coordination of Mo, which is tetrahedral in β-$CoMoO_4$ and essentially octahedral in α-$CoMoO_4$. [4] The results are in agreement with the literature. Iron in MC-1 and MC-2 catalysts was found to be present under the form of

$Fe_2(MoO_4)_3$, which is confirmed by the diffraction peaks at *d*-values 3.89, 3.48, 4.01, 4.36 and 2.97 Å.[6]

Table 2: Phase composition of multicomponent catalysts

Catalyst	Composition/ wt.% silica	Phases obtained	*d*-spacing[a], Å	Relative Intensity, I[b]	Ratio[c]
MC-1	$Co_{4.5}Ni_{2.5}Fe_3BiK_{0.07}P_{0.5}Mo_{12}O_{55}$/17.5	β-$CoMoO_4$ $Fe_2Mo_3O_{12}$ γ-Bi_2MoO_6 α-$Bi_2Mo_3O_{12}$	3.36 3.88 3.15 3.19	100 38.6 39.1 15.8	2.6
MC-2	$Co_{4.5}Ni_{2.5}Fe_3BiK_{0.07}P_{0.5}Mo_{12}O_{55}$/17.5	β-$CoMoO_4$ $Fe_2Mo_3O_{12}$ γ-Bi_2MoO_6 α-$Bi_2Mo_3O_{12}$	3.36 3.87 3.13 3.19	100 27.3 39.6 14.7	2.6
MC-5	$Co_{4.5}Ni_{2.5}Fe_3BiK_{0.07}P_{0.5}Mo_{12}O_{55}$	α-$CoMoO_4$ β-$CoMoO_4$ $Fe_2Mo_3O_{12}$ γ-Bi_2MoO_6 α-$Bi_2Mo_3O_{12}$	3.13 3.36 3.88 3.15 3.19	34.2 100 39.5 24.5 16.3	1.5
MC-6	$Co_{4.5}Ni_{2.5}Fe_3BiK_{0.07}P_{0.5}Mo_{12}O_{55}$/ 50	α-$CoMoO_4$ β-$CoMoO_4$ $Fe_2Mo_3O_{12}$ α-$Bi_2Mo_3O_{12}$	3.14 3.36 3.87 3.19	70.9 100 19 3.37	0
MC-7	$Co_{4.5}Ni_{2.5}BiMo_8O_{33}$/ 17.5	α-$CoMoO_4$ β-$CoMoO_4$ γ-Bi_2MoO_6 α-$Bi_2Mo_3O_{12}$ MoO_3	3.13 3.37 3.15 3.19 3.82	68.7 100 43.7 71.2 55	0.6
MC-8	$Co_{4.5}Ni_{2.5}Fe_3BiMo_{12}O_{49}$/17.5	α-$CoMoO_4$ β-$CoMoO_4$ $Fe_2Mo_3O_{12}$ γ-Bi_2MoO_6 α-$Bi_2Mo_3O_{12}$	3.12 3.36 3.88 3.15 3.19	13.9 100 34.7 44 20.3	2.1
MC-11	$Co_7Fe_3BiK_{0.07}P_{0.5}Mo_{12}O_{55}$/ 17.5	β-$CoMoO_4$ $Fe_2Mo_3O_{12}$ γ-Bi_2MoO_6 α-$Bi_2Mo_3O_{12}$	3.37 3.88 3.15 3.19	100 26.3 36.3 8.3	4.37
MC-12	$Ni_7Fe_3BiK_{0.07}P_{0.5}Mo_{12}O_{55}$/ 17.5	α-$NiMoO_4$ β-$NiMoO_4$ $Fe_2Mo_3O_{12}$ γ-Bi_2MoO_6 α-$Bi_2Mo_3O_{12}$	3.10 3.34 3.88 3.15 3.20	36.4 100 43.8 37.7 8.9	4.37
MC-14	$Co_{4.5}Ni_{2.5}Fe_3K_{0.07}P_{0.5}Mo_{12}O_{42}$/17.5	α-$CoMoO_4$ β-$CoMoO_4$ $Fe_2Mo_3O_{12}$ α-$NiMoO_4$	3.12 3.36 3.87 6.25	47.9 100 41.8 41.3	-

MC-15	$Cu_7Fe_3BiK_{0.07}P_{0.5}Mo_{12}O_{55}$/ 17.5	β-$CuMoO_4$ $Fe_2Mo_3O_{12}$ γ-Bi_2MoO_6 α-$Bi_2Mo_3O_{12}$	3.38 3.88 3.15 3.19	100 78 70.2 43.9	1.6
MC-16	$Mg_7Fe_3BiK_{0.07}P_{0.5}Mo_{12}O_{55}$/ 17.5	β-$MgMoO_4$ $Fe_2Mo_3O_{12}$ γ-Bi_2MoO_6 α-$Bi_2Mo_3O_{12}$	3.38 3.88 3.15 3.19	100 51.5 57.8 33.1	1.74
MC-17	$Co_{4.5}Ni_{2.5}Cr_3BiK_{0.07}P_{0.5}Mo_{12}O_{55}$/ 17.5	α-$CoMoO_4$ β-$CoMoO_4$ $Cr_2Mo_3O_{12}$ γ-Bi_2MoO_6 α-$Bi_2Mo_3O_{12}$	3.12 3.36 3.85 3.15 3.18	11.6 100 27.8 13.9 10.9	1.27
MC-18	$Co_{4.5}Ni_{2.5}Al_3BiK_{0.07}P_{0.5}Mo_{12}O_{55}$/ 17.5	α-$CoMoO_4$ β-$CoMoO_4$ $Al_2Mo_3O_{12}$ γ-Bi_2MoO_6 α-$Bi_2Mo_3O_{12}$	3.13 3.36 3.81 3.15 3.19	17.9 100 32.9 29.3 41.3	0.71

[a] *d*- spacing is the interplanar spacing,
[b] Relative Intensity I is the intensity of the main line of the corresponding phase, as a percentage of the line intenstity of β-$CoMoO_4$
[c] Ratio of relative intensities of γ-Bi_2MoO_6 and α-$Bi_2Mo_3O_{12}$ phases

Bismuth in the catalysts can be present in two different phases: γ-Bi_2MoO_6, and α-$Bi_2Mo_3O_{12}$. The peaks observed at *d*-spacing values of3.19 and 3.06 Å were assigned to α-$Bi_2Mo_3O_{12}$, while the presence of γ-Bi_2MoO_6 phase was indicated from the peak at 3.15 Å after comparison with pure γ-Bi_2MoO_6 phase (Figure 1). However, this value is also common to the β-$CoMoO_4$ phase, but with lower intensity. Hence, the high intensity in our catalyst strongly suggests that a γ-Bi_2MoO_6 phase is present.[1]

The absence of phosphorus and potassium in the catalyst composition shows minor effect on the observed phases. In catalyst MC-8, small amounts of cobalt were crystalized as α-$CoMoO_4$. Nevertheless, iron and bismuth appear in similar phases as in MC-1 catalyst.

The MC-7 and MC-14 catalysts prepared without iron and bismuth, respectively, show the presence of both β-$CoMoO_4$ and α-$CoMoO_4$, meaning that the formation of α-$CoMoO_4$ is possible in the absence of iron and bismuth even at high calcination temperature. Furthermore, in MC-7 catalyst in the absence of iron the α-$Bi_2Mo_3O_{12}$ phase appears to be relatively better defined than γ-Bi_2MoO_6 indicating that the presence of iron tends to promote the formation the γ-phase.[7] A similar trend is observed in the catalysts where iron is replaced by other trivalent

cations, *i.e.*, Cr^{3+} and Al^{3+} (MC-17 and MC-18). In the chromium-containing catalysts, the bismuth molybdate phases occur with almost similar but low intensities, whereas the α phase dominates over γ-Bi_2MoO_6 in Al-containing catalyst. The trivalent cations Cr and Al forms $Cr_2Mo_3O_{12}$ and $Al_2Mo_3O_{12}$ structures, which are isomorphous with $Fe_2(MoO_4)_3$.[8, 9]

The catalysts containing only cobalt in the system (MC-11) has identical phase composition with MC-1 catalyst with the presence of only the β-$CoMoO_4$ phase. On the other hand, the catalyst with only nickel (MC-12) leads to the formation of a mixture of α and β-$NiMoO_4$.[10] The γ and α bismuth molybdate phases exhibit identical intensity patterns in both the catalysts. In Cu-Fe-Bi (MC-15) and Mg-Fe-Bi (MC-16), copper and magnesium are present as β-$CuMoO_4$ and β-$MgMoO_4$[11] respectively, which have isomorphous structure with β-$CoMoO_4$. The other phases $Fe_2(MoO_4)_3$, γ-Bi_2MoO_6 and α-$Bi_2Mo_3O_{12}$ appear to be highly crystalized in both Cu- and Mg-containing catalysts.

4.4 Bulk composition of catalysts

4.4.1 ICP-OES

The bulk composition of the catalyst was determined by ICP-OES analysis and the results are shown in Table 3.

Table 3: Elemental composition of the catalysts from ICP-OES analysis

Catalyst	Co		Ni		Fe		Bi		Mo		P		K	
	Ex	Me	Ex	Me	Ex	Me	Ex	Me	Ex	Me	Ex	Me	Ex	Me
MC-1	4.5	4.8	2.5	2.4	3	3	1	1	12	11.4	0.5	0.6	0.07	0.09
MC-2	4.5	4.8	2.5	2.4	3	4.2	1	1	12	13.2	0.5		0.07	
MC-5	4.5	4.5	2.5	2.4	3	3	1	1	12	11	0.5	0.6	0.07	0.07
MC-6	4.5	4.1	2.5	2.2	3	3.2	1	1	12	10.1	0.5	0.0	0.07	0.06
MC-7	4.5	4.3	2.5	2.3	-	-	1	1	8	10.9	-	-	-	-
MC-8	4.5	4.2	2.5	2.2	3	2.5	1	1	12	10.8	-	-	-	-
MC-9	-	-	-	-	-	-	1	1	0.5	0.5	-	-	-	-
MC-11	7	6.7	-	-	3	2.8	1	1	12	10.9	0.5	0.6	0.07	0.05
MC-12	-	-	7	5.6	3	2.7	1	1	12	10.4	0.5	0.6	0.07	0.05
MC-14	4.5	4.5	2.5	2.7	3	3	-	-	10	12	0.5	0.6	0.07	0.06
MC-15	7*	6.9	-	-	3	2.8	1	1	12	11.3	0.5	0.4	0.07	0.05
MC-16	-	-	7**	6.3	3	2.7	1	1	12	10.7	0.5	0.5	0.07	0.06
MC-17	4.5	4	2.5	2.1	3[a]	1.5	1	1	12	9	0.5	0.5	0.07	0.08
MC-18	4.5	4.2	2.5	2.3	3[b]	2.8	1	1	12	10.5	0.5	0.5	0.07	0.05

Ex – Expected, Me - Measured
***Cu, **Mg, [a]Cr and [b]Al**

The molar ratio of each element was calculated with respect to bismuth. From these figures, one can see that the theoretical and the experimental compositions are close in all cases. Nevertheless, there are some exceptions such as in the iron content of the MC-2 catalyst, which is higher than the theoretical value (3 *vs.* 4.2) and also in the Ni content of the MC-12 catalyst, which is found to be lower than expected, whereas Cr and Mo values in MC-17 catalyst are far lower than the theoretical composition.

4.4.2 EDX

The elemental compositions of the calcined catalysts were also determined by EDX spectroscopy and the results are summarized in Table 4. The corresponding technique is capable to analyze up to 2 microns in depth, meaning that the results are representative for the bulk composition.

Table 4: Elemental composition of the catalyst (atomic %)

Catalyst	Co		Ni		Fe		Bi		Mo		Si		O	
	Ex	**Me**	**Ex**	**Me**	**Ex**	**Me**	**Ex**	**Me**	**Ex**	**Me**	**Ex**	**Me**	**Ex**	**Me**
MC-1	4.5	3.4	2.5	2	3	4.1	1	1	12	13.5	17.5	10.6	55	66.5
MC-2	4.5	8.6	2.5	5.6	3	1.9	1	-	12	16.8	17.5	11.2	55	56
MC-5	4.5	8.1	2.5	5	3	3.5	1	1.8	12	14.6	17.5	-	55	62.5
MC-6	4.5	3.6	2.5	1.9	3	2.4	1	1.3	12	5.7	17.5	21	55	63
MC-7	4.5	6.8	2.5	3.7	-	-	1	1.2	8	13.2	17.5	5.9	33	67.8
MC-8	4.5	7.3	2.5	4.5	3	2.3	1	1.3	12	11.4	17.5	9.1	49	64.2
MC-9	-	-	-	-	-	-	22	28.2	11	14	-	-	67	57.8
MC-11	7	9.3	-	-	3	3.5	1	1.8	12	10.8	17.5	7.3	55	67.3
MC-12	-	-	7	9.9	3	2.9	1	1.4	12	11.3	17.5	8.6	55	65.9
MC-14	4.5	6	2.5	3.3	3	4.5	-	-	10	11.5	17.5	7.2	43	67.4
MC-15	7*	7.2	-	-	3	3.9	1	1.8	12	9.7	17.5	10.4	55	66.5
MC-16	-	-	7**	7.4	3	4	1	1.8	12	11.2	17.5	7.8	55	67.8
MC-17	4.5	6.1	2.5	3.6	3[a]	3.3	1	1.6	12	12.8	17.5	9.3	55	63.3
MC-18	4.5	5.7	2.5	3.4	3[b]	4.8	1	1.2	12	11.7	17.5	07.3	55	65.9

Ex – Expected, Me – Measured
***Cu, **Mg, [a]Cr and [b]Al**

The observed elemental composition of γ-Bi_2MoO_6 (MC-9) is very close to its theoretical value of Bi/Mo = 2.

From the quantitative results, we can see that catalysts MC-1, MC-11, MC-12 and MC-14 have atomic compositions close to the theoretical ones. On the other hand, catalysts MC-2, MC-5, MC-7 and MC-8 show increased amounts of cobalt and nickel. P and K are not detected due to their very small concentrations. This also supports the hypothesis of shell and core model of multicomponent catalyst proposed by Wolf *et al.*, suggesting that divalent metal molybdates (Co, Ni, Cu or Mg) tend to concentrate in the inner core of the catalysts, while Bi is present on the surface as bismuth molybdate.[12] In order to get more information on the surface composition, the catalysts were analyzed by XPS in the followings.

4.5 Surface composition of the catalysts

The surface composition of the multicomponent catalyst MC-1 before and after calcination was determined by X-ray photoelectron spectroscopy and the results are given in Table 5.

Table 5: Surface compositions of MC-1 catalyst before and after calcination

	Bi	Co	Ni	Fe	Mo	O	Si
BC	0.12	2.27	2.42	1.26	0.18	62.39	18.3
AC	1.17	0.93	0.75	0.78	8.11	67.09	20.66

BC- Before calcination, AC- After calcination

With respect to our results, it is worth discussing the XPS results of Wolf *et al.* obtained for unsupported multicomponent catalysts with compositions $Co_8Fe_3BiMo_{12}O_X$ and $Mg_8Fe_{2.5}BiMo_{12}O_X$.[12] They reported that only Bi, Mo and O were present on the surface after single sputtering of the surface. Based on these results, they suggested a shell and core model for the multicomponent catalyst, where Bi is present as a thin shell of bismuth molybdate on the surface, while the inner core contains a mixture of $Fe_2(MoO_4)_3$ and $Me^{II}MoO_4$ where Me^{II} = Co or Mg.

Our XPS data for the calcined MC-1 ($Co_{4.5}Ni_{2.5}Fe_3BiK_{0.07}P_{0.5}Mo_{12}O_{55}$/17.5 Si) catalyst, however, show the presence of all the elements, *i.e.*, Co, Bi, Ni, Fe, Mo, Si and O on the catalyst

surface, except P and K, which are not detected probably due to their very small concentrations. Nevertheless, we observed the migration of bismuth molybdate phase to the surface during the calcination of the catalyst. From Table 5, one can see that the surface of the calcined catalyst is enriched with Bi (1.17% *vs.* 0.12%) and Mo (8.11% *vs.* 0.18%), simultaneously, whereas there is a depletion in surface concentrations of Co, Ni and Fe, indicating that these elements migrated towards the inner core of the catalysts during calcination. Hence, the above shell and core model proposed by Wolf *et al.* is only partially valid for our catalyst. Furthermore, this phenomenon is also supported with the bulk composition obtained by EDX analysis (Table 4), where we can see that Co, Ni and Fe are rich in their bulk compositions compared to surface compositions.

The X-ray photoelectron spectra of the elements detected on the surface of the calcined MC-1 catalyst are shown in Figure 3. Two distinct types of oxygen are detected: the higher binding energy (532.6 eV) oxygen, O_I is associated with silica and the lower one O_{II} (530.4 eV) with metal oxide species.[2]

Comparison of the published binding energy values for these elements is summarized in Table 6. From the observed binding energies, we can conclude that Mo is present as Mo^{6+}, Bi is present as Bi^{3+}, Co is present as Co^{2+}, Ni as Ni^{2+}, Fe as Fe^{3+} and Si is present as Si^{4+}.

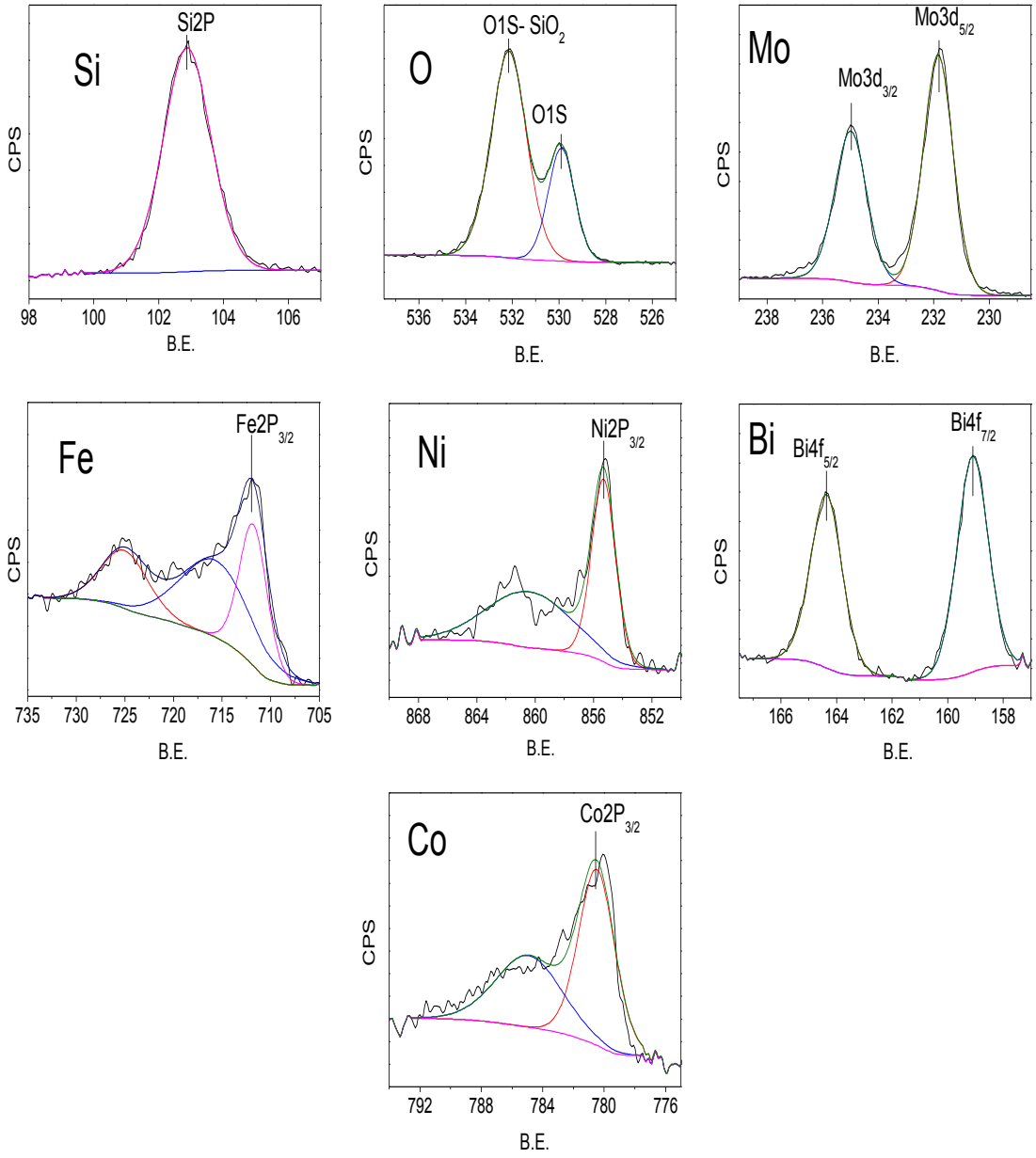

Figure 3: XPS spectra of multicomponent catalyst (MC-1)

Table 6: Oxidation states of the elements in catalyst

Elements	Binding energy, eV	Oxidation state	Reference
Bi	159.1	+3	[23]
Co	780.4	+2	[24]
Fe	712	+3	[25]
Ni	855.4	+2	[26]
Mo	231.8	+6	[23]
Si	102.9	+4	[27]

The surface compositions of the selected catalysts are given in Table 7. The bare bimetallic MC-9 catalyst showed a Bi/Mo ratio of 2.15 on the surface, which is very close to the theoretical value in γ-Bi_2MoO_6.

Table 7: Surface compositions of different multicomponent catalysts

Catalyst	Bi	Mo	O	Fe	Co	Ni	Si
MC1	1.17	8.11	67.09	0.78	0.93	0.75	20.66
MC2	0.99	6.65	67.45	1.46	1.08	0.78	21.58
MC5	1.32	13.89	79.47	1.46	2.15	1.90	-
MC7	1.13	8.09	67.53	-	0.96	0.47	21.82
MC11	0.93	5.81	67.61	0.59	1.20	-	23.87
MC15	0.37	3.37	68.94	1.25	0.97*	-	22.70
MC18	1.11	10.23	58.20	1.87**	1.36	0.77	14.76
MC9	20.97	9.77	61.66	-	-	-	-

*** Cu, ** Al**

From the bulk (EDX, Table 4) and surface composition results, it can be observed that all the catalysts are subjected to the migration phenomena for bismuth molybdate phase and the bivalent

(Co, Ni, Cu) and trivalent metals (Fe, Al). Whereas the bismuth molybdate is enriched at the surface, the bivalent and trivalent metals migrate towards the inner core.

The amount of bismuth on the surface was finally compared in terms of the ratio of the amount of bismuth on the surface to the amount of bivalent and trivalent metals. The corresponding results are shown in Figure 4. One can see that the MC-1 catalyst shows higher $Bi/(M^{II}+M^{III})$ ratio (M^{II} = Co, Ni and M^{III} = Fe) than the MC-2 catalyst (0.48 *vs.* 0.30), indicating the relative enrichment of bismuth at the surface. From the XRD results, we have seen that bismuth is present in the form of γ-Bi_2MoO_6, and α-$Bi_2Mo_3O_{12}$ in both catalysts. While the relative intensity ratios (XRD, Table 2) of these two phases is similar for the MC-1 and MC-2 catalysts (ratio 2.6), MC-1 exhibits a higher bismuth molybdate content on the surface compared to MC-2 (Figure 4). It is worth mentioning that the MC-5 catalyst prepared without silica shows an even lower bismuth amount (0.24) on the surface than the MC-1 catalyst.

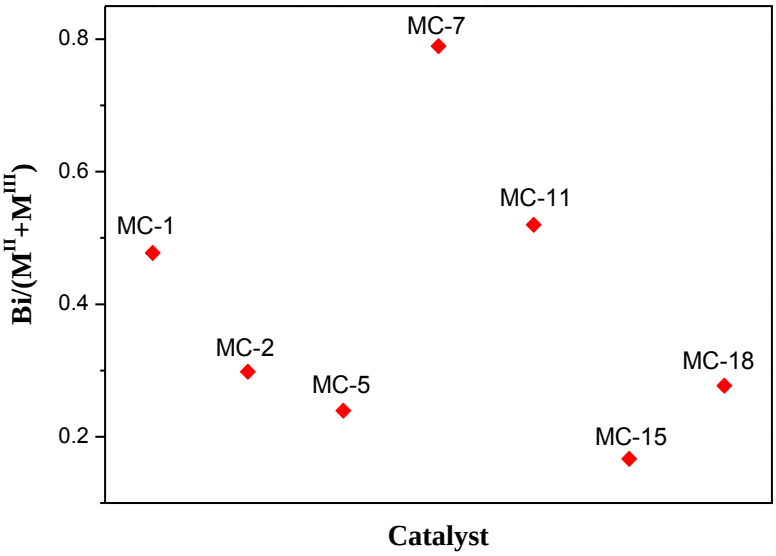

Figure 4: $Bi/(M^{II}+M^{III})$

The $Bi/(M^{II}+M^{III})$ ratio is higher for the MC-7 catalyst, probably because of the absence of iron in the ratio. Also, most of the bismuth molybdate in this catalyst is under form of α-$Bi_2Mo_3O_{12}$ rather than γ-Bi_2MoO_6 (XRD, Table 2).

Furthermore, the MC-11 catalyst containing a Co-Fe-Bi-Mo combination shows a ratio of 0.5 very close to that of MC-1 catalyst revealing the similar composition pattern on the surface. However, the MC-15 catalyst containing copper as a bivalent metal shows a very low $Bi/(M^{II}+M^{III})$ ratio (0.17) due to low bismuth content on the surface. Moreover, the MC-18 catalyst in which aluminum replaced iron also shows a lower bismuth amount on its surface than the MC-1 catalyst.

4.6 UV/Visible Diffuse Reflectance Spectroscopy (DRS)

In order to get more information about the coordination of the cations by oxygen, DRS measurements were carried out and the spectra are given in Figure 5.

a) Molybdenum – The spectra of the molybdate exhibits charge-transfer transitions between O^{2-} and Mo^{6+} in the range starting from 480 nm.[13] The γ-Bi_2MoO_6 (MC-9) catalyst showed a broad peak at 360 nm, which is characteristic of Mo in octahedral coordination. All the multicomponent catalysts show unusually broad peaks at around 245 nm and 360 nm, which were assigned to tetrahedral and octahedral molybdenum species, respectively.[4,14] The β-$CoMoO_4$ and β-$MgMoO_4$ phases observed by XRD are in agreement with the Mo in tetrahedral coordination, whereas octahedral Mo is assigned to the γ-Bi_2MoO_6, α-$CoMoO_4$ and α-$NiMoO_4$ phases.[4]

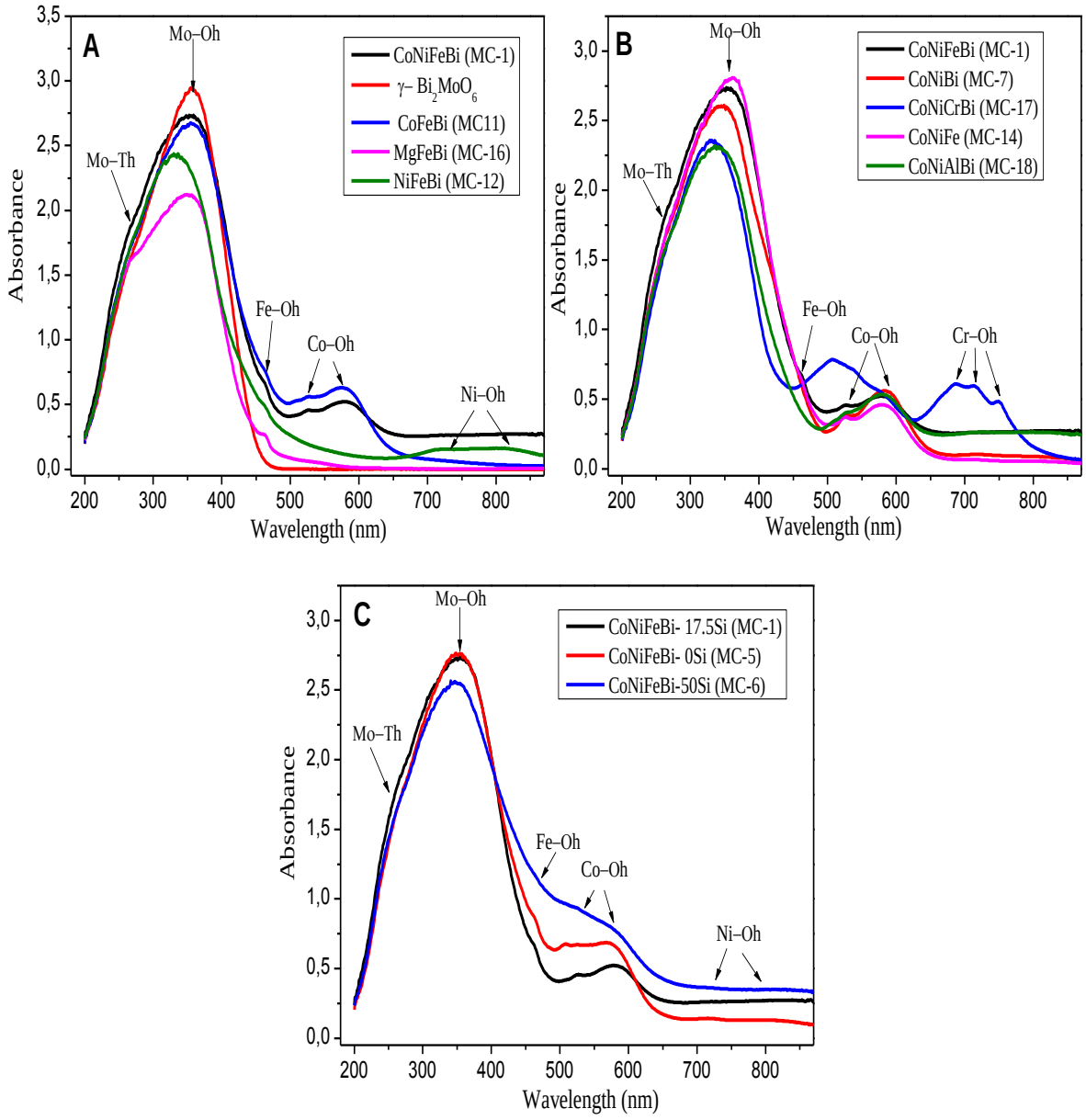

Figure 5: UV/Vis diffuse reflectance spectra of multicomponent catalysts

b) Bivalent Metals (Co, Ni, Mg) – The CoFeBi (MC-11) catalyst (Figure 5A) showed two bands at 525 and 580 nm, indicating that Co is octahedrally coordinated by oxygen, suggesting the presence of the β-$CoMoO_4$ structure also found by XRD.[15] All the catalyst containing cobalt shows absorption in this region.

The Ni-Fe-Bi catalyst (MC-12) containing only nickel, exhibits two bands at around 710 and 780 nm, suggesting that the Ni^{2+} is in octahedral coordination of oxygen.[16] However, for the Cr-containing catalyst (MC-17), these bands are covered by the stronger reflections of chromium molybdate (Figure 5B).

The magnesium-containing catalyst (MC-16) shows characteristics band of tetrahedral molybdenum. However, there is no specific band information observed as to the coordination of Mg.[11]

c) Trivalent Metals – The iron-containing catalysts always show a maximum at 460 nm, which is a characteristic band of Fe^{3+} in octahedral coordination as in the $Fe_2(MoO_4)_3$ phase.[7] This is also confirmed by the absence of the 460 nm band in the iron-free MC-7 (Figure 5B) catalyst. We may conclude therefore that the iron in our catalysts forms the $Fe_2(MoO_4)_3$ phase, which is also supported by the XRD results.

Catalyst MC-8 prepared without phosphorus and potassium did not show any difference in the spectra.

The reflection spectra of CoNiCrBi (MC-17) catalyst in Figure 5B shows three maxima at 685, 710 and 745 nm with a broad band at 487 nm, which are characteristic bands of Cr in six fold oxygen coordination just as in $Cr_2(MoO_4)_3$.[4]

The spectra of Al-containing catalyst (MC-18) did not show any peak that can be ascribed to this metal ion.

d) Silica content – The silica-free catalyst (MC-5) and the one with 17.5% content (MC-1) showed identical reflection patterns. However, the catalyst with 50% silica (MC-6) strongly absorbed in the Co-Oh region and the peak at 460 nm for $Fe_2(MoO_4)_3$ did not appear, maybe due to the lower crystallization of latter phase (Figure 5C).

4.7 Infra-red spectra analysis

The presence of octahedral and tetrahedral Mo coordination is also revealed by infra-red spectroscopy.

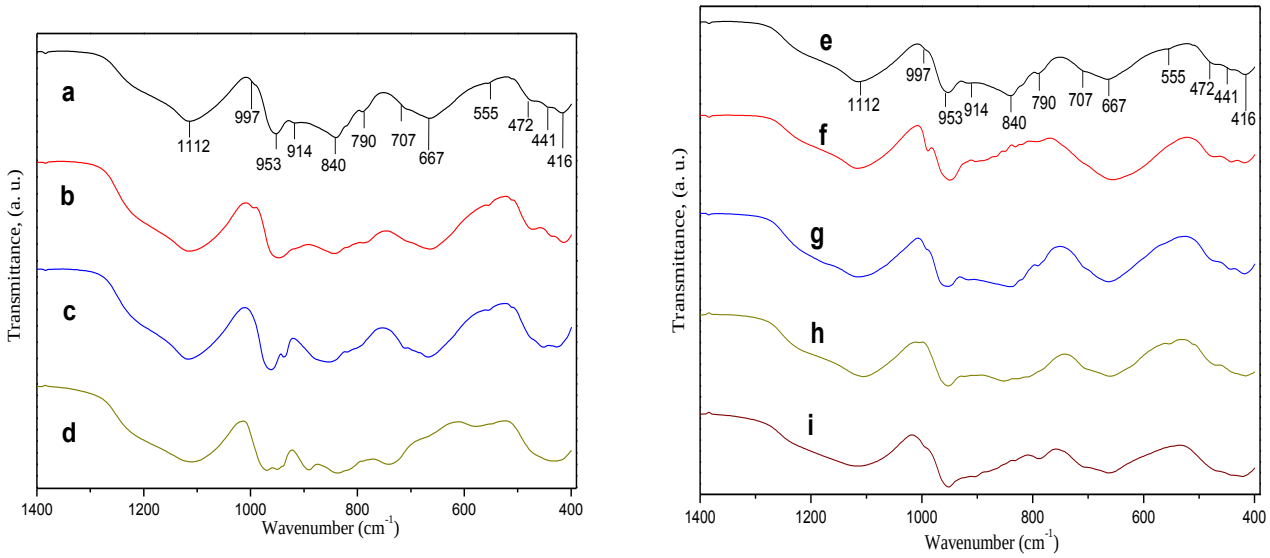

Figure 6: Infra-red spectroscopy of multicomponent catalysts

a & e - CoNiFeBi (MC-1); **b -** CoFeBi (MC-11); **c -** NiFeBi (MC-12); **d-** MgFeBi (MC-16); **f -** CoNiBi (MC-7); **g -** CoNiFe (MC-14); **h -** CoNiCrBi (MC-17); **i -** CoNiAlBi (MC-18).

The FTIR spectra of the catalyst with the combination CoNiFeBi (MC-1) is complex with broad absorption bands at 1112, 953, 840 and 667 cm^{-1} together with shoulders at 992, 914, 790, 555 and a triplet at 472, 441 and 416 cm^{-1} (Figure 6a). The broad peak at 1112 cm^{-1} and the peak at 472 cm^{-1} in all the catalysts are attributed to amorphous silica.[17,18] It can be inferred from the IR spectra that Mo is present in both the tetrahedral and octahedral coordinations. The broad bands at 840 and 790 cm^{-1} are characteristic for tetrahedral Mo, more specifically the band at 840 cm^{-1} is attributed to the Th-Mo in $Fe_2(MoO_4)_3$. The bands at 997, 953 and 667 cm^{-1} are characteristics bands of Mo in octahedral oxygen surrounding.[3,7] Moreover, some literature reported that a shoulder at 992 cm^{-1} is also due to the free Mo=O double bond in octahedral MoO_3.[19,20] Hence, it is difficult to make exact assignments to identify the individual molybdates based only on infrared analysis. Trifiro *et al.* classified the molybdates depending on the nature of IR spectra whereby molybdate presenting bands between 940-970 cm^{-1} are assigned to individual Mo-O

bonds in transition metal molybdates (953 cm^{-1} in our case), whereas bands between 900 and 930 cm^{-1} are assigned to Mo-O bonds in Bi and Al molybdates.[20] Hence, the band at 914 cm^{-1} in the MC-1 catalyst may be attributed to bismuth molybdate. Matsuura *et al.*[21] assigned the doublet at 416 and 441 cm^{-1} to α-$Bi_2Mo_3O_{12}$. However, Carrazan *et al.* stated these bands at 443 and 416 cm^{-1} to the deformation bands in $CoMoO_4$.[13] It is noteworthy that we observed this doublet even in the catalyst without bismuth (MC-14, Figure 6g) and also in the catalyst MC-11 with CoFeBi combination (Figure 6b). Therefore, these bands are more likely due to the deformation in $CoMoO_4$.

The NiFeBi catalyst (MC-12, Figure 6c) shows bands at 960, 935, 450 and 420 cm^{-1}, which are characteristic of α-$NiMoO_4$[22] along with the band at 840 cm^{-1} of $Fe_2(MoO_4)_3$. The Mg-containing catalyst (MC-16, Figure 6d) exhibits bands at 970, 945, 890, 735, 445 and 424 cm^{-1}, characteristics of β-$MgMoO_4$[22], which is also in agreement with the XRD results (Table 2).

The catalyst prepared without iron (MC-7, Figure 6f) show bands at 953 and 665 cm^{-1}, which are normally characteristics of $Fe_2(MoO_4)_3$. Nevertheless, in the case of MC-17, (Figure 6h) since no Fe is present, the appearance of a band at 840 cm^{-1} indicates that the Cr forms $Cr_2Mo_3O_{12}$ phase, which is isomorphic with $Fe_2(MoO_4)_3$. However, Al-containing catalyst (MC-18, Figure 6i) shows very weak absorption in this region although it should form the same structure as the Fe and Cr molybdate.

The FTIR spectra of catalyst prepared with different silica content are shown in Figure 7.

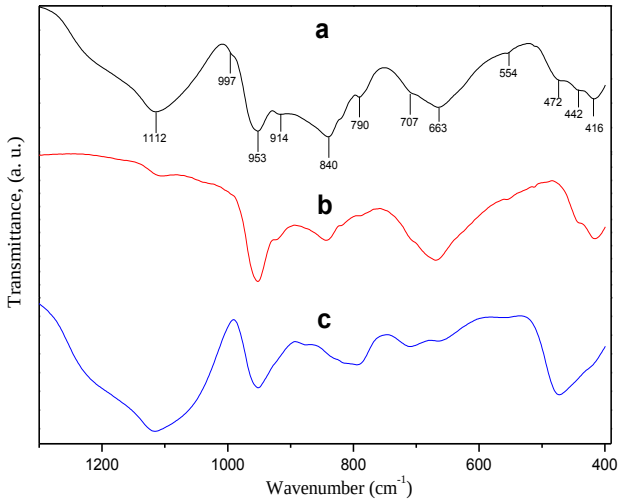

Figure 7: IR spectra of catalyst with different silica content

a – 17.5% Silica (MC-1)**; b** – 0% Silica (MC-5) and **c** – 50% Silica (MC-6)

It can be seen that the MC-1 (Figure 7a) and MC-5 (Figure 7b) catalysts show only small differences in the absorption bands arising from silica. The bands at 1112 and 472 cm^{-1} attributed to silica are absent in MC-5 catalyst, but the other characteristic bands were the same. However, the IR spectra of the MC-6 (Figure 7c) catalyst is dominated by the bands of silica, as can be seen from very broad band at 1112 and strong band at 472 cm^{-1}.[18]

4.8 Conclusion

The multicomponent Bi-Mo catalysts with general formula $Me_7^{II}Me_3^{III}BiMo_{12}O_X$ were prepared by the coprecipitation method, as multiple mixed oxide molybdate phases, which gave complex X-ray diffraction patterns. The bismuth is present as γ-Bi_2MoO_6, and α-$Bi_2Mo_3O_{12}$. The bivalent metals forms MMo_4 phases, which are found to be present as α and β isomorphs. In α-$M^{II}Mo_4$, the Mo-O coordination is octahedral whereas it is tetrahedral in its β counterpart. The trivalent metal is present as $M^{III}Mo_3O_{12}$, where Mo is in tetrahedral coordination whereas Me-O coordination is octahedral for all the metals. The presence of theses phases and their oxygen coordination was further confirmed by the UV-DRS and FTIR studies. Interestingly, the formations of α or β isomorphs of bivalent metal molybdates and of α or γ phases of bismuth molybdate were found to be affected by the presence of trivalent metals, and especially of iron.

The elemental compositions derived from ICP-OES of all the catalysts are consistent with their theoretical formula, suggesting the successful formation of the catalysts by the coprecipitation method. Moreover, EDX analysis shows that the bulk of the solids is enriched in bivalents (Co, Ni, Mg or Cu) and trivalent (Fe, Cr or Al) elements as compared to the bismuth. Surface depletion of Bi is confirmed by the XPS analysis. The surface composition of the catalysts before and after calcination reveals a migration phenomenon of M^{II} and M^{III} metals to the inner core, whereas Bi and Mo move towards the surface. However, the amount of bismuth on the surface with respect to other elements is different between the different catalysts, which could be one of the determining factors in their acrolein ammoxidation performances. This will be studied in the next chapter.

4.9 References

[1] D. Carson, G. Coudurier, M. Forissier, J. C. Vedrine, A. Laarif, F. Theobald, *Journal of the Chemical Society, Faraday Transactions 1: Physical Chemistry in Condensed Phases* **1983**, *79*, 1921-1929.
[2] T. S. R. P. Rao, P. G. Menon, *Journal of Catalysis* **1978**, *51*, 64-71.
[3] D. Klissurski, Y. Pesheva, N. Abadjieva, I. Mitov, D. Filkova, L. Petrov, *Applied Catalysis* **1991**, *77*, 55-66.
[4] M. W. J. Wolfs, P. H. A. Batist, *Journal of Catalysis* **1974**, *32*, 25-36.
[5] T. Ono, N. Ogata, Y. Miyaryo, *Journal of Catalysis* **1996**, *161*, 78-86.
[6] A. P. V. Soares, M. Farinha Portela, A. Kiennemann, L. Hilaire, J. M. M. Millet, *Applied Catalysis A: General* **2001**, *206*, 221-229.
[7] P. A. Batist, C. G. M. van de Moesdijk, I. Matsuura, G. C. A. Schuit, *Journal of Catalysis* **1971**, *20*, 40-57.
[8] W. T. A. Harrison, *Materials Research Bulletin* **1995**, *30*, 1325-1331.
[9] P. D. Battle, A. K. Cheetham, W. T. A. Harrison, N. J. Pollard, J. Faber Jr, *Journal of Solid State Chemistry* **1985**, *58*, 221-225.
[10] F. J. Maldonado-Hódar, L. M. Palma Madeira, M. Farinha Portela, *Journal of Catalysis* **1996**, *164*, 399-410.
[11] Y. J. Zhang, I. Rodríguez-Ramos, A. Guerrero-Ruiz, *Catalysis Today* **2000**, *61*, 377-382.
[12] I. Matsuura, M. W. J. Wolfs, *Journal of Catalysis* **1975**, *37*, 174-178.
[13] S. Carrazan, C. Martin, V. Rives, R. Vidal, *Spectrochimica Acta Part A: Molecular and Biomolecular Spectroscopy* **1996**, *52*, 1107-1118.
[14] N. Giordano, M. Padovan, A. Vaghi, J. C. J. Bart, A. Castellan, *Journal of Catalysis* **1975**, *38*, 1-10.
[15] G. Smith, J. Ibers, *Acta Crystallographica* **1965**, *19*, 269-275.
[16] C.-J. Zhou, C.-J. Huang, W.-G. Zhang, H.-S. Zhai, H.-L. Wu, Z.-S. Chao, *Studies in Surface Science and Catalysis* **2007**, *165*, 527-530.
[17] D. G. Filkova, L. A. Petrov, D. M. Shopov, *Journal of Catalysis* **1984**, *88*, 119-124.
[18] K. Liu, Q. Feng, Y. Yang, G. Zhang, L. Ou, Y. Lu, *Journal of Non-Crystalline Solids* **2007**, *353*, 1534-1539.
[19] P. Forzatti, P. L. Villa, N. Ferlazzo, D. Jones, *Journal of Catalysis* **1982**, *76*, 188-207.
[20] F. Trifirò, P. Centola, I. Pasquon, *Journal of Catalysis* **1968**, *10*, 86-88.
[21] I. Matsuura, R. Schut, K. Hirakawa, *Journal of Catalysis* **1980**, *63*, 152-166.
[22] I. Matsuura, S. Mizuno, H. Hashiba, *Polyhedron* **1986**, *5*, 111-117.
[23] B. Grzybowska, J. Haber, W. Marczewski, L. Ungier, *Journal of Catalysis* **1976**, *42*, 327-333.
[24] A. W. Armour, P. C. H. Mitchell, B. Folkesson, R. Larsson, *Journal of the Less Common Metals* **1974**, *36*, 361-365.
[25] Q. Xu, G. Jia, J. Zhang, Z. Feng, C. Li, *The Journal of Physical Chemistry C* **2008**, *112*, 9387-9393.
[26] A. Kaddouri, E. Tempesti, C. Mazzocchia, *Materials Research Bulletin* **2004**, *39*, 695-706.
[27] K. E. Coulter, A. G. Sault, *Journal of Catalysis* **1995**, *154*, 56-64.

5. Catalytic Performance in ammoxidation of acrolein

5.1 Preliminary experiments

5.1.1 Blank test

Preliminary blank experiments were carried out without any catalyst in order to determine if thermal activation takes place. It is reported that the ammoxidation reaction proceeds in the temperature range of 320 to 480 °C, with a NH_3/AC ratio between 1 to 5 and O_2/AC ratio in the range of 0.5 to 4. Therefore, we chose moderate conditions as stated in Table 1 for preliminary tests.[1] [2]. A marginal acrolein conversion of 2% was observed. This result is within the accuracy limitations of the analytics and the experimental setup. Furthermore, no acrylonitrile was observed. One can thus conclude that the thermal deactivation is negligible and that the reactor material exhibited no catalytic activity on the reactants.

Table 1: Reaction conditions for preliminary blank experiments

Conditions	Value
Reaction temperature	350 °C
Acrolein feed	0.42 g/h
NH_3/AC ratio	1.5
O_2/AC ratio	2.4
Pressure	Atmospheric

5.1.2 Reproducibility of catalytic tests

The reproducibility of the catalytic tests, in terms of conversion of acrolein and of selectivity towards the desired product acrylonitrile was studied by repeating a selected experiment under identical reaction conditions with the MC-1 catalyst (same catalyst batch). The obtained results are presented in Figure 1.

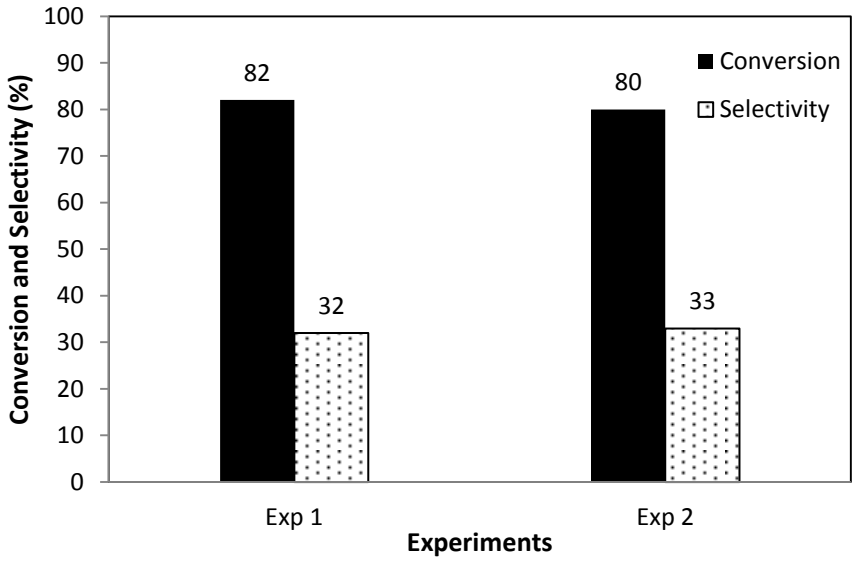

Figure 1: Investigation of reproducibility; Selectivity and conversion

Reaction conditions: Temperature - 350°C, Pressure – 1 bar, Catalyst wt. – 7 g, Contact time – 1 s, Acrolein feed - 0.42 g/h, Air feed – 79 mL/min, Ammonia feed - 4.7 mL/min, Feed molar composition - Acr:NH_3:O_2:N_2: H_2O = 1.8:2.8:4.7:37:54.

From the results, we can see that the acrolein conversion and acrylonitrile selectivity are well reproduced under the applied reaction conditions. The results of both experiments are within the accuracy of the test and analytics. Thus, the results imply that the reproducibility is acceptable.

5.1.3 Reproducibility of catalyst synthesis

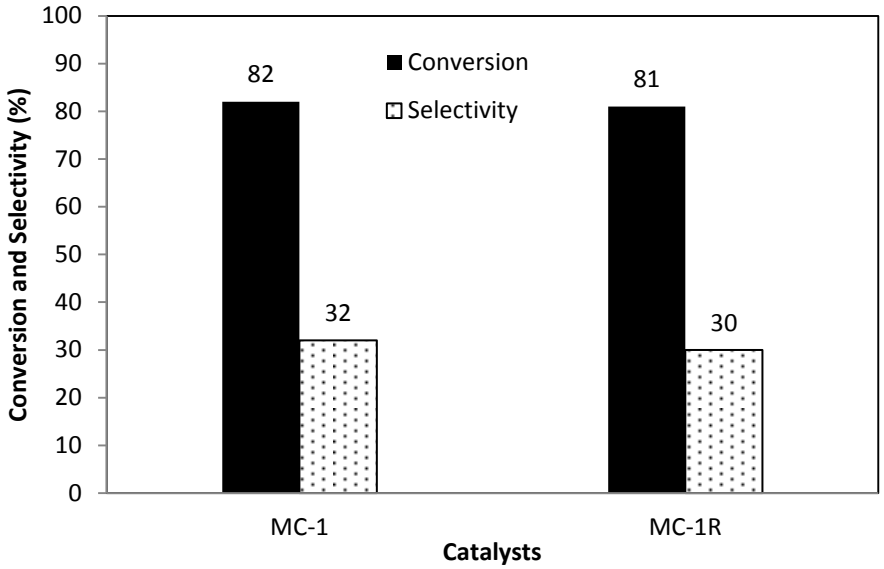

Figure 2: Reproducibility of catalysts synthesis

Reaction conditions: Temperature - 350°C, Pressure – 1 bar, Catalyst wt. – 7 g, Contact time – 1 s, Acrolein feed - 0.42 g/h, Air feed – 79 mL/min, Ammonia feed - 4.7 mL/min, Feed molar composition - Acr:NH_3:O_2:N_2:H_2O = 1.8:2.8:4.7:37:54.

The MC-1 catalyst was resynthesized and tested for acrolein ammoxidation in order to check about the reproducibility of the coprecipitation synthesis method. The results given in Figure 2 show that the catalyst synthesis is successfully reproduced. The acrolein conversion (MC-1 X = 82% *vs.* MC-1R X = 81%) and the acrylonitrile selectivity (MC-1 S = 32% *vs.* MC-1R S = 30%) vary in a negligible extent within the range of accuracy of the test and analytics.

5.1.4 Influence of catalyst synthesis method

The catalysts MC-1 and MC-2 prepared by different methods (*cf.* section 3.3.2) were tested for the ammoxidation of acrolein in order to compare their respective performances. The difference between the two catalysts is notably the sequential addition of the nitrate precursors in the MC-2 catalyst whereas they are added as a mixture in the MC-1 catalyst. The results are shown in Figure 3. The MC-1 catalyst shows a slightly higher conversion for acrolein than MC-2 (80 *vs.* 74%). Furthermore, the selectivity to acrylonitrile is significantly higher over MC-1 than over MC-2 (33 *vs.* 20%).

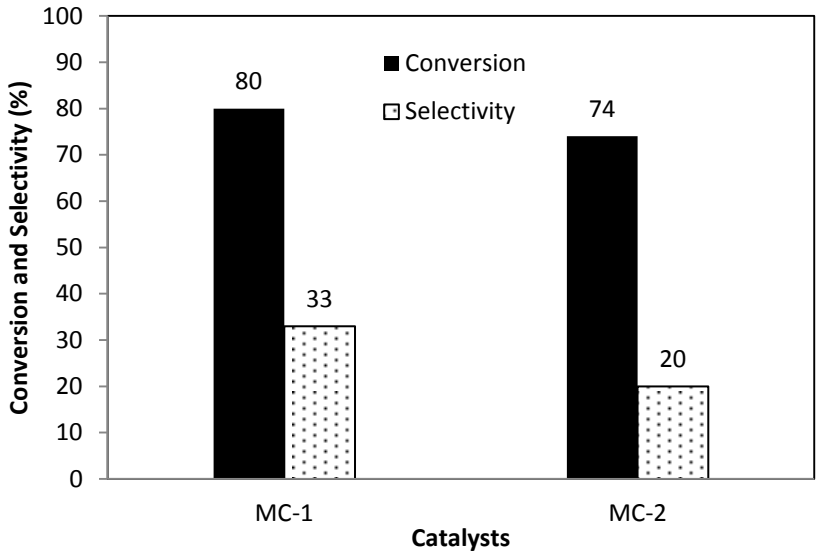

Figure 3: Influence of the catalyst synthesis method

Reaction conditions: Temperature - 350°C, Pressure – 1 bar, Catalyst wt. – 7 g, Contact time – 1 s, Acrolein feed - 0.42 g/h, Air feed – 79 mL/min, Ammonia feed - 4.7 mL/min, Feed molar composition - Acr:NH_3:O_2:N_2: H_2O = 1.8:2.8:4.7:37:54.

Regarding the results from the characterization of the catalysts, we did not find any major difference neither in the textural properties obtained by BET analysis (*cf.* section 4.1, Table 1) nor on the structural characteristics deduced from the XRD diffractograms. In fact, both catalysts exhibit identical crystalline phases, and the γ-Bi_2MoO_6 and α-$Bi_2Mo_3O_{12}$ phases were identified from XRD analysis in similar ratios (*cf.* section 4.3, Table 2). On the other hand, a major difference is found in their bulk and surface composition. The bulk composition determined by EDX showed an increased amount of oxygen content for the MC-1 catalyst compared to the MC-2 catalyst. The increased performance over MC-1 might correlate to the larger amount of oxygen stored in the bulk (*cf.* Section 4.4.2 EDX, table 4), thus promoting oxidation reactions.

Furthermore, concerning the surface composition, no difference in the oxidation states of the elements was evidenced by XPS. It is noteworthy that the elemental composition of the MC-1 catalyst exhibits enrichment of bismuth and molybdenum on the surface compared to the MC-2 catalyst. This can be seen from the surface ratio of Bi to Co+Ni+Fe (*cf.* section 4.5, Figure 4), which is higher for the MC-1 catalyst (0.48) than for MC-2 (0.3). This could be explained by the formation of larger amounts of bismuth molybdate phase, in the case of the MC-1 catalyst.

Thus, the increased surface concentration in the bismuth molybdate phase, which is reported to be the active and selective phase for ammoxidation reaction,[3],[4] together with the increased amount of oxygen in the bulk of MC-1 might be responsible for the observed superior performance in the reaction of acrolein ammoxidation over the MC-1 catalyst.[5] Therefore, the basic procedure used for the synthesis of the MC-1 catalyst was kept for the other catalysts prepared by varying their relative compositions and the nature of the contained elements, for the purpose of catalyst screening (*cf.* Section 3.3.2).

5.2 Catalyst screening

In order to study the role of each element in the multicomponent catalyst, a series of catalysts with different composition was prepared as shown in Section 3.3.2 (Table 2). The general composition of the catalysts is:

$$Me_7^{II}Me_3^{III}BiMo_{12}O_X$$

Therefore, it is convenient to separate the catalysts mainly in two groups, the first one *a)* with Me^{II} = Co, Ni, Co-Ni, Cu and Mg and the second one *b)* Me^{III} = Fe, Cr and Al. Additionally, the effect of promoters like P and K and of the amount of silica binder on the conversion and selectivity was also studied. The catalysts were screened under slightly modified reaction conditions, which were in fact obtained by a specific study (Table 2).

Table 2: Optimized reaction parameters for catalyst screening

Parameter	Value
Reaction temperature	390 °C
Contact time (catalyst amount)	0.5 s (3.5 g)
Acrolein feed	0.42 g/h
NH_3/AC ratio	1.75
O_2/AC ratio	2.7
Pressure	Atmospheric

5.2.1 Effect of bivalent metals substitution

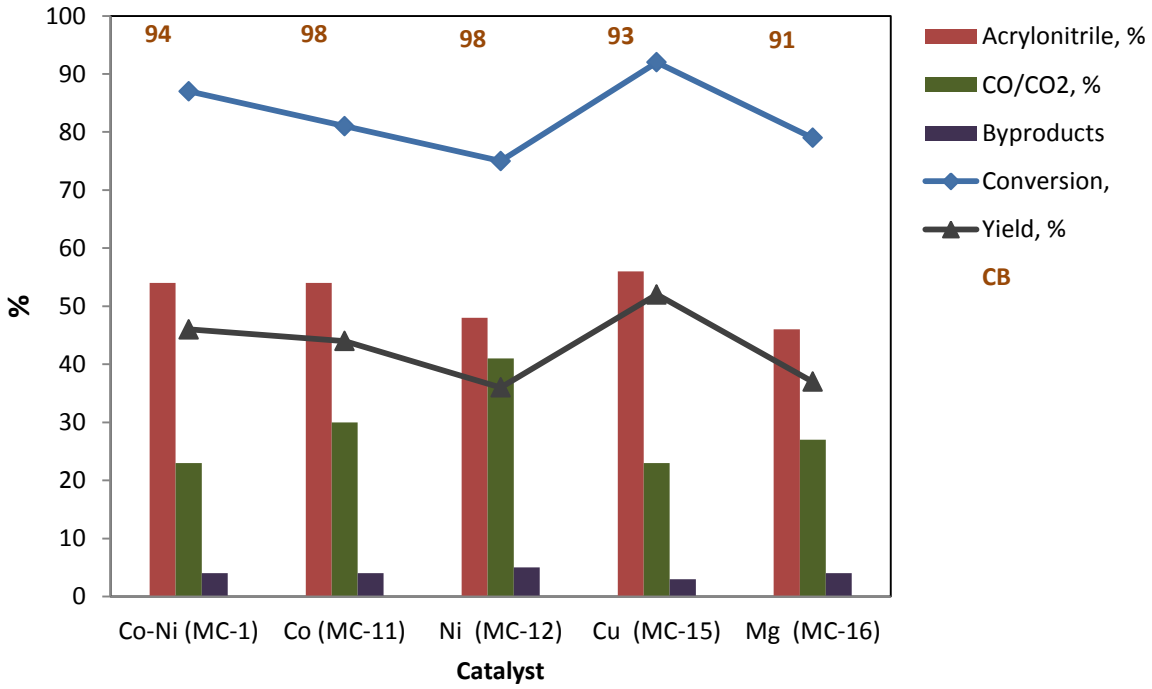

Figure 4: Effect of bivalent metal substitution on conversion and selectivity

Figure 4 shows the performances results of the catalysts containing different bivalent metals. The catalyst containing a combination of Co and Ni (MC-1) shows a higher acrolein conversion (87%) than those of the catalysts containing one of these metals alone (81% for MC-11-Co and 75% for MC-12-Ni). The selectivity to acrylonitrile is rather the same (54%) for the catalysts containing Co-Ni (MC-1) or only Co (MC-11). However, the Ni containing catalyst (MC-12) comparatively exhibits a lower selectivity to acrylonitrile (48%) and leads to a larger proportion of total oxidation products (41% selectivity to CO/CO_2). In other words, Co and Ni when used together (MC-1) give better performances in terms of acrylonitrile yield than when used alone.

A possible explanation for the superior performance of the Co-Ni-based catalyst (MC-1) and of the only Co-containing catalyst (MC-11) is linked with the existence of the metastable β-$CoMoO_4$, phase, which is reported to give a high activity (*cf.* Section 4.3, Table 2).[3, 6] On the other hand, the high selectivity of the Co (MC-11) catalyst could be attributed to the large γ-Bi_2MoO_6/α-$Bi_2Mo_3O_{12}$ ratio of 4.37 calculated from the XRD study (*cf.* Section 4.3, Table 2),

which implies, as least in the bulk, a larger quantity of γ-Bi_2MoO_6 compared to that of α-$Bi_2Mo_3O_{12}$, while the former is, as aforementioned, reported to be the more active and selective phase among both ones.[3, 7] Furthermore, the catalyst has a surface enriched in Bi with a Bi/(Co+Ni+Fe) ratio of 0.52, which is quite close to ratio in MC-1 catalyst (*cf.* section 4.5, Figure 4). The Ni catalyst (MC-12) has a similar γ-Bi_2MoO_6/α-$Bi_2Mo_3O_{12}$ ratio of 4.37, but the relatively lower activity of this Ni-containing catalyst could be due to the presence of α-$NiMoO_4$ as compared to metastable β-$CoMoO_4$ in MC-1 and MC-11.

Interestingly, among the bivalent metals, the highest performance was observed over the copper-containing catalyst (MC-15). From Figure 4, it can be seen that the maximum acrolein conversion of 92% with 56% of selectivity to acrylonitrile was obtained over MC-15. According to Simons *et al.*, CuO is more active than Co_3O_4, Fe_2O_3 or NiO in the oxidation reaction due to its ability to easily donate the oxygen.[8] In our case, the high activity could be attributed to the β-$CuMoO_4$ phase. However, the same authors stated that CuO is more selective towards total oxidation products, *i.e.*, to CO_2. Therefore, the higher selectivity to acrylonitrile over the MC-15 catalyst is surprising because the XPS study shows that MC-15 has a low bismuth content on the surface compared to the MC-1 catalyst (*cf.* Section 4.5, Figure 4). Also, the γ-Bi_2MoO_6/α-$Bi_2Mo_3O_{12}$ ratio obtained by XRD is 1.6 (*cf.* Section 4.3, Table 2) in the catalyst is comparatively lower than that observed on MC-1 and MC-11, but the relative intensities of the main peaks of these two phases are higher, *i.e.*, 70.2 and 43.9, respectively, which are further the highest values among all the catalysts, suggesting these two phases are highly crystallized. However, XRD being a bulk analysis, we have to be prudent when correlating the results with catalytic results.

The MC-16 catalyst containing Mg as a bivalent element shows an acrolein conversion of 79% with a selectivity to acrylonitrile of 46%, giving an overall yield of 37%, which is similar to that of the Ni-containing catalyst (MC-12). Among the metal molybdates, the lower activity of $MgMo_4$ compared to Co and Ni molybdates is already reported in the literature. Wolf *et al.* observed that, among the Bi-containing catalysts, the Co- and Ni-containing ones have higher activity than the Mg-containing one in the *1*-butene oxidation reaction.[3] Haber *et al.* reported that the lower activity of Mg^{2+} complexes is due to their very weak bonding with allylic species in the propylene oxidation compared to Co^{2+} and Ni^{2+} species.[9]

As a conclusion, the Me^{II}-containing catalysts show the following order of catalytic performances for acrolein ammoxidation in terms of acrylonitrile yield: Cu > Co-Ni > Co > Mg > Ni.

5.2.2 Effect of trivalent metals

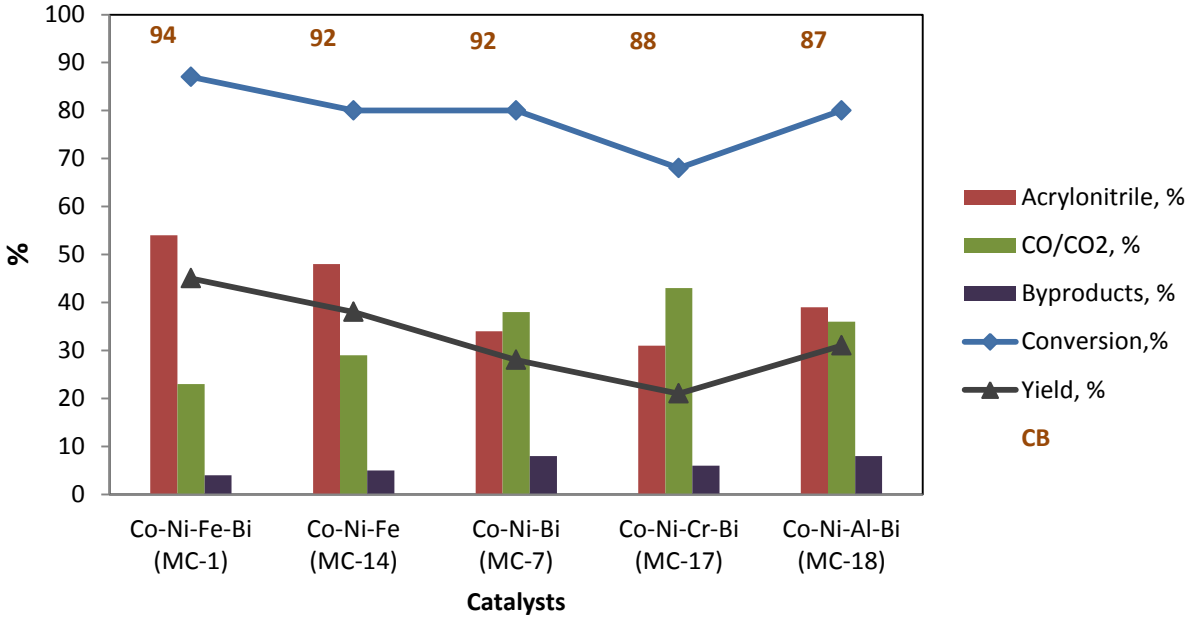

Figure 5: Effect of trivalent metal substitution on conversion and selectivity

The influence of trivalent metal substitution was studied by removing or replacing Fe from the MC-1 catalyst with Cr or Al. The results are shown in Figure 5. The iron-free Co-Ni-Bi catalyst (MC-7) shows a relatively low acrolein conversion (80%) as well as a very low acrylonitrile selectivity (28%) compared to the iron-containing MC-1 catalyst (87% conversion and 54% selectivity). Catalyst activity is significantly dropped when iron is replaced by Cr and Al, where Cr (MC-17) shows the lowest performance with 68% acrolein conversion and 31% of selectivity to acrylonitrile, whereas for the Al-containing catalyst (MC-18) these values are 80% and 39%, respectively. Therefore, the performances of trivalent metal-containing catalysts in terms of acrylonitrile yield follows the order Fe > Al > Cr.

The effect of iron can be explained from the molybdate phase formation as observed by XRD (*cf.* Section 4.3, Table 2). In the catalyst prepared without iron (MC-7), the α-$Bi_2Mo_3O_{12}$ phase (relative intensity 71.2) is formed predominantly compared to γ-Bi_2MoO_6 (relative intensity 43.7) with a γ-Bi_2MoO_6/α-$Bi_2Mo_3O_{12}$ ratio of 0.6. However, the catalyst with iron (MC-1) has γ-Bi_2MoO_6 as a dominant phase with a ratio of 2.6. This implies that iron promotes the formation of the γ-Bi_2MoO_6 phase rather than the α-$Bi_2Mo_3O_{12}$ phase. Batist *et al.* studied the promotion effect of Fe_2O_3 and Cr_2O_3 when added to the α-$Bi_2Mo_3O_{12}$ phase. They reported that the promotion caused the formation of the Koechlinite γ-Bi_2MoO_6 phase.[10] A similar observation is reported by Wolf *et al.* who claimed that the relative intensity ratio of γ-Bi_2MoO_6/α-$Bi_2Mo_3O_{12}$ increases with increasing the iron content of the catalyst, confirming the promotion effect of iron on the γ-Bi_2MoO_6 phase formation.[3]

The XRD study showed that the Co-Ni-Fe-Bi catalyst (MC-1) exhibited the exclusive formation of the metastable β-$CoMoO_4$ phase for cobalt while the iron-free Co-Ni-Bi catalyst showed the formation of the α-$CoMoO_4$ phase along with the β–type phase. This indicates that the metastable β-$CoMoO_4$ phase is stabilized in the presence of iron. Wolf *et al.* drew up the explanation that in α-$CoMoO_4$ both metal ion and Mo are in octahedral oxygen coordination and connected *via* the edges. However, in β-$CoMoO_4$ the metal ion are in octahedral coordination and Mo is in tetrahedral coordination and connection occurs *via* the corners. In the $Fe_2(MoO_4)_3$ phase, the Fe-O octahedra and Mo-O tetrahedra are connected *via* the corners just like in β-$CoMoO_4$. Furthermore, the sequence of layers of Co, Mo and of Fe, Mo along the *c*-axes is closely similar. Therefore, the predominance of β-$CoMoO_4$ instead of α-$CoMoO_4$ in the presence of iron can be explained by assuming that the β-$CoMoO_4$ structure is better suited to fit the $Fe_2(MoO_4)_3$ structure.

Trivalent cations, and especially iron, are also reported to have several roles in the multicomponent catalysts. Grasselli[1] stated that iron serves as an efficient redox couple ($Fe^{3+/2+}$), capable of efficient lattice oxygen transfer to the Bi-Mo-O active site in its Fe^{3+} oxidation state. Indeed, in its 2+ oxidation state, it efficiently chemisorbs dioxygen and dissociates it to lattice oxygen (O^{2-}) with further incorporation into the lattice. Since during the reaction it is difficult to maintain a sufficient number of Fe^{2+} surface sites in an overall oxidizing gaseous atmosphere, it is necessary to structurally stabilize the Fe^{2+} state. In this scenario,

divalent elements like Co, Ni, Mg and Mn form stable molybdates isostructural with Fe^{2+} molybdate, and thus stabilize the Fe^{2+} state. In other words, Ni, Co, Mg and Mn have the function of providing the host structure for Fe^{2+} in the multiphase catalysts.

The activity of the catalyst is strongly depending on which trivalent cation is used, and it decreased in the sequence Fe, Al, Cr. This indicates that $Fe_2(MoO_4)_3$ has a stronger promotion effect than $Cr_2Mo_3O_{12}$ and $Al_2Mo_3O_{12}$.

5.2.3 Effect of P, K and silica binder

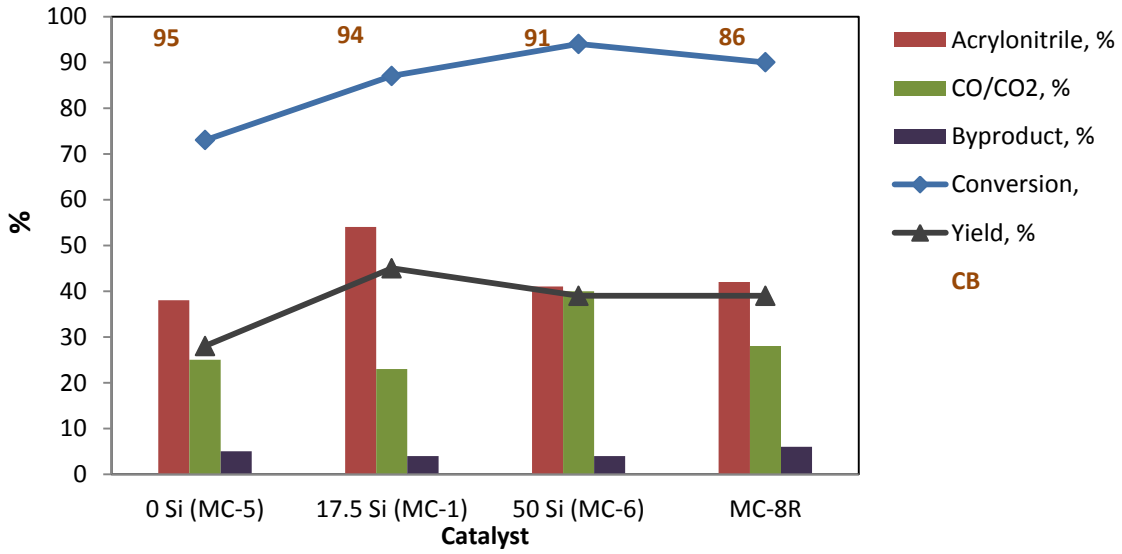

Figure 6: Effect of P, K and silica binder on conversion and selectivity

The effect of the amount of silica on the activity of the catalyst is shown in Figure 6. Silica was added to the catalyst as a binder to provide a better mechanical strength. From Figure 6, we can see that acrolein conversion gradually increases with increasing the silica amount. The lowest conversion was observed for the silica-free MC-5 catalyst (73%). It increased to 87% for MC-1 with 17.5% silica and further to 94% for MC-6 with 50% silica. The acrylonitrile selectivity

however first increased from 38% to 54% for MC-1 catalyst and then decreased to 41% with further increasing the silica content to 50%.

The increase in conversion could be attributed to the surface area of the catalyst. The surface area of the catalysts increases with increasing the silica content from 0, 17.5 and 50% in the following order: 4.5, 15 and 55 m^2/g (*cf.* Section 4.1, Table 1), respectively. Furthermore, the XRD and IR spectra study of MC-6 catalyst shows the dominant formation of α and β cobalt molybdates, which leads to its higher conversion of 94%. The XRD study shows that the MC-5 catalyst (0% Si) has a lower γ-Bi_2MoO_6/α-$Bi_2Mo_3O_{12}$ ratio than the MC-1 catalyst (17.5% Si), namely 1.5 *vs.* 2.6, indicating the high content of γ-Bi_2MoO_6 phase in MC-1 (*cf.* Section 4.3, Table 2). The surface composition determined from the XPS study also shows that the MC-1 catalyst has a higher amount of bismuth on its surface than the MC-5 catalyst (*cf.* Section 4.5, Figure 4). This accounts for the increased selectivity to acrylonitrile over the MC-1 catalyst. Furthermore, the MC-6 catalyst with high Si content (50%) shows the formation of only poorly defined α-$Bi_2Mo_3O_{12}$ phase of bismuth leading to lower acrylonitrile selectivity as compared to the MC-1 catalyst.

The effect of additives like phosphorus and potassium can be seen from catalyst MC-8R. Surprisingly, the catalyst without theses additives shows comparatively a higher conversion of 90% than the MC-1 catalyst (87%). On the other hand, the selectivity is lower compared with the MC-1 catalyst (42% *vs.* 54%).

The amounts of P and K that are added to the formulation are very low, and, therefore, there is no significant amount of separate phases formed from these elements. Also, no traces of P and K could be found on the surface in the XPS study. Therefore, it is difficult to explain the impact of P and K on the catalytic performance. The only difference is found in the surface area, which decreased from 15 m^2/g (MC-1) to 10 m^2/g in the presence of P and K (MC-8R).

The role of these additives is not clear. Nevertheless, Grasselli[11] claimed that the alkali metal action is to annihilate the most acidic cracking sites of the catalyst, and to serve as a spacer and contact enhancer of the two functionally distinct but epitaxially matched catalytic phases. Grasselli stated that there are two phases, the first one being Fe^{3+}-containing the catalytically active bismuth molybdate phase and the second one being a Fe^{2+}-containing (Ni, Co, Mg)

molybdate phase. For multiphase oxidation catalysts with superior performances, these two phases must be in the utmost proximity one to another, and are ineffective if they are remotely separated. For this reason, catalysts should have at least one face essentially epitaxially matched (principle of phase cooperation).

5.3 Design of Experiment

The optimization of the reaction conditions (reaction temperature, contact time and NH_3/Acrolein ratio) was performed using a computer assisted experimental design (Design-Expert version 5.0.8) based on a Box-Behnken response surface methodology. The multicomponent bismuth molybdenum catalyst MC-1 was selected, as it exhibited medium values in terms of selectivity towards acrylonitrile (54%) and conversion of acrolein (87%) resulting in an overall yield for acrylonitrile of 45%.

The variation limits of the used parameters are depicted in Table 3, and the performed experiments are detailed in Table 4.

Table 3: Variation limits for parameter optimization with MC-1

Parameter	Value
Reaction Temperature	350 °C – 450 °C
Amount of catalyst	3.5 g – 10 g
(Contact time)	(0.5 s – 1.5 s)
NH_3/AC molar ratio	1 – 2.5

Table 4: Performed experiments

Std	Run	Block	Factor A: Temperature °C	Factor B: Ammonia/AC	Factor C: Contact time s	Response conversion %	Response selectivity ACN %	Response yield ACN %
5	1	Block 1	350	1.75	1.5	86	31	26
16	2	Block 1	400	1.75	1	98	57	56
15	3	Block 1	400	1.75	1	99	57	56
9	4	Block 1	400	1	1.5	94	53	50
6	5	Block 1	450	1.75	1.5	96	54	52
2	6	Block 1	450	1	1	93	44	41
14	7	Block 1	400	1.75	1	100	57	56
13	8	Block 1	400	1.75	1	98	59	56
4	9	Block 1	450	2.5	1	97	59	58
1	10	Block 1	350	1	1	82	30	24
11	11	Block 1	400	1	0.5	77	69	53
12	12	Block 1	400	2.5	0.5	86	63	54
8	13	Block 1	450	1.75	0.5	92	63	58
7	14	Block 1	350	1.75	0.5	64	30	19
3	15	Block 1	350	2.5	1	89	28	25
30	16	Block 1	450	1	0.5	80	63	51
10	17	Block 1	400	2.5	1.5	97	49	48
18	18	Block 1	450	2.5	1.5	96	66	64
17	19	Block 1	400	1.75	0.5	89	74	66
19	20	Block 1	350	1.75	1	85	32	27
20	21	Block 1	400	1	1	89	49	44
21	22	Block 1	400	2.5	1	99	62	61
24	23	Block 1	350	2.5	0.5	66	24	16
23	24	Block 1	350	1	0.5	67	35	23
22	25	Block 1	450	1.75	1	97	59	57
25	26	Block 1	450	2.5	0.5	89	60	53
26	27	Block 1	350	1	1.5	85	30	25
27	28	Block 1	350	2.5	1.5	94	27	25
28	29	Block 1	400	1.75	1.5	95	58	55

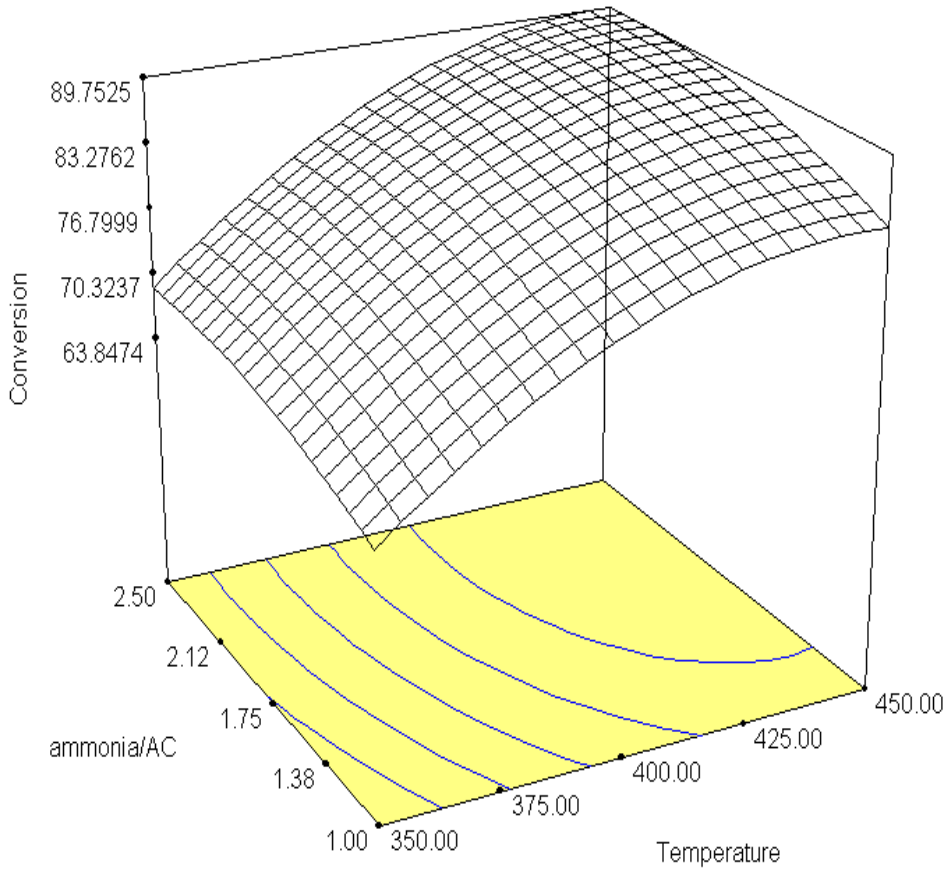

Figure 7: Acrolein (AC) conversion as a function of the reaction temperature and the NH_3/AC molar ratio

Reaction conditions: Pressure – 1 bar, contact time - 0.5 s, Acrolein/O_2 ratio - 0.38

The effect of the variation of reaction temperature and NH_3/AC ratio on acrolein conversion is depicted in Figure 7. One can see that the acrolein conversion increases with both the reaction temperature and the NH_3/AC ratio. Thereby, it exhibits the overall minimum value of 64% at 350 °C and at a NH_3/AC ratio of 1. The conversion increases gradually with the temperature, whereby a maximum conversion of 90% is predicted for a temperature of 425 °C with a NH_3/AC ratio of around 2. This suggests that a high temperature is required for the activation of ammonia on the catalytic surface.

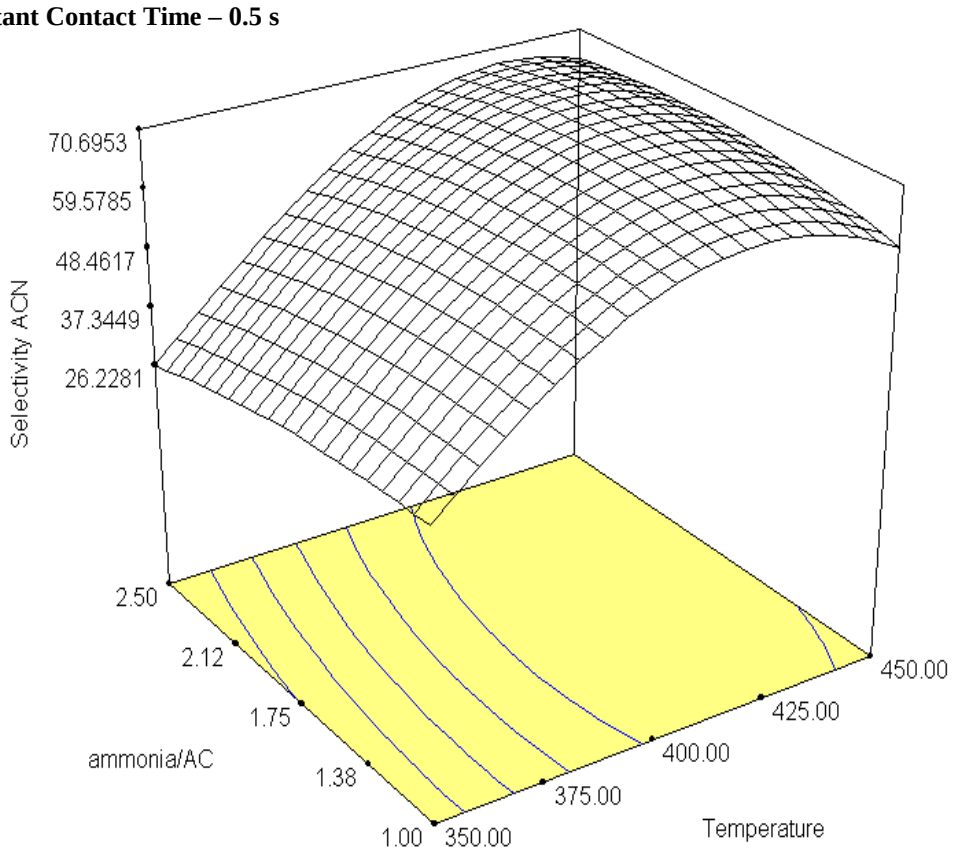

Figure 8: Acrolein (AC) selectivity as a function of the reaction temperature and the molar NH_3/AC ratio

Reaction conditions: Pressure – 1 bar, contact time - 0.5 s, Acrolein/O_2 ratio - 0.38

Figure 8 illustrates the influence of the reaction temperature and the NH_3/AC molar ratio on the selectivity to acrylonitrile. At the relatively low reaction temperature of 350 °C and NH_3/AC ratio of 1, the ACN selectivity exhibits the overall minimum of 26%. In relation to the reaction temperature and the NH_3/AC ratio, the best selectivity of 67% is predicted at 425 °C with a NH_3/AC ratio of 2. The decrease in selectivity at temperatures higher than 425°C may be ascribed to the decomposition of acrolein or of the formed acrylonitrile. Furthermore, it is noteworthy that a higher amount of ammonia also leads to the formation of nitrogen-containing by-products such as acetonitrile, propionitrile and pyridine.

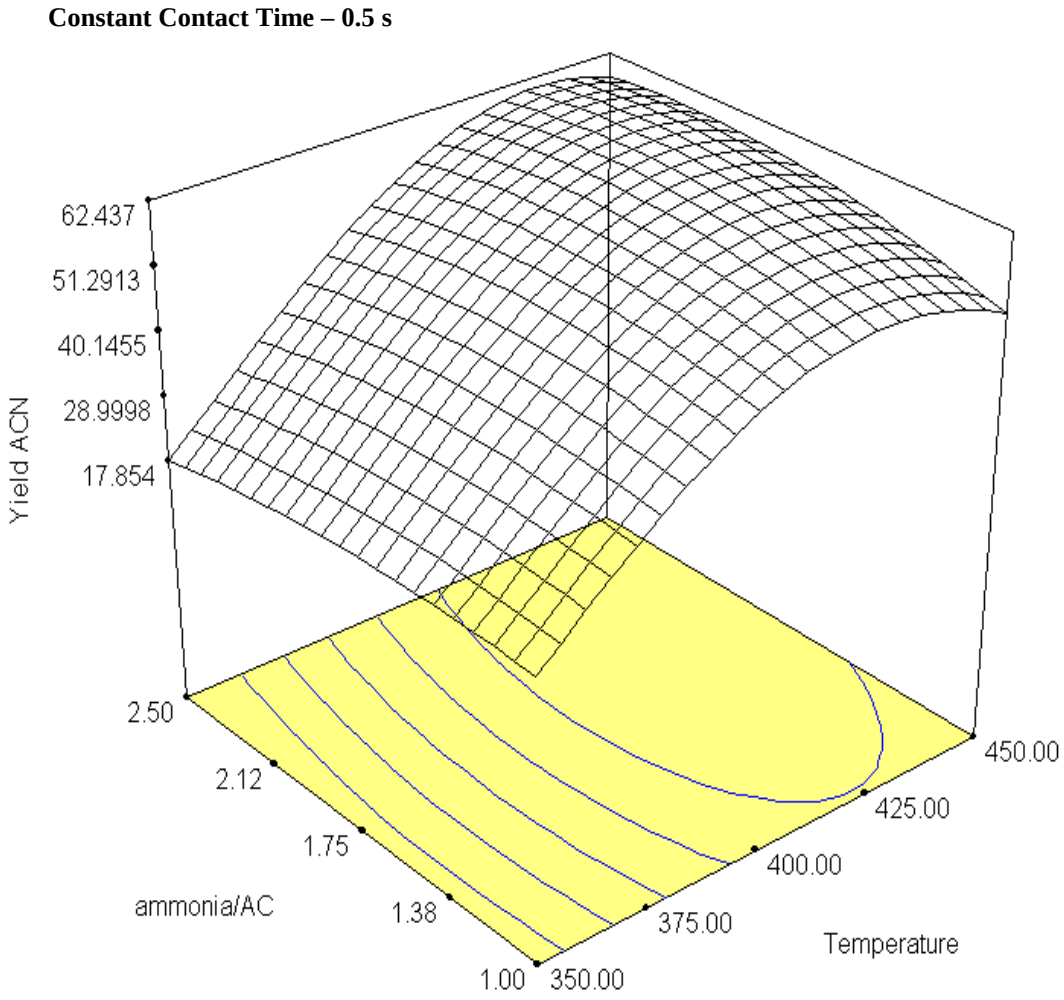

Figure 9: **Acrylonitrile (ACN) yield as a function of the reaction temperature and the NH_3/AC molar ratio**

Reaction conditions: Pressure – 1 bar, contact time - 0.5 s, Acrolein/O_2 ratio - 0.38

Figure 9 shows the influence of the reaction temperature and the NH_3/AC molar ratio on the acrylonitrile yield. The lowest yield is 18% at 350 °C, irrespective of the NH_3/AC ratio. This yield increases with the reaction temperature, and the highest yield is predicted at 425 °C. Concerning the NH_3/AC ratio, the highest yield of 61% is predicted for a NH_3/AC ratio of around 2.

In order to validate the model, the parameters predicting the highest catalytic performance (temperature of 425 °C, NH_3/AC molar ratio of 2 and contact time of 0.5 s) were experimentally verified. The predicted and measured catalytic performances are compared in

Figure 10. The predicted and the experimental values are very close, as the observed acrolein conversion is of 93% *vs.* 90% for the value predicted by the model issued from DOE. The observed selectivity to acrylonitrile was 63% *vs.* 67% for the prediction, and, therefore, the obtained overall yield of acrylonitrile was 59% *vs.* 62% for the predicted value, which confirms the excellent agreement between the experimental values and the model-derived values, thus validating the model.

Nevertheless, it is noteworthy that, in the experiments carried out during the design of experiments methodology, a slightly higher yield to acrylonitrile was obtained for another set of parameters. As a matter of fact, the highest yield to acrylonitrile (66%) was obtained with 89% acrolein conversion and 74% ACN selectivity at 400 °C at a NH_3/AC molar ratio of 1.75 (Table 4, entry 17). In fact the predicted reaction parameters are derived from the software-generated model, which tries to fit the maximum points of set of parameters. However, there is the possibility that some points might be excluded during the fitting.

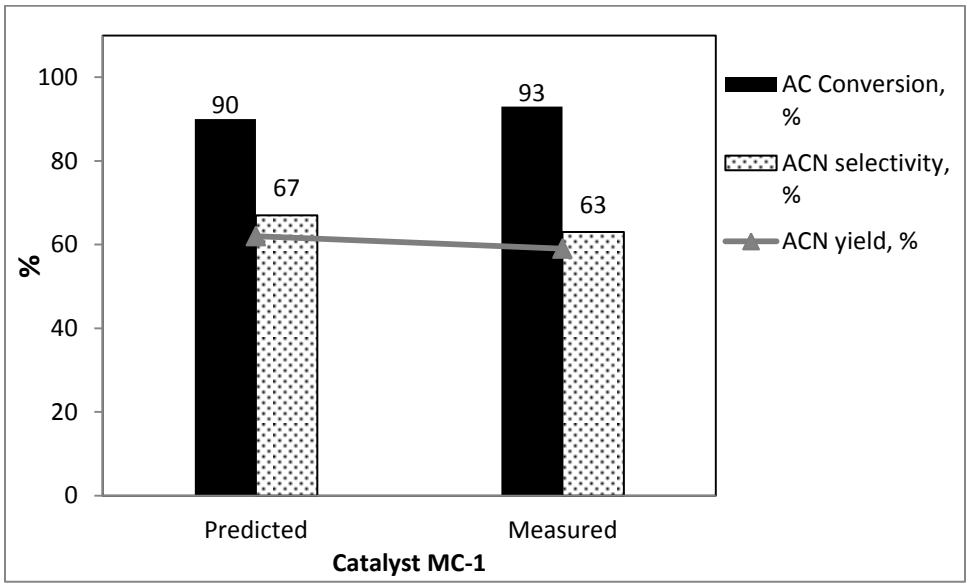

Figure 10: Comparison of predicted and measured results for optimized parameters predicted by the DoE results-derived model
Reaction conditions: Temperature – 425 °C, catalyst amount – 3.5 g, NH_3/AC ratio – 2

Table 5 shows the values of the varied operating conditions before and after the experimental design.

Table 5: Key operating conditions before and after the experimental design (DOE)

Parameter	Value before DOE	Value after DOE
Reaction temperature	400 °C	425 °C
Amount of catalyst (Contact time)	3.5 g (0.5 s)	3.5 g (0.5 s)
NH_3/AC molar ratio	1.75	2

5.4 Conclusion

The multicomponent bismuth molybdate catalysts with the general formula $Me_7^{II}Me_3^{III}BiMo_{12}O_X$ were very active and selective in the reaction of acrolein ammoxidation to acrylonitrile. From our study, it can be seen that the catalysts' synthesis method affects their performance. Despite a complex composition, the catalysts can be successfully reproduced by the coprecipitation method.

The catalysts have complicated structures, basically comprising the bismuth molybdate phase together with additional promoters that can be categorized in two groups: bivalent metal molybdates, and trivalent metal molybdates. Among the bivalent metals used, the highest performance was observed for the Cu-containing catalyst with a 52% acrylonitrile yield. The second best performance was observed over the Co-containing catalyst, and on a formulation containing a Co-Ni mixture. The presence of the metastable β-$CoMoO_4$ phase and Bi-enriched catalyst surface was responsible for the high activity of the Co and Co-Ni catalysts, whereas the lower activity of the only Ni-containing catalyst was due to the presence of the α-$NiMoO_4$ phase. Among the bivalent metals used, we observed the order of catalytic performances as Cu > Co-Ni > Co > Mg > Ni in terms of acrylonitrile yield.

In multicomponent catalysts, the role of the trivalent element is crucial because it is supposed to provide an efficient redox cycle in the ammoxidation reaction. We also observed that there is a significant decrease in the catalytic performances in the absence of iron. The characterization study showed that the iron has a significant promotion effect on the formation of the metastable β-$CoMoO_4$ phase of cobalt and of the Koechlinite γ-Bi_2MoO_6 phase of bismuth, which leads to a better activity of the iron-containing catalysts. Among the trivalent metal-containing catalysts, the activity order was observed as Fe > Al > Cr in terms of acrylonitrile yield. The silica added as a binder improved the catalytic performance, where the best performance was achieved with 17.5% silica content, while a further increase in silica content decreased the selectivity to acrylonitrile. Furthermore, a very small concentration of promoters like P and K marginally improved the selectivity, but the role of these elements is not clear as they do not form any identified separate phase in the solids.

The catalytic performance in acrolein ammoxidation reaction was also sensitive to the applied reaction conditions. The DOE study showed that the reaction temperature and the NH_3/AC ratio have a significant effect on activity and selectivity of the catalyst. The optimal reaction conditions obtained from the DOE model were further experimentally validated with a maximum acrylonitrile yield of 64 ± 2%.

5.5 References

[1] (The Standard Oil Co.), GB1319190, **1973**.
[2] F. J. Bellringer, T. Bewley, H. M. Stanley, (The Distillers Co. Ltd.), GB709337, **1954**.
[3] M. W. J. Wolfs, P. H. A. Batist, *Journal of Catalysis* **1974**, *32*, 25-36.
[4] J. C. Jung, H. Kim, Y. S. Kim, Y.-M. Chung, T. J. Kim, S. J. Lee, S.-H. Oh, I. K. Song, *Applied Catalysis A: General* **2007**, *317*, 244-249.
[5] J.-H. Park, K. Row, C.-H. Shin, *Catalysis Communications* **2013**, *31*, 76-80.
[6] I. I. Zakharov, G. Y. Popova, T. V. Andrushkevich, *React Kinet Catal Lett* **1982**, *19*, 367-371.
[7] J. C. Jung, H. Lee, H. Kim, Y.-M. Chung, T. J. Kim, S. J. Lee, S.-H. Oh, Y. S. Kim, I. K. Song, *Catalysis Letters* **2008**, *124*, 262-267.
[8] J. Simons Th. G, M. Verheijen E. J, A. Batist Ph, A. Schuit G. C, in *Oxidation of Organic Compounds, Vol. 76*, American Chemical Society, **1968**, pp. 261-275.
[9] J. Haber, M. Witko, *Accounts of Chemical Research* **1981**, *14*, 1-7.
[10] P. A. Batist, C. G. M. van de Moesdijk, I. Matsuura, G. C. A. Schuit, *Journal of Catalysis* **1971**, *20*, 40-57.
[11] R. K. Grasselli, *Catalysis Today* **1999**, *49*, 141-153.

6. General discussion and Perspectives

6.1 General Discussion

In this work, the selective gas-phase ammoxidation of acrolein to acrylonitrile was studied over multicomponent Bi-Mo-O*x* catalysts containing various promoters such as M^{II} (Co, Ni, Mg or Cu) and M^{III} (Fe, Cr or Al). The textural properties, crystal phases, bulk and surface composition and metal molybdate-oxygen coordination of the catalyst were determined using different characterization techniques in order to correlate key properties of the catalysts with their catalytic activities in the acrolein ammoxidation reaction. Furthermore, the optimized reaction conditions such as temperature and NH_3/AC ratio were obtained by performing experiments under various conditions and deriving a model using a design of experiment software, which was further experimentally validated.

The multicomponent bismuth molybdate catalyst has the general formula of $Me^{II}_7Me^{III}_3BiMo_{12}Ox$. The impact of each element was studied by varying the Me^{II} and Me^{III} metals in the composition.

The reaction mechanism of the ammoxidation over multifunctional bismuth molybdate catalysts is very complex. However, it is widely reported that the basic active site is the bismuth molybdate phase, which is responsible for the chemisorption of the reactant molecule as well as the insertion of N to form acrylonitrile. Grasselli *et al*.[1] studied the mechanism of propylene ammoxidation over bismuth molybdate catalysts. They reported that the kinetics of ammoxidation reaction over a bismuth molybdate catalyst follows the Mars-van Krevelen mechanism, where lattice oxygen of the catalyst takes part in the reaction resulting in the reduction of the catalyst. In a following step, the catalyst is reoxidized by molecular oxygen. In the case of propylene, the reaction is initiated by the α-hydrogen abstraction with the formation of an allylic intermediate. The detailed mechanism of propylene ammoxidation over a bismuth molybdate catalyst is shown in figure 1.

1) The reaction starts with the formation of the active ammoxidation site by replacing lattice O^{2-} of Mo with isoelectronic NH^{2-}
2) The oxygen bound to the bismuth is responsible for α-hydrogen abstraction

3) Mo acts as the center for chemisorption of the propylene through a correspondingly formed allylic intermediate, where NH^{2-} insertion occurs prior to the abstraction of a second hydrogen species to form acrylonitrile.

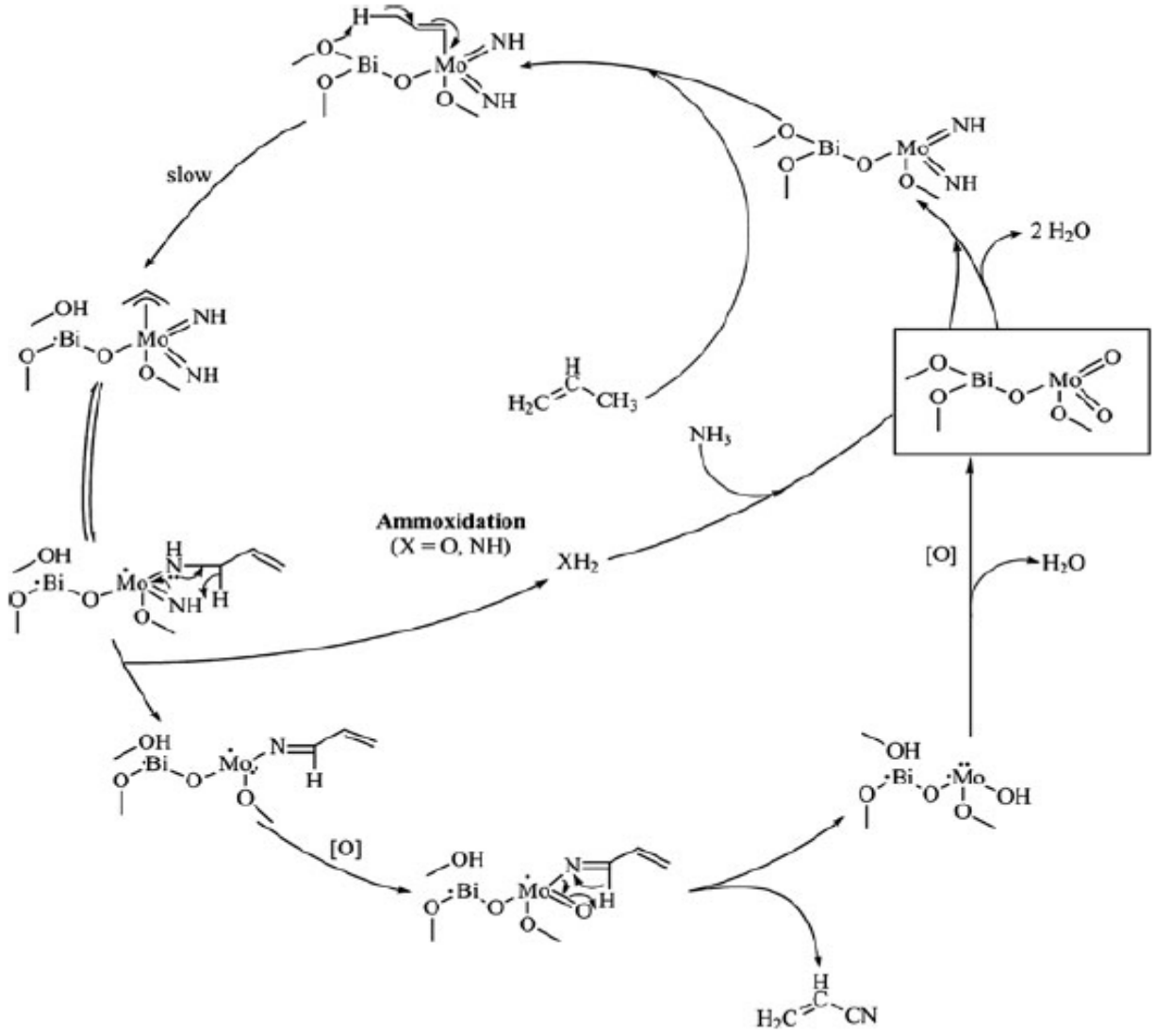

Figure 1: Mechanism of selective propylene ammoxidation to acrylonitrile over a bismuth molybdate catalyst.[1]

However, the ammoxidation of partially oxidized substrates like allyl alcohol do not follow the same pathway through α-hydrogen abstraction from bismuth. Burrington *et al.*[2] postulated a specific reaction mechanism for the ammoxidation of allyl alcohol, which is given in Figure 2.

First, ammonia is chemisorbed on MoO_3 to give a Mo=NH entity **1** by substitution of Mo=O. Then, allyl alcohol is chemisorbed on molybdenum by abstracting the hydroxy hydrogen and forming a σ-allyl molybdate species **2** which is thereafter transformed to a σ-N allyl complex **3** Finally, the formation of acrylonitrile proceeds by two hydrogen abstraction steps. From the mechanism below, we can see that molybdenum has a substantial activity towards allyl alcohol ammoxidation, whereby the role of bismuth is not clear. Burrington *et al.* reported that the presence of bismuth increases the reaction rate either by abstraction of hydrogen *via* Bi-O bond (propylene mechanism) or by providing a sink for the molybdenum to which it can transfer electrons after hydrogen abstraction by molybdenum oxygens. Hence, in the case of allyl alcohol, bismuth acts by providing a sink for molybdenum.

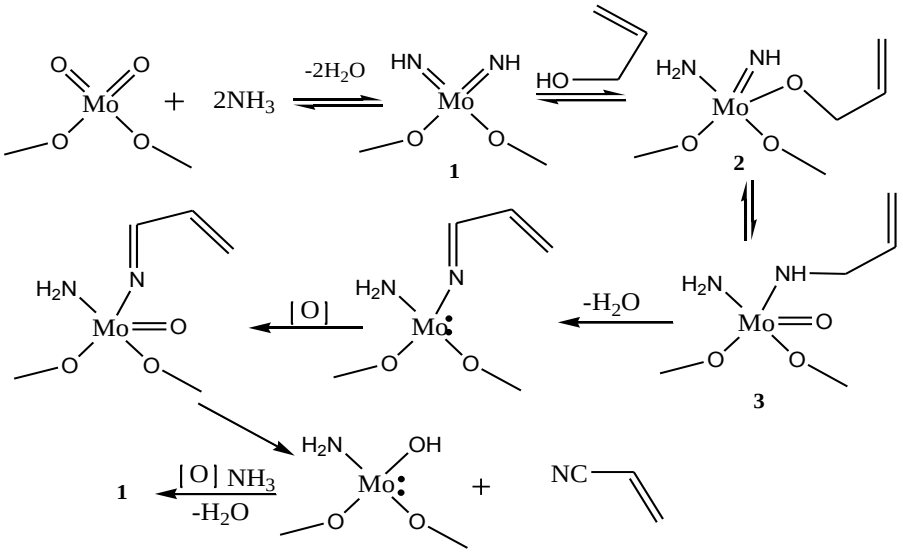

Figure 2: Mechanism of selective allyl alcohol ammoxidation to acrylonitrile over a bismuth molybdate catalyst.[2]

In the case of acrolein, the mechanism will not follow the same pathway, since it is already more oxidized than propylene and allyl alcohol. Therefore, the chemisorption of acrolein is not possible nor by α-hydrogen abstraction neither by hydroxy hydrogen abstraction. Andrushkevich *et al.*[3] reported that acrolein can adsorb on an aprotic center by the formation of coordinatively bonded π-complex. Therefore, we propose the mechanism depicted in Fig 3 for the acrolein ammoxidation.

We propose that the reaction starts with the formation of the ammoxidation site **1** by chemisorption of NH_3 on Mo to form a Mo=NH species, similary to the mechanism for allyl

alcohol. Further, acrolein forms a coordinate bond through carbonyl oxygen, which then further transforms into a σ-N allyl complex **3.** Thereafter, acrylonitrile is formed by abstraction of hydrogen, leaving behind the reduced Mo catalyst **5,** which is then reoxidized by molecular oxygen.

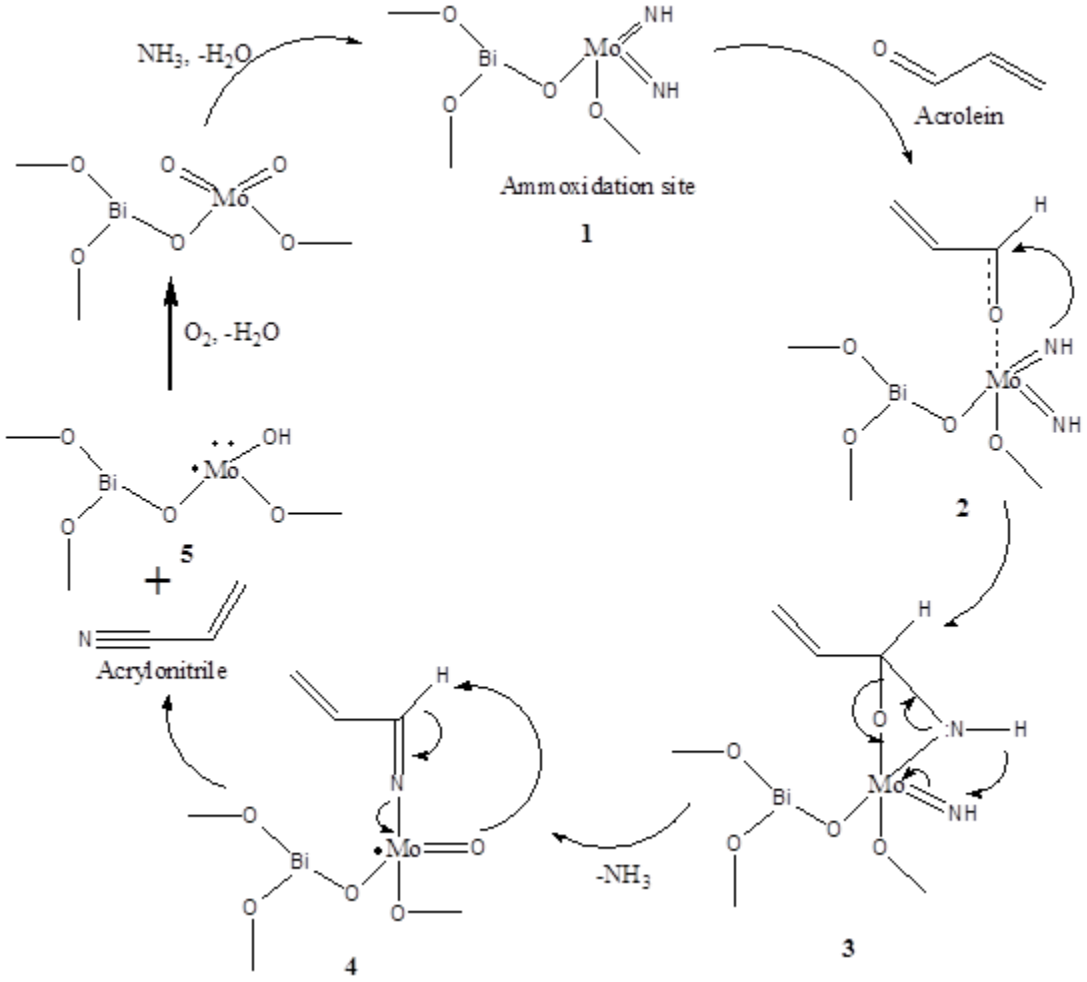

Figure 3: Proposed mechanism of acrolein ammoxidation over bismuth molybdate catalyst

From all the three mechanisms stated above, we can see that the following steps are in common:

1) Removal of lattice oxygen from the catalyst results into the reduction of the catalyst as well as the creation of an oxygen vacancy. 2) These lattice oxygen vacancies migrate through the bulk of the catalyst from the reaction sites to separate reoxidation sites.

3) The catalyst is reoxidized at this separate site, where O_2 is dissociated to lattice O^{2-} and the latter diffuses from the reoxidation site to the ammoxidation reaction site for another catalytic cycle.

Therefore, the ammoxidation catalyst should have two phases: the first one where the actual reaction occurs with removal of lattice oxygen, and the second one which provides the reoxidation center for the dissociation of molecular oxygen to lattice oxygen. In this context, the multicomponent catalyst based on bismuth molybdate contains various elements, with each of them bringing a specific function in the catalytic act.

The catalysts we studied with the general formula $Me^{II}_7Me^{III}_3BiMo_{12}Ox$ contains bismuth molybdate, which primarily functions as active phase for ammoxidation (Figure 3). The trivalent metal, and especially iron, acts as a redox couple, Fe^{3+}/Fe^{2+} in the case of iron. Iron in its Fe^{3+} oxidation state is capable of efficient lattice oxygen transfer to the Bi-Mo-O site, where in its 2+ state it is capable of dioxygen chemisorption and formation of lattice oxygen O^{2-} and its incorporation into lattice.[4] Therefore, we saw a significant improvement in the catalyst activity in the presence of iron (28% acrylonitrile yield for MC-7 *vs.* 45% yield for MC-1, *c.f.* section 5.2.2, Figure 5).

The screening of the catalysts in the presence and the absence of trivalent metal showed that 1) activity and selectivity significantly dropped in the absence of iron 2) the iron has the strongest promoting effect compared to the other trivalent metals such as Cr^{3+} and Al^{3+}. The XRD and IR studies of the catalysts showed that iron is present as $Fe_2(MoO_3)_4$. Another positive effect of iron was the promotion of the active γ-Bi_2MoO_6 phase formation as well as the formation of the metastable β-$CoMoO_4$ phase. Chromium and aluminium also showed this promotion effect, but in a less extent compared to iron.

Grasselli[5] reported the cooperation between the two phases: one is a Fe^{3+}-containing bismuth molybdate phase [$Fe_2(MoO_4)_3$], which is the actual catalytic phase, the other one is a and Fe^{2+}-containing phase (β-$FeMoO_4$), which acts as a reoxidation center. However, since it is very difficult to maintain a sufficient number of Fe^{2+} surface sites in an overall oxidizing gaseous atmosphere, it is necessary to stabilize Fe^{2+} structurally. In the presence of divalent metals (Me^{II}) such as Co, Ni, Mg and Cu, stable molybdates isostructural to β-$FeMoO_4$ are formed and, thus,

this latter compound is stabilized. Hereby, the β-$CoMoO_4$ phase is more favorable to stabilize the β-$FeMoO_4$ phase, because they are isostrucural, where Mo is in tetrahedral coordination while in α-$CoMoO_4$, the Mo-O coordination is octahedral. In other words, bivalent Me^{II} metals have the function of providing the host structure for Fe^{2+} in the multicomponent catalyst.

This also could be the reason behind the better performance of MC-1 and MC-11 catalysts, where there is formation of exclusively β-$CoMoO_4$. The lower performance of Ni-containing catalyst can be explained due the formation of α-$NiMoO_4$, where Mo is octahedrally coordinated, which is not isostructural to β-$FeMoO_4$ (*c.f.* section 5.2.1, Figure 4).

The catalyst containing Mg also exhibited a lower activity despite the formation of β-$MgMoO_4$. The lower performance could arise from the weak bonding of magnesium complexes with adsorbed acrolein molecules.[6] Therefore, the choice of the bivalent metal has an impact on the performances of the catalyst.

Overall, the results marked synergistic effect when both divalent promoters and iron molybdate are present together with the catalytically active bismuth molybdate phase. Millet *et al.*[7] studied the synergy effect between bismuth molybdate and mixed iron and cobalt molybdate, where they reported that the $Fe_XCo_{(1-X)}MoO_4$ phase also plays a role for the fast electron transfer, which enhances the efficiency of the redox mechanism. This facilitates the transfer of electrons from reaction site (bismuth molybdate) to the highly conductive $Fe_XCo_{(1-X)}MoO_4$ and the transfer of lattice oxygen to the active site as shown in Figure 4.

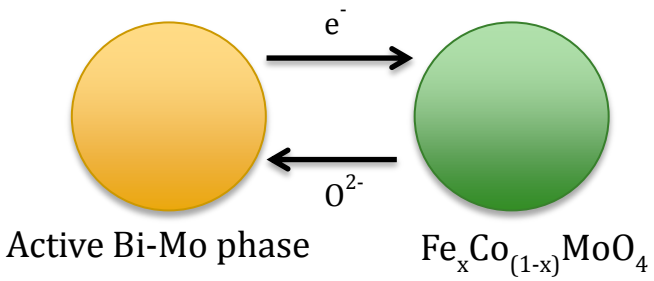

Figure 4: Redox process in multicomponent catalysts

The role of additional promoters such as Si, P and K is not very clear. However, most of the commercial multicomponent catalysts contain silica as a binder.[8, 9] The addition of silica increased the catalytic activity, and the highest yield of acrylonitrile was obtained for the catalyst

with 17.5% silica. However, further increase in silica amount to 50% increased the acrolein conversion, but the acrylonitrile selectivity was significantly decreased resulting in a lower acrylonitrile yield. The acrolein conversion varied linearly with the surface area of the catalyst as shown in Figure 5. However, the selectivity to acrylonitrile was maximal for the catalyst with 17.5% silica, and then decreased for the catalyst with a higher silica content. The increased selectivity of the MC-1 catalyst (17.5% silica) was due to a bismuth-enriched surface, and also to a higher γ-Bi_2MoO_6/α-$Bi_2Mo_3O_{12}$ ratio. Furthermore, silica also plays the role of a binder in the catalyst, which provides enhanced mechanical strength and long term stability.[10]

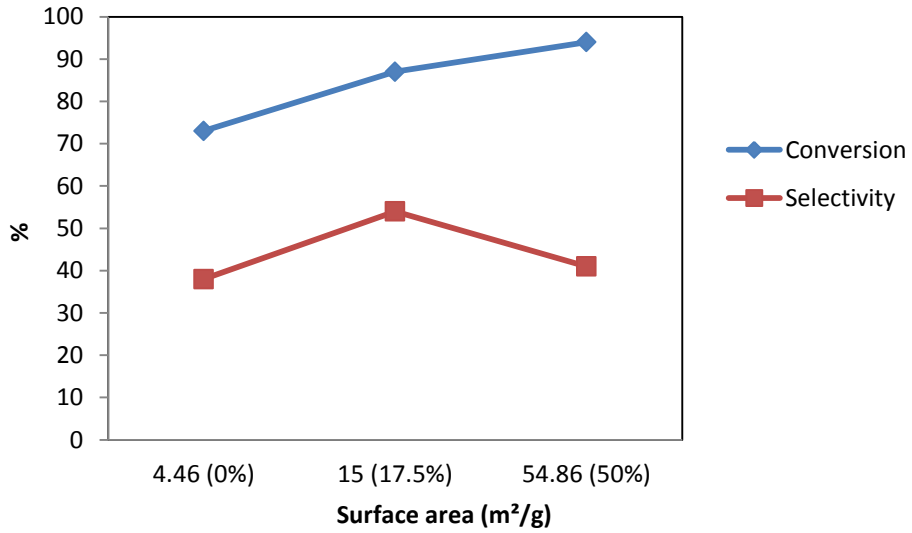

Figure 5: Evolution of conversion and selectivity as a function of the surface area of the catalyst

Furthermore, the addition of small amounts of alkali metal and phosphorus showed improvement in the selectivity for acrylonitrile. The characterization of the catalyst however did not showed any significant difference, except the surface area, which was increased with P and K addition in the catalyst. No P- or K-containing separate phases were detected due to their very small concentrations. The role of phosphorus was reported to increase the long term stability of the multicomponent catalyst in the oxidation of methanol to formaldehyde,[10] whereas the alkali metal was reported to neutralize the most acidic cracking sites and to enhance contact between two functionally distinct phases in the multicomponent catalyst (active phase and reoxidation phase).[5]

The elements in the multicomponent catalysts and their possible roles in the reaction are then summarized in table 1.

Table 1: Elements and their roles in the multicomponent catalyst

Elements	Role
Bi, Mo	Active phase
Fe, Cr or Al	Redox cycle, electric conductivity
Co, Ni, Cu or Mg	Stabilization of reduced Fe^{2+} phase
K	Cation vacancy, suppress acidic cracking sites
P, Si	Long term stability, mechanical strength

Finally, the influence of the key reaction parameters such as temperature, NH_3/AC ratio on the catalyst performance was investigated on the MC-1 catalyst. The models obtained from the design of experiment demonstrated that the molar NH_3/AC ratio and the reaction temperature has a strong influence on the acrolein conversion and the acrylonitrile selectivity. The acrolein conversion increased with increasing the temperature and the NH_3/AC ratio, and reached a maximum at 450°C for a NH_3/AC ratio of 2.5. However, the selectivity to acrylonitrile initially increased with the temperature from 350°C to 425°C after which it decreased with further increase in temperature to 450°C. The overall best performance was obtained with 89% acrolein conversion, 74% selectivity and 66% yield for acrylonitrile at 400 °C and with a NH_3/AC ratio of 1.75.

6.2 Perspectives

From the above results, it can be concluded that the multicomponent bismuth molybdate catalysts are very efficient systems for the acrolein ammoxidation reaction. While a great deal of work has been performed on mechanistic studies on propylene ammoxidation, the acrolein ammoxidation mechanism has not been investigated deeply yet. We have proposed a mechanism for acrolein ammoxidation, but more concrete characterization data are needed to fully support the hypotheses we formulated on the various mechanism steps. Furthermore, there is still room for studying the actual composition of surface and bulk phases of the catalyst and the interaction of acrolein with the surface species. For this purpose, the detailed study of interaction of acrolein and ammonia with a catalyst surface could be studied by *in-situ* spectroscopic techniques, optionally coupled with microcalorimetric studies.

Moreover, from the given ammoxidation mechanisms, we can see that the availability of lattice oxygen as well as the reduction-reoxidation properties play an important role in catalyst performance. Therefore, emphasis could also be put on deeply studying the oxygen capacity, the oxygen mobility within the bulk and also the ease of reoxidation of the catalyst.

Another approach may be to develop more simple catalysts with single phases, which are capable of multiple functions. This so-to-speak catalyst deformulation could lead to a better understanding of the mechanism of the ammoxidation reaction as the structure and the functioning of multicomponent catalyst is very complex due to the presence of multiple phases.

From the DoE, we see that a high temperature is needed to activate ammonia, which causes cracking reactions and waste CO*x* formation. Therefore, finding catalysts capable of activating ammonia at a lower temperature would be a possible target.

Furthermore, as acrolein can be obtained by dehydration of bio-glycerol, it can be combined with acrolein ammoxidation process for the sustainable synthesis of acrylonitrile. The indirect route with integrated two reactions processes, where glycerol is first dehydrated to acrolein and then the as-formed acrolein is ammoxidated to acrylonitrile will be effective for acrylonitrile production. This approach enables us to choose different catalysts and reaction conditions for both reactions.

6.3 References

[1] R. K. Grasselli, J. D. Burrington, *Advances in Catalysis* **1981**, *30*, 133-163.
[2] J. D. Burrington, C. T. Kartisek, R. K. Grasselli, *Journal of Catalysis* **1980**, *63*, 235-254.
[3] T. V. Andrushkevich, G. Y. Popova, *Russian Chemical Reviews* **1991**, *60*, 1023.
[4] R. Grasselli, *Topics in Catalysis* **2001**, *15*, 93-101.
[5] R. K. Grasselli, *Catalysis Today* **1999**, *49*, 141-153.
[6] J. Haber, M. Witko, *Accounts of Chemical Research* **1981**, *14*, 1-7.
[7] J. M. M. Millet, H. Ponceblanc, G. Coudurier, J. M. Herrmann, J. C. Vedrine, *Journal of Catalysis* **1993**, *142*, 381-391.
[8] T. S. R. P. Rao, P. G. Menon, *Journal of Catalysis* **1978**, *51*, 64-71.
[9] (The Standard Oil Co.), GB1319190, **1973**.
[10] D. Klissurski, Y. Pesheva, N. Abadjieva, I. Mitov, D. Filkova, L. Petrov, *Applied Catalysis* **1991**, *77*, 55-66.